Parent-of-Origin inference and its role in the genetic architecture of complex traits: evidence from ~220,000 individuals

Robin J. Hofmeister[1,2,3,4,✉], Théo Cavinato[1,3], Adriaan van der Graaf[1,3], Fanny-Dhelia Pajuste[4], Jaanika Kronberg[4], Nele Taba[4], Estonian Biobank research team[*], Reedik Mägi[4], Simone Rubinacci[5], Lili Milani[4,6], Olivier Delaneau[7], and Zoltán Kutalik[1,2,3,✉]

[1]Department of Computational Biology, University of Lausanne, Lausanne, Switzerland, [2]University Center for Primary Care and Public Health, Lausanne, Switzerland, [3]Swiss Institute of Bioinformatic (SIB), University of Lausanne, Lausanne, Switzerland, [4]Estonian Genome Centre, Institute of Genomics, University of Tartu, Estonia , [5]Institute for Molecular Medicine Finland, Helsinki, Finland, [6]Estonian Biobank, Institute of Genomics, University of Tartu, Estonia, [7]Regeneron Genetics Center, Tarrytown, NY, USA, [*]Lists of authors and their affiliations appear at the end of the paper, ✉Corresponding authors: Robin J. Hofmeister and Zoltán Kutalik

Abstract

Parent-of-origin effects (POEs) occur when the impact of a genetic variant depends on its parental origin. Traditionally linked to genomic imprinting, these effects are believed to have evolved from parental conflict over resource allocation to offspring, which results in opposing parental genetic influences. Despite their potential importance, POEs remain heavily understudied in complex traits, largely due to the lack of parental genomes.

Here, we present a multi-step approach to infer the parent-of-origin of alleles without parental genomes, leveraging inter-chromosomal phasing, mitochondrial and chromosome X data, and sibling-based crossover inference. Applied to the UK Biobank (discovery cohort) and Estonian Biobank (replication cohort), this scalable approach enabled parent-of-origin inference for up to 221,062 individuals, representing the largest dataset of its kind.

GWAS scans for more than 60 complex traits and over 2,400 protein levels contrasting maternal and paternal effects identified over 30 novel POEs and confirmed more than 50% of testable known associations. Notably, approximately half of our POEs exhibited a bipolar pattern, where maternal and paternal alleles exert conflicting effects. These effects were particularly prevalent for traits related to growth (e.g., IGF-1, height, fat-free mass) and metabolism (e.g., type 2 diabetes, triglycerides, glucose). Replication in the Estonian Biobank validated over 70% of testable associations.

Overall, our findings shed new light on the influence of POEs on diverse complex traits and align with the parental conflict hypothesis, providing compelling evidence for this understudied evolutionary phenomenon.

Introduction

Genome-wide association studies (GWAS) have traditionally focused on identifying additive genetic effects, where the phenotypic impact depends on the number of copies of a given allele. This approach assumes that alleles inherited from the mother and father contribute equally to the examined trait. However, some sequence variants can have distinct phenotypic effects depending on whether they are maternally or paternally inherited, a phenomenon known as parent-of-origin effects (POEs). Traditionally, POEs have been linked to genomic imprinting, where only one parental gene is expressed depending on its parental origin. This selective expression is thought to have evolved under the parental conflict hypothesis, which suggests opposing evolutionary pressures on maternal and paternal alleles over resource allocation to offspring: paternally inherited alleles are believed to enhance offspring growth even at the cost of maternal resources, favoring paternal genetic fitness, while maternally inherited alleles conserve resources for future reproduction[1]. This dynamic can result in opposite parental effects at imprinted loci, particularly for traits related to growth, metabolism, and energy storage. However, since most studies have identified only isolated instances of POEs without a systematic evaluation of their abundance, there is only scarce examples to support the conflict hypothesis across a wide array of traits.

While the conflict hypothesis provides a compelling framework for understanding genomic imprinting, the observation of POEs in non-imprinted genes raise the possibility of more complex inheritance patterns influencing certain complex traits[2,3]. Alternatively, some of these effects might also reflect environmental or parental rearing influences rather than strictly genetic mechanisms. This broader perspective underscores the importance of extending investigations beyond classical imprinted regions to open avenues to explore new mechanisms leading to POEs.

Studying POEs at a genome-wide scale requires large cohorts with parent-of-origin (PofO) information. Traditional approaches rely on extensive collections of parent-offspring trios or duos or detailed genealogical data to identify relatives as surrogate parents[4,5]. However, large-scale biobanks often lack both substantial parental genomic data and comprehensive genealogies[6]. Our previous work introduced a method leveraging chromosome X sharing to identify maternal relatives without genealogical information[3], which opened new research opportunities and significantly increased the sample size. However, this method is limited to male participants, prohibiting sex-specific POE detection, constraining sample size and hence reducing statistical power.

To overcome these challenges, we developed a novel multi-step approach for inferring the PofO of sequence variants in many additional pedigree situations. First, we partition the genome into maternal and paternal haplotypes through statistical inter-chromosomal phasing, using inferred surrogate parents. To determine the PofO of these haplotypes, we integrate several predictors: beyond leveraging chromosome X data for males, we also use mitochondrial DNA whole-genome sequencing (WGS). In addition, we infer crossover positions in sibling pairs and assign their PofO using sex-specific recombination maps[7,8] (Figure 1). Using these predictors, our approach probabilistically determines the PofO of variants, maximizing sample size while minimizing misclassification errors inherent to strict parent assignments used in our prior study[3].

We initially applied this method to the UK Biobank, successfully inferring the PofO for 123,716 individuals at over 7.6 million variant sites — a fivefold increase in sample size compared to our previous work[3]. We then extended this approach to the Estonian Biobank, adding 97,346 individuals with PofO information, which served as a replication cohort. This combined dataset of 221,062 individuals enabled a systematic investigation of POEs across a broad range of human traits, including anthropometric characteristics, blood biomarkers, diseases, and protein levels. Our analysis identified over 30 novel POEs, particularly on traits tied to resource allocation, such as growth-related and metabolic traits, as well as protein levels. Many of these effects aligned with the parental conflict hypothesis, primarily through bi-polar effects, where maternal and paternal alleles exert opposing influences. These findings highlight the genetic and evolutionary significance of POEs in shaping complex traits and diseases, offering new insights into their broader biological roles.

Results

We developed a comprehensive, multi-step strategy to infer the PofO of sequence variants in large-scale biobanks. A brief summary of the methods is outlined below, followed by a detailed analysis of POEs.

Summary of the methods

Surrogate parent-based inter-chromosomal phasing

We used kinship estimates, age and sex to identify parent-offspring trios, duos and siblings. For individuals with more distant relatives, we utilized a clustering approach to segregate relatives by parental sides[3], thereby classifying them into "one family side" versus "the other family side". This could be done for a total of 274,525 UK Biobank participants (Supplementary Figure 1). In subsequent sections we refer to those family groups as "surrogate parents". Within this subset, 2,141 individuals also had directly available parental genomes. This group served as a "validation cohort" for assessing the accuracy of our method by comparing surrogate parent-based inferences against true parental genotypes (Supplementary Figure 2). We then used identity-by-descent (IBD) information from surrogate parents to conduct inter-chromosomal phasing, effectively identifying sets of variants inherited together from the same parent across different chromosomes (Figure 1A). This phasing method was applied to 274,525 UK Biobank participants, achieving an average inter-chromosomal phasing accuracy of 99% (Supplementary Figure 3). In subsequent analyses, we refer to this dataset as "inter-chromosomally phased".

Parent-of-origin determination for 123,716 individuals

We leveraged our inter-chromosomally phased data to infer the PofO of each complete parental haplotype set simultaneously. We used two key approaches depending on the available surrogate parents.

First, for second- to fourth-degree relatives, the PofO was determined by identifying whether the surrogate parent was on the maternal or paternal side. Once the PofO of a single haplotype segment was established through its IBD status with the used surrogate parents, this assignment could be confidently extended to the entire parental haplotype set. To determine whether the used surrogate parents are on the maternal or on the paternal side, we leveraged chromosome X genotype data and mtDNA whole-genome sequence data, while also demonstrating the potential value of including chromosome Y whole-genome sequences (Figure 1A, see Methods). Chromosome X is maternally inherited in males, and mtDNA is maternally inherited in both sexes, allowing us to identify maternal relationships (Supplementary Figures 4-8). Although chromosome Y data can reliably identify paternal relationships (Supplementary Figure 9), we found this approach to be less cost-effective and therefore chose not to implement it broadly. By analyzing IBD sharing with surrogate parents on these specialized chromosomes, we were able to determine whether the surrogate parent (and, consequently, all IBD segments shared on other chromosomes) belonged to the maternal or paternal side.

For siblings, who cannot be assigned exclusively to a single parental side since they inherit

genomes from both parents, we applied a different strategy. Specifically, we inferred crossover positions in siblings and probabilistically assigned them a PofO using sex-specific recombination maps[7,8] (Figure 1B). This approach prioritized inter-chromosomally phased data that improved accuracy by aggregating crossovers events across chromosomes (see methods, Supplementary Figures 10-12).

We combined these different kinds of PofO predictors (see Methods) with inference made from available parental genomes to obtain PofO estimates for a set of 286,666 individuals. Notably, over 40% of these individuals (N=123,716) had an estimated PofO probability between 0.99 and 1 (Figure 2A and Supplementary Figure 13A). For 31,008 individuals, multiple predictors were available, and these consistently indicated the same PofO in over 94% of cases (N=29,154 individuals), further reinforcing the reliability of these assignments (Supplementary Figure 13B). Using the validation cohort (where the PofO of the alleles is know) we estimated the accuracy of our inference to be 97.94% at heterozygous sites (Figure 2B, Supplementary Figure 14). Notably, the majority of individuals ($> 80\%$) showed accuracy greater than 99%. This high level of accuracy demonstrates the reliability of our method for determining the PofO of alleles across the genome.

Next, we used the resulting PofO of alleles to perform PofO specific association scans on 59 selected complex traits (Supplementary Table 1) and 2,414 proteins. We selected complex traits primarily from biomarkers and morphological measures, to assess POEs across a diverse range of phenotypes while including traits associated with resource allocation, such as growth-related traits (e.g., height and fat-free mass), metabolic traits (e.g., glucose, lipids, and basal metabolic rate), and energy storage traits (e.g., regional fat percentages and BMI), allowing us to test the conflict hypothesis. Our analysis employed three main approaches: (i) a genome-wide scan to identify novel POEs without prior assumptions, and two targeted strategies, (ii) focusing on regions with additive associations with the trait (referred to as "additive regions" in subsequent discussions) and (iii) examining imprinted regions with established imprinting potential to detect loci most likely to exhibit POEs.

Replicating known POE associations

We first replicated POEs previously reported in the literature[3,4,5,9,10,11,12,13], both to validate known POEs and to validate our PofO assignment. No consensus method is currently used to identify POEs and many studies simply claim POEs if the effect is significant (at an arbitrary threshold) when the allele came from one parent, but not significantly associated when it came from the other parent. Therefore, we first pre-filtered claimed POEs by rigorously testing for a differential paternal *vs* maternal alleles effect and kept only published hits where the differential test P-value P_D was lower than 10^{-3}, to ensure more robust evidence for POE.

We identified 23 known POEs meeting this criterion, of which 22 could be tested for replication in our cohort (same variant-trait pair). We successfully replicated 12 of them (54.5%) at $P_D < 0.05/22$. Interestingly, of the 8 POEs reported for birth weight, none were replicated in our cohort. For the other traits, we successfully replicated $> 85\%$ (12/14) POEs, with the same parental effect and the same direction of effect (Supplementary Table 2).

Parent-of-origin association genome-wide

We conducted a genome-wide scan for POEs across the 59 selected traits (Supplementary Table 1), identifying 6 significant associations ($P_D < 1 \times 10^{-9}$). However, this approach did not reveal any additional significant associations beyond those identified through the targeted strategies presented below. Consequently, we focused on the more informative results from the targeted analyses.

Novel associations in additive regions

To identify novel POEs within "additive regions", we first performed additive association testing (ignoring the PofO of the alleles) for 59 selected traits (Supplementary Table 1) and identified 1,812 significant (P-value $< 1 \times 10^{-9}$, see Methods) LD-pruned additive associations. We then sought to detect whether some of these associations may involve POEs. To this end, we applied a differential POE GWAS scan (see Methods) restricted to these SNP-trait pairs. This approach "additive regions" is geared towards the identification of POEs where the maternal and paternal effects are not in opposite direction and hence even the simple additive effect is non-zero. While this strategy allows us to detect only a subset of POE scenarios (Supplementary Figure 15), it also drastically reduces the multiple testing burden, increasing the significance threshold to $0.05/1812 = 2.75 \times 10^{-5}$ (see Methods).
This approach revealed 6 significant POEs (Table 1). Among these, two associations — the 11p15.5 region with standing height and the 14q32.2 region with platelet count — have been previously reported (for standing height) or are in high linkage disequilibrium (LD) with associations documented in earlier studies ($r^2 > 0.89$ for platelet count, see replication section). Two additional associations were found to be in moderate to low LD with previously reported variants. At the 5p15.33 locus, the POE of rs7705526 on telomere length exhibited moderate LD ($r^2 = 0.27$) with rs2735940, a variant previously implicated in telomere length in our earlier work[14]. Notably, our additive region approach focuses on assessing the PofO specificity of the lead additive variant at a locus, which may not always pinpoint the true lead POE variant. For telomere length, the lead POE variant was also rs2735940 (Figure 3A,B; see replication section). Additionally, the association of rs2237895 with glycated hemoglobin (HbA1c) exhibited low LD ($r^2 = 0.047$) with rs2237892, a variant previously associated with type 2 diabetes (T2D) in a parent-of-origin context[5]. Since HbA1c is a known proxy for T2D[15], we conducted a conditional analysis to test whether the POEs of these two variants on HbA1c were independent. The results indicated that the two SNPs are not independently associated with HbA1c, with rs2237895 emerging as the lead variant driving the observed POE at this locus ($P_D(cond.) = 2.4 \times 10^{-4}$ and 0.045 for rs2237895 and rs2237892, respectively).
We also identified two novel, independent POEs on telomere length (Figure 3). First, the T allele of rs11100479 on chromosome 4, an eQTL for the gene *NAF1*, was associated with an increase in telomere length when inherited from the father. We also observed a moderate effect of the maternal T allele, albeit the effect of the paternal T allele was significantly stronger ($\widehat{\beta}_P = 0.078$, $\widehat{\beta}_M = 0.022$, $P_P = 1.8 \times 10^{-22}$, $P_M = 6.6 \times 10^{-3}$, $P_D = 6.25 \times 10^{-7}$, Figure 3A,C). Additionally,, the C allele of rs2293607 on chromosome 3, located within the *TERC* gene (non-coding transcript exon), was found to be associated with decreased telom-

ere length when inherited from either parent, albeit the effect is significantly stronger when paternally inherited ($\widehat{\beta}_P = -0.12$, $\widehat{\beta}_M = -0.068$, $P_P = 2.2 \times 10^{-55}$, $P_M = 5.3 \times 10^{-18}$, $P_D = 5.7 \times 10^{-7}$, Figure 3A,D).

In less stringent analysis, where the testing burden is reduced by evaluating each trait individually, we identified six additional suggestively significant POEs (Supplementary Table 3), two of which (both novel) with IGF-1. The maternal T allele of the first lead variant rs17145750, intronic to *MLXIPL*, was associated with increased IGF-1 levels, and we observed no effect from the paternal T allele ($\widehat{\beta}_P = 0.015$, $\widehat{\beta}_M = 0.063$, $P_P = 0.09$, $P_M = 9.07 \times 10^{-13}$, $P_D = 1.18 \times 10^{-4}$). The second association is located within the 11p15.5 imprinted region. The lead variant rs3213217, intronic to *IGF2*, demonstrated asymmetric polar effects, with both maternal and paternal T alleles associated with increased IGF-1 levels, albeit to different extents ($\widehat{\beta}_P = 0.096$, $\widehat{\beta}_M = 0.058$, $P_P = 1.4 \times 10^{-34}$, $P_M = 2.0 \times 10^{-13}$, $P_D = 5.7 \times 10^{-4}$). While these findings did not meet the stringent significance threshold when focusing on additive regions, they highlight potential POEs with moderate effects.

Novel associations in imprinted regions

Another way to reduce multiple testing burden in a meaningful way is to restrict our POE analysis to variants located within a 500kb window of known imprinted regions, which are more likely to harbor POEs (Supplementary Table 4)[5]. We applied this approach to the same 59 selected traits (Supplementary Table 1) and identified a total of 26 POEs with significant (0.05/16,574, see Methods) POE difference P-value P_D (Table 2). Interestingly, the majority of these loci exhibited opposite parental effects on the examined trait, i.e the trait is increased by the allele inherited from one parent, but decreased when the allele is inherited from the other parent. These opposite parental effects align with a pattern of bi-polar dominance[16,17], emphasizing the distinct and opposing contributions of each parent's allele to the trait. Notably, such effects are often missed by traditional additive GWAS, where these parental effects cancel out at heterozygotes (Supplementary Figure 15).

A novel bi-polar dominant effect on standing height at 11p15.5

We detected three independent loci associated with standing height in a parent-of-origin dependent fashion at the 11p15.5 imprinted region (Table 2, Figure 4). Two of these, rs143840904 and rs77708343, are in high LD ($r^2 > 0.6$) with variants that were associated with height in previous POE studies[9,12,13] (see replication section).

At the same locus, we discovered an independent and novel POE of rs7105710, located more than 120kb away and in relatively low LD with both previously reported lead SNPs ($r^2 = 0.021$ and 0.022 with rs77708343 and rs147239461, respectively). This variant exhibits a clear bi-polar pattern, with the maternal C allele associated with decreased, and the paternal C allele associated with increased height ($\widehat{\beta}_P = 0.017$, $\widehat{\beta}_M = -0.014$, $P_P = 1.84 \times 10^{-5}$, $P_M = 2.6 \times 10^{-4}$, $P_D = 1.99 \times 10^{-8}$, Figure 4E). The variant is a splicing QTL (sQTL) for the maternally expressed *H19* gene and also acts as an sQTL and eQTL for *MRPL23* and *TNNT3*[18].

To better understand the independence of the POEs at these three loci, we conducted a conditional analysis by including our three primary variants - rs143840904, rs77708343, and

rs7105710 - in a single regression model. This approach allowed us to assess whether the effect of each variant remains significant after accounting for the others, ensuring that the observed effects are not due to linkage disequilibrium. The conditional analysis confirmed that each variant independently contributed to the observed POEs ($P_D(cond.) = 9.2 \times 10^{-8}, 5.81 \times 10^{-4}$, and 6.17×10^{-8} for rs143840904, rs77708343, and rs7105710, respectively), underscoring their distinct roles in standing height regulation at this locus. Notably, due to their bi-polar dominant effects, the associations of both rs77708343 and rs7105710 were not detected by the traditional additive GWAS.

Finally, we evaluated these variants for POEs on sitting height, to understand how these loci can differentially impact various growth parameters. We successfully replicated two associations at a significance threshold of $0.05/3 = 0.016$ ($P_D = 3.8 \times 10^{-4}$ and 4.1×10^{-9} for rs143840904 and rs77708343, respectively), with parental effects aligned to those observed on standing height (Supplementary Table 5). Interestingly, while the significance and effect sizes of rs143840904 decreased for sitting height, the association of rs77708343 remained relatively stable, indicating that it may contribute equally to trunk size as it does to overall height. On the other hand, we did not replicate the association of rs7105710, although reaching nominal significance ($P_D = 0.041$). This suggests that this variant likely contributes more to femoral length rather than to trunk size.

Novel bi-polar dominant effects on metabolic traits at 11p15.5

We uncovered novel bi-polar POEs on metabolic rate and body composition traits within the 11p15.5 imprinted region (Table 2). Specifically, the paternal G allele of rs77708343 was associated with a decrease in metabolic rate, while the maternal G allele showed an increase ($\widehat{\beta}_P = -0.048$, $\widehat{\beta}_M = 0.035$, $P_P = 1.2 \times 10^{-5}$, $P_M = 1.3 \times 10^{-3}$, $P_D = 7.5 \times 10^{-8}$). Given that basal metabolic rate is estimated from height and weight, we further examined the effects of rs77708343 on these individual traits. Both height and weight were impacted by the variant, with the paternal G allele associated with decreased, and the maternal G allele associated with increased trait levels ($\widehat{\beta}_P = -0.054$ and -0.064, $\widehat{\beta}_M = 0.033$ and 0.031, $P_P = 2.2 \times 10^{-7}$ and 1.3×10^{-5}, $P_M = 1.0 \times 10^{-3}$ and 3.1×10^{-2}, $P_D = 2.1 \times 10^{-9}$ and 3.8×10^{-6} for standing height and weight, respectively).

Due to the correlation between height and weight, we further explored associations of rs77708343 with additional morphological traits, including waist and hip circumference, as well as fat, fat-free and water mass measurements for legs, arms, trunk and whole body. The analysis revealed that rs77708343 influenced waist circumference, fat-free mass and whole body water mass, while no significant effect was observed on hip circumference or fat percentage. Specifically, the paternal G allele was associated with decreased and the maternal G allele with increased trait levels ($\widehat{\beta}_P = -0.056$, -0.052, -0.032, -0.038 and -0.043, $\widehat{\beta}_M = 0.039$, 0.032, 0.030, 0.034 and 0.033, $P_P = 1.0 \times 10^{-3}$, 1.2×10^{-6}, 1.8×10^{-3}, 1.9×10^{-4} and 1.0×10^{-5}, $P_M = 1.7 \times 10^{-2}$, 2.0×10^{-3}, 3.1×10^{-3}, 8.0×10^{-4} and 1.2×10^{-3}, $P_D = 7.0 \times 10^{-5}$, 1.8×10^{-8}, 1.6×10^{-5}, 5.5×10^{-7} and 1.6×10^{-7} for waist circumference, leg, arm, and trunk fat-free mass, and whole-body water mass, respectively). Notably, leg and trunk fat-free mass, and whole body water mass also met our significance threshold specific to imprinted regions at this locus (Table 2).

Distinct bi-polar dominant and maternal effects on blood glucose biomarkers and type 2 diabetes

We identified novel associations with type 2 diabetes (T2D), HbA1c and glucose levels at two variants in high LD ($r^2 > 0.99$), rs10838787 and rs4417225 ($P_D = 1.8 \times 10^{-9}, 2.7 \times 10^{-17}$ and 7.4×10^{-8}, respectively, Table 2). Specifically, we found the paternal A allele of rs10838787 to be associated with increased T2D prevalence, while the maternal A allele appears to be protective ($\widehat{\beta}_P = 0.136$, $\widehat{\beta}_M = -0.09$, $P_P = 3.8 \times 10^{-7}$, $P_M = 7.4e \times 10^{-4}$, $P_D = 1.8 \times 10^{-9}$, Figures 5A,B). We also found bi-polar dominant effects on HbA1c and glucose, with paternal alleles associated with increased, and maternal alleles associated with decreased trait levels ($\widehat{\beta}_P = 0.05$ and 0.029 , $\widehat{\beta}_M = -0.028$ and -0.028, $P_P = 2.3 \times 10^{-14}$ and 9.2×10^{-5}, $P_M = 1.8 \times 10^{-5}$ and 2.0×10^{-4} for HbA1c and glucose, respectively, Figures 5C,D). Although these variants are novel, they are in high LD ($r^2 > 0.9$) with a variant previously associated with T2D in a parent-of-origin manner[5].

We identified a novel, independent POE of rs2299620 with HbA1c ($P_D = 2.2 \times 10^{-6}$), a variant located 1.1 Mb away and not in LD with the previously discussed variants ($r^2 < 0.01$, Table 2, Figure 5C). The maternal T allele was associated with decreased HbA1c levels ($\widehat{\beta}_M = -0.12$, $P_M = 1.3 \times 10^{-13}$), while the paternal T allele has no detectable effect. Here again, while being novel for HbA1c, the variant is in high LD ($r^2 = 0.5$) with rs2237892, a variant previously associated with T2D[5]. Although the association of rs2299620 with T2D does not reach our conventional significance threshold, we observed a moderate protective effect of the maternal T allele ($\widehat{\beta}_M = -0.36$, $\widehat{\beta}_P = -0.01$, $P_M = 3.2 \times 10^{-7}$, $P_P = 0.42$, $P_D = 2.2 \times 10^{-3}$, Figure 5A). To disentangle the observed signal at this locus, we performed a conditional analysis for HbA1c, which revealed that the two SNPs are not independently associated with HbA1c. SNP rs2299620 emerged as the lead variant driving the observed HbA1c association at this locus ($P_D(cond.) = 2.19 \times 10^{-4}$ and 0.054 for rs2299620 and rs2237892, respectively).

Novel bi-polar dominant effects on renal function indicators at 11p15.5

We identified three novel POEs on cystatin C, creatinine and urate levels ($P_D = 5.9 \times 10^{-14}, 4.9 \times 10^{-11}$ and 2.2×10^{-7}, respectively, Table 2) at a locus located over 300kb away and not in LD with other known POEs on blood biomarkers ($r^2 < 0.001$). We observed bi-polar effects of lead SNPs rs170102 and rs217215 ($r^2 > 0.98$) for both cystatin C and creatinine, respectively. Specifically, we found the paternal A allele of rs170102 associated with decreased, but the maternal A allele associated with increased cystine C levels ($\widehat{\beta}_P = -0.041$, $\widehat{\beta}_M = 0.026$, $P_P = 5.9 \times 10^{-11}$, $P_M = 3.1 \times 10^{-5}$). We also found the paternal G allele of rs217215 associated with increased, but the maternal G allele associated with decreased creatinine levels ($\widehat{\beta}_P = 0.03$, $\widehat{\beta}_M = -0.024$, $P_P = 2.5 \times 10^{-7}$, $P_M = 2.6 \times 10^{-5}$). For urate, we found the G allele of rs4264135 associated with decreased urate levels when paternally inherited, and observed no effect when maternally inherited ($\widehat{\beta}_P = -0.033$, $\widehat{\beta}_M = 0.014$, $P_P = 1.8 \times 10^{-7}$, $P_M = 0.033$).

We evaluated the independence of these effects using co-localization analysis, and found that cystatin C and creatinine probably share the same causal variant and are likely influenced by a common genetic regulatory mechanism (posterior probability $H_4 > 0.88$). On the other

hand, we found lower co-localization probabilities for urate (posterior probability = 0.39 and 0.64 with cystatin C and creatinine, respectively).

7q32.2 revealed novel bi-polar dominant effects on lipid-related profiles

We identified novel POEs of rs62471721, rs4731690 and rs10239342 on triglycerides (TG), HDL-cholesterol (HDL-C) and sex hormone-binding globulin (SHBG) levels, respectively ($P_D = 6.5 \times 10^{-9}, 1.9 \times 10^{-6}$ and 1.8×10^{-6}, respectively, Table 2, Figure 6). These variants are in moderate to high LD ($r^2 > 0.4$) with each other, but are not in LD with other previously reported POE associations ($r^2 < 0.001$). These novel POEs revealed clear bi-polar dominant effects, where parental alleles influence traits in opposite directions.

We found the maternal A allele of rs62471721, which is an eQTL for the imprinted genes *KLF14*, *MEST*, *COPG2* and *CPA4* in adipose tissue[18], to be associated with increased, and the paternal A allele with decreased TG levels ($\widehat{\beta}_P = -0.023$, $\widehat{\beta}_M = 0.033$, $P_P = 9.7 \times 10^{-4}$, $P_M = 1.5 \times 10^{-6}$, Figure 6D).

We also identified a bi-polar dominant POE of rs4731690 on HDL-cholesterol levels, a variant also influencing *MEST*, *COPG2* and *CPA4* expression levels in adipose tissue[18]. Specifically, we found the paternal G allele to be associated with increased, but the maternal G allele associated with decreased HDL-C levels ($\widehat{\beta}_P = 0.019$, $\widehat{\beta}_M = -0.022$, $P_P = 1.9 \times 10^{-3}$, $P_M = 2.7 \times 10^{-4}$, Figure 6E).

Lastly, we found a bi-polar dominant POE of rs10239342, also eQTL for imprinted genes *KLF14*, *MEST* and *COPG2*[18], on SHBG levels, with the paternal G allele associated with increased, but the maternal G allele associated with decreased SHBG level ($\widehat{\beta}_P = 0.022$, $\widehat{\beta}_M = -0.024$, $P_P = 1.3 \times 10^{-3}$, $P_M = 4.1 \times 10^{-4}$, Figure 6F). We evaluated the independence of these effects using co-localization analysis, which found that all three traits (HDL-C, TG and SHBG) likely share the same causal POE variant (posterior probability $H_4 > 0.99$ for HDL-TG and SHBG-TG, $H_4 = 0.75$ for HDL-SHBG).

A novel maternal effect on hip circumference at 7q32.2

We discovered a novel POE of rs6467315 on hip circumference, a variant eQTL for the maternally expressed gene *KLF14* in multiple tissues, located within the 7q32.2 imprinted region (Table 2). We found the maternal G allele of rs6467315 associated with increased hip circumference and we observed no effect of the paternal G allele ($\widehat{\beta}_M = -0.042$, $\widehat{\beta}_P = 0.001$, $P_M = 5.8 \times 10^{-11}$, $P_P = 0.9$, $P_D = 2.2 \times 10^{-6}$). The variant is in high LD ($\mathbf{R^2} = 0.96$) with a variant reported to exhibit maternal effects on TG, HDL-C, and T2D by previous studies (see replication section, Supplementary Table 2)[4,5]. Consistently, we found moderate associations when testing rs6467315 for POEs on these traits ($P_D = 6.9 \times 10^{-3}$, 8.9×10^{-4} and 4.6×10^{-4} for T2D, TG and HDL-C, respectively), with maternal effects aligning to those previously reported. For example, we found the maternal G allele of rs6467315 to be associated with increased T2D prevalence, while the paternal G allele had no effect ($\widehat{\beta}_M = 0.088$, $\widehat{\beta}_P = -0.010$, $P_M = 6.6 \times 10^{-4}$, $P_P = 0.69$).

A novel locus with bi-polar dominant effects on body fat composition at 20q13.32

We identified a novel POE of rs80116540 on body fat percentage within the 20q13.32 imprinted region. The paternal G allele was associated with increased in body fat percentage, while the maternal G allele showed the opposite effect ($\widehat{\beta}_P = 0.037$, $\widehat{\beta}_M = -0.037$, $P_P = 2.6 \times 10^{-4}$, $P_M = 2.2 \times 10^{-4}$, $P_D = 2.0 \times 10^{-7}$). To assess which parts of body fat this effect is driven by, we examined its POE on arm-, leg-, and trunk fat percentages. Significant POEs were observed for all these traits ($\widehat{\beta}_P = 0.025, 0.035$, and 0.042; $\widehat{\beta}_M = -0.024, -0.042$, and -0.039; $P_P = 2.8 \times 10^{-3}, 4.3 \times 10^{-4}$, and 3.6×10^{-4}; $P_M = 3.5 \times 10^{-3}, 2.0 \times 10^{-5}$, and 1.0×10^{-3}; $P_D = 2.9 \times 10^{-5}, 3.4 \times 10^{-8}$, and 1.3×10^{-6} for leg, arm, and trunk fat percentages, respectively). Notably, these traits met the significance threshold specific to imprinted regions at this locus, though some exhibited different lead variants (Table 2). These lead variants were identified as either sQTLs for *STX16* or *CTSZ* in adipose tissue[18] or eQTLs for the *GNAS* imprinted gene in blood[19], underscoring their potential functional relevance in the observed POEs.

Novel and distinct maternal and paternal effects on IGF-1 at 6q24.2 and 16p13.3

We identified a novel POE of rs12528876 on IGF-1 levels at the 6q24.2 locus, located in an intron of the *PLAGL1* gene ($P_D = 2.9 \times 10^{-6}$, Table 2). Specifically, we found the paternal C allele of rs12528876 to be associated with decreased IGF-1 levels and the maternal allele having no effect ($\widehat{\beta}_P = -0.036$, $\widehat{\beta}_M = 0.021$, $P_P = 2.5 \times 10^{-5}$, $P_M = 0.016$).
We identified a second independent and novel POE of rs7188903 on IGF-1 at 16p13.3 ($P_D = 6.1 \times 10^{-7}$, Table 2), which is an eQTL in blood for two maternally expressed genes, *ZNF597* and *NAA60*. We found the maternal G allele of rs7188903 to be associated with increased IGF-1 levels and the paternal allele having no effect ($\widehat{\beta}_M = 0.041$, $\widehat{\beta}_P = -0.012$, $P_M = 5.3 \times 10^{-8}$, $P_P = 0.1$).

Novel bi-polar dominant effect on total protein levels at 15q12

Lastly, we identified a novel POE of rs146982369 on total blood protein levels within the 15q12 imprinted region, located in the intro of *ATP10A* ($P_D = 2.5 \times 10^{-6}$, Table 2). We found the paternal G allele of rs146982369 associated with an increase in blood protein levels, while the maternal G allele has the opposite effect ($\widehat{\beta}_P = 0.101$, $\widehat{\beta}_M = -0.106$, $P_P = 1.8 \times 10^{-3}$, $P_M = 9.9 \times 10^{-4}$).

Parent-of-origin effects on childhood traits

We examined the timing of POEs on complex traits to assess whether these effects manifest in early childhood or are specific to adult traits. For this purpose, we tested three loci associated with standing height for significant POEs on "comparative body height at age 10" and three loci linked to obesity-related traits (fat percentage, basal metabolic rate, and T2D) for POEs on "birth weight" and "comparative body size at age 10." We identified two significant (0.05/9) POEs for "comparative body height at age 10" (Supplementary Table 6). Specifically, the paternal G allele of rs77708343 was associated with a decrease in body height at age 10, while the maternal G allele showed an increase ($\widehat{\beta}_P = -0.11$, $\widehat{\beta}_M = 0.07$,

$P_P = 2.3 \times 10^{-3}$, $P_M = 6.2 \times 10^{-2}$, $P_D = 4.0 \times 10^{-4}$). Additionally, the maternal T allele of rs143840904 was associated with a decrease in body height at age 10, whereas the paternal T allele had no significant effect ($\widehat{\beta}_P = -0.07$, $\widehat{\beta}_M = -0.32$, $P_P = 0.21$, $P_M = 2.0 \times 10^{-8}$, $P_D = 2.7 \times 10^{-3}$). Notably, these observed effects on body height at age 10 aligned with those seen on adult standing height, suggesting that POEs at these loci may influence early growth trajectories.

Evidence of sex-specific bi-polar POE on glucose levels

Recognizing that complex traits often exhibit sex-specific variation[20,21], we investigated whether POEs also display sex-specific patterns. To explore this, we conducted POE analyses separately for males and females across the 32 loci identified in this study.

We identified one significant sex-specific difference, for the POE of rs4417225 on glucose levels (Supplementary Table 7, Supplementary Figure 16). The POE was significant in male individuals ($P_{D_{males}} = 4.7 \times 10^{-9}$), but not in female individuals ($P_{D_{females}} = 0.19$). Specifically, the T allele of rs4417225 was associated with increased glucose levels in men when paternally inherited, and with decreased levels when maternally inherited ($\widehat{\beta}_P = 0.045$, $\widehat{\beta}_M = -0.040$, $P_P = 1.0^{-4}$, $P_M = 1.3 \times 10^{-5}$), while we observed no effect of neither paternal nor maternal T alleles in women ($P_P = 0.3$, $P_M = 0.38$). Additionally, we formally tested for significant sex differences in POE by comparing male and female GWAS effect sizes using a Z-score approach, applying a significance threshold of $P_Z < 0.05/32 = 1.56 \times 10^{-3}$ (see Methods). This analysis confirmed a significant sex-specific POE for glucose levels ($P_{Z_D} = 1.3 \times 10^{-3}$, Supplementary Table 7). Interestingly, although this locus is also associated with HbA1c and type 2 diabetes risk in a POE fashion, no sex-specific effects were detected for these traits (Supplementary Table 7).

Parent-of-Origin SNP heritability for complex traits

We used Linkage Disequilibrium Score Regression (LDSC) to estimate SNP heritability ($\mathbf{h^2}$), which represents the proportion of phenotypic variability explained by Single Nucleotide Polymorphisms (SNPs). Instead of the traditional SNP-based $\mathbf{h^2}$ computation that considers additive effects, we estimated h^2 separately for the maternal effects, the paternal effects, and for the parental differential effects at heterozygous sites (as derived from our maternal, paternal and differential GWAS scans, respectively; see Methods).

Our genome-wide estimates reveal that for most traits, the paternal and maternal haplotypes contribute similarly to SNP-based heritability (Figure 7A). Next, we focused our analysis within imprinted regions. While the paternal and maternal contributions remained balanced for most traits, we observed several interesting trait-specific patterns (Figure 7B): for arm fat percentage and type 2 diabetes, we found a trend for a larger maternal *vs* paternal SNP heritability, while we found larger point estimates for paternal SNP heritability for the remaining ones.

Finally, we estimated POE SNP heritability (h^2_{POE}) within and outside imprinted regions. Our findings revealed that six traits exhibited significantly higher h^2_{POE} within imprinted regions compared to non-imprinted regions (Figure 7C), namely for IGF-1, triglycerides, eosinophil count, lymphocyte count, birth weight and basophil count. Reassuringly, no

traits showed significantly greater h^2_{POE} outside known imprinted regions, hinting that a disproportionately large POE heritability is due to genomic imprinting.

Parent-of-Origin Protein Quantitative Trait Loci

In addition to our investigation of POEs on complex traits, we explored the UK Biobank plasma proteomics data to identify parent-of-origin protein quantitative trait loci (POE-pQTLs). Since protein levels widely correlate with transcript abundance, we hypothesized that imprinting mechanisms acting on gene expression levels may detectably propagate to protein levels. Our analysis focused on two main objectives: first, determining whether variants exhibiting POEs on complex traits identified in this study also exhibit POE-pQTL effects on their associated genes, and second, assessing whether previously established pQTLs[22] exhibit associations in a PofO fashion.

Parent-of-Origin pQTLs at known POEs

Across the genes associated with variants exhibiting POEs on complex traits identified in this study (Tables 1 and 2), two genes, *CPA4* and *GNAS*, had available protein quantification data. To investigate potential POEs at the protein level, we tested five variant-protein pairs: rs62471721 and rs4731690 with *CPA4*, and rs80116540, rs6026426, and rs3730173 with *GNAS*. Among these, we identified one significant (0.05/5) POE-pQTL for *CPA4*. Specifically, the G allele of rs4731690, previously identified as exerting a bi-polar effect on HDL-C, was found to increase *CPA4* protein levels only when paternally inherited ($\widehat{\beta}_M = -0.01$, $\widehat{\beta}_P = 0.08$, $P_M = 0.58$, $P_P = 6.3 \times 10^{-4}$, $P_D = 5.7 \times 10^{-3}$). In contrast, no significant POE-pQTLs were observed for *GNAS*.
Co-localization analysis revealed that the observed POE signals for HDL-C and *CPA4* are distinct (posterior probability $H_4 = 0.04$).

Novel Parent-of-Origin pQTLs among additive pQTLs

Beyond exploring POE-pQTLs at variants regulating complex traits in a parent-of-origin fashion, we also evaluated a set of established additive pQTLs[22] for potential POEs. From the 14,287 lead pQTL associations spanning 2,414 proteins reported in a previous study[22], we could directly test 10,611 associations in our dataset, where the same SNP and protein data were available, and we used proxy variants selected based on LD ($r^2 > 0.8$) for the remaining ones. We identified four significant ($P_D < 0.05/14285 = 3.5 \times 10^{-6}$) POE associations, with namely *DLK1*, *CPA4*, *ADAM23* and *PER3* protein levels (Table 3, Supplementary Figure 17).
Two of these associations involved known imprinted genes: *DLK1* and *CPA4*. Specifically, we found the paternal C allele of rs12881545 associated with higher *DLK1* protein levels compared to the maternal C allele, consistent with the paternal expression of the *DLK1* gene ($\widehat{\beta}_P = 0.82$, $\widehat{\beta}_M = 0.18$, $P_P = 2.2 \times 10^{-274}$, $P_M = 1.2 \times 10^{-15}$, $P_D = 3.0 \times 10^{-84}$, Table 3, Supplementary Figure 17A). For *DLK1*, the lead pQTL reported in the previous study was also our lead POE-pQTL. In addition, we found the maternal T allele of rs34587586 associated with lower *CPA4* protein levels compared to the paternal T allele, consistent with the maternal expression of the *CPA4* gene ($\widehat{\beta}_M = -0.63$, $\widehat{\beta}_P = -0.43$, $P_M = 4.4 \times 10^{-149}$,

$P_P = 2.7 \times 10^{-71}$, $P_D = 5.6 \times 10^{-9}$). For *CPA4*, the lead pQTL reported in the previous study was not our lead POE-pQTL: we found a stronger POE association with *CPA4* protein levels for another variant, rs12538292, in high LD with rs34587586 ($r^2 = 0.77$). Specifically, we found the maternal A allele of rs12538292 associated with lower *CPA4* protein levels compared to the paternal one ($\widehat{\beta}_M = -0.66$, $\widehat{\beta}_P = -0.43$, $P_M = 2.3 \times 10^{-151}$, $P_P = 4.8 \times 10^{-65}$, $P_D = 3.5 \times 10^{-11}$, Table 3, Supplementary Figure 17B).

We found two POE associations where genes were located outside known imprinted regions: for *ADAM23* and *PER3* protein levels. Firstly, we found the paternal A allele of rs72933203 associated with higher *ADAM23* protein levels compared to the maternal one ($\widehat{\beta}_P = 1.01$, $\widehat{\beta}_M = 0.72$, $P_P = 1.4 \times 10^{-190}$, $P_M = 9.0 \times 10^{-102}$, $P_D = 1.2 \times 10^{-9}$). For *ADAM23*, the lead pQTL reported in the previous study was not our lead POE-pQTL: we found a stronger POE association with *ADAM23* for another variant, rs13429599, located over 100 kb away from rs72933203 and in low LD with it ($r^2 = 0.046$). For this variant, we found the paternal A allele associated with higher *ADAM23* protein levels compared to the maternal one ($\widehat{\beta}_P = 0.71$, $\widehat{\beta}_M = 0.45$, $P_P = 5.9 \times 10^{-204}$, $P_M = 9.3 \times 10^{-84}$, $P_D = 4.3 \times 10^{-15}$, Table 3, Supplementary Figure 17C). In addition, we found the paternal A allele of rs228647 associated with higher *PER3* protein levels compared to the maternal A allele ($\widehat{\beta}_P = 0.50$, $\widehat{\beta}_M = 0.24$, $P_P = 6.8 \times 10^{-110}$, $P_M = 4.1 \times 10^{-26}$, $P_D = 1.9 \times 10^{-16}$). Again for *ADAM23*, the lead pQTL reported in the previous study was not our lead POE-pQTL: we found a stronger POE association with *PER3* for another variant, rs228682, in moderate LD with rs228647 ($r^2 = 0.3$). Here again, we found the paternal C allele of rs228682 associated with higher protein levels compared to the maternal C allele ($\widehat{\beta}_P = 0.54$, $\widehat{\beta}_M = 0.24$, $P_P = 4.3 \times 10^{-121}$, $P_M = 1.0 \times 10^{-25}$, $P_D = 5.4 \times 10^{-20}$, Table 3, Supplementary Figure 17D).

Replication analyses in the Estonian Biobank

To replicate the POEs identified in our study, we leveraged the high level of cryptic relatedness within the Estonian Biobank (EstBB) cohort[23]. Our analysis followed a similar approach to that applied to the UK Biobank cohort.

Among the 211,259 EstBB participants, we identified 14,063 parent-offspring trios, 37,686 parent-offspring duos, over 55,000 individuals with at least one sibling and more than 150,000 individuals with more distant relatives. Notably, 95% of individuals had at least one close relative (up to the fourth degree), which were then clustered in surrogate parent groups, allowing us to leverage inter-chromosomal statistical phasing via shared IBD haplotype segments for almost the entire cohort. This extensive relatedness in EstBB enabled an inter-chromosomal phasing error rate of only 0.56%, compared to 1% in the UK Biobank (Supplementary Figure 18).

For individuals without directly available parental genomes, we inferred the PofO of parental haplotype sets by analyzing chromosome X inheritance in male individuals (Supplementary Figure 19) and by using crossover inference combined with sex-specific recombination maps in sibling pairs (Supplementary Figures 20 and 21). Using this approach, we successfully inferred PofO of haplotypes in a total of 113,921 EstBB individuals, of which more than 85% (N=97,346) had a probability greater than 0.99, and achieving an average error rate at heterozygous sites of just 0.89%, compared to 2.06% in the UK Biobank (Supplementary

Figure 22).

Due to the limited overlap of phenotypes in the EstBB cohort, we were able to test 8 of the 32 POEs identified in our study using the exact same variants. For 6 additional associations, we utilized proxy variants selected based on the highest LD available in the dataset. Out of these 14 associations, we successfully replicated 10 ($P_D < 0.05/14 = 3.35 \times 10^{-3}$), with three additional associations at nominal significance (Supplementary Table 8).

Discussion

We introduce a novel multi-step approach to infer the parent-of-origin (PofO) of haplotypes, providing substantial improvements over existing methods. This innovation enables the production of the largest cohort to date with PofO information, paving the way for discoveries of parent-of-origin effects (POEs) at an unprecedented scale across complex traits, diseases, and protein levels. In the scope of this study, we applied this approach on the UK Biobank and on the Estonian Biobank, scaling up to 221,062 individuals and uncovering more than 30 novel POEs.

Advantages and limitations of the methodology

Our novel approach addresses significant limitations of traditional methods that rely on parental genomes, known genealogies, or chromosome X sharing in male individuals, thereby limiting scalability and applicability. By contrast, our method enables PofO inference without these constraints, greatly enhancing sample sizes and improving the detection of POEs. Instead of relying exclusively on chromosome X sharing in males, we also leverage mtDNA data from whole-genome sequencing (WGS). This allows us to infer PofO in female individuals, increasing the overall sample size and allowing us to examine sex differences in POEs. However, this approach is limited to cohorts with available WGS data. To overcome this limitation, we introduced a sibling-based crossover inference method, which provides a promising alternative for datasets derived from SNP arrays alone. This strategy allows extending PofO inference to a broader range of close relatives.

Despite its advantages, our method has several limitations. The accuracy of PofO inference depends on the availability of haplotype segments shared IBD across chromosomes, which in turn is influenced by cohort structure and data availability. Sample sizes vary across chromosomes, with fewer individuals available for smaller chromosomes where detecting IBD segments is more challenging. This variability restricts the analysis power, particularly in cohorts with limited data on related individuals. This limitation is evident when comparing inferences between the UK Biobank and the Estonian Biobank. While the UK Biobank includes an average of 1.6 relatives per individual, the Estonian Biobank includes approximately 12 relatives per individual. This difference results in larger sample sizes per chromosome and reduces error rates by half in the Estonian Biobank.

Our method is also highly dependent on the degree of relatedness among individuals. Higher accuracy and call rate is achieved with closer relatives, as seen with mtDNA minor variant sharing (MVS), where second-degree relatives can be use to predict both paternal and maternal side, versus accurately predicting only maternal side when using more distant relatives. Consequently, biobanks enriched with closer familial relationships, such as the Estonian Biobank, provide a larger proportion of the cohort with accurate PofO inference. Indeed, approximately half of the Estonian Biobank cohort had PofO probabilities exceeding 0.99, compared to only about a quarter of the UK Biobank cohort.

Another potential limitation that was previously discussed[14] relates to consanguinity within populations. Higher levels of consanguinity could lead to individuals sharing chromosome X or mtDNA from both sides of the family, potentially introducing errors in PofO assignment. However, our observations in the Estonian Biobank do not support this hypothesis. Despite

significantly higher average Runs-of-Homozygosity in the Estonian Biobank compared to the UK Biobank, we observed lower error rates and better PofO inference coverage in the Estonian cohort. This is likely due to the larger number of close relatives per individual and our rigorous clustering approach for relatives. We excluded individuals for whom relatives could not be clustered into two distinct groups or for whom group clustering was ambiguous. Together, these measures ensure the robustness of our multi-step approach, even in populations with high consanguinity.

A further weakness of our approach is that we cannot distinguish between parental rearing and true imprinting effects. The effect of a maternal transmitted allele may emerge through changing maternal behavior impacting how a child is raised (starting from intra-uterine effects to child education), or it may exert its effect directly in the offspring via suppressed gene expression. This weakness can be addressed in the future by inferring untransmitted parental effects and comparing them to that of the transmitted one.

Parent-of-origin on complex traits revealed a novel asymmetric pattern

The detection power of the POE analysis is comparable to that of additive GWAS: The expected test statistic for additive GWAS is $\approx (\beta_M + \beta_P)/2 \cdot \sqrt{N} \cdot \sqrt{2q(1-q)}$. On the other hand, only heterozygous samples are informative to detect POEs, hence its test statistic is $\approx (\beta_M - \beta_P) \cdot \sqrt{N} \cdot \sqrt{q(1-q)/2}$, where β_M and β_P are the per allele maternal and paternal effect size, respectively. In classical POEs scenario, when a SNP has an effect only when it comes from one of the parents (e.g. $\beta_P = 0$), the test statistics become equal. Note that in these situations, an additive effect should also be detectable. The fact that we detect much less POEs is therefore likely driven by the lack of classical patterns (i.e, strict paternal or maternal effect). Thus, besides the genome-wide scan, we explored two additional strategies to boost power: focus on (i) SNPs that show an additive association (since apart from the scenario of $\beta_M = -\beta_P$, the additive effect will not be zero); (ii) imprinted regions (where POEs are more likely). These filters reduce multiple testing burden and hence lead to milder P-value thresholds and can improve statistical power.

These analyses uncovered a wide range of POEs, offering insights into previously uncharacterized genetic mechanisms. Our additive regions-focused scan revealed two novel POEs on telomere length, the first associated with the *TERC* gene, and the second with the *NAF1* gene, both well-known regulators of telomere biology[24,25,26]. Although these associations do not fall within imprinted regions, they align with earlier hypotheses suggesting that telomere length regulation may involve imprinting mechanisms[27,28,29]. The identification of these loci broadens our understanding of telomere length regulation, suggesting that genomic imprinting mechanisms may operate beyond established imprinted regions, warranting further investigation. Notably, these POEs exhibit a pattern distinct from the current classification of POEs, termed here "asymmetric polar" parental effects: both parental alleles affect the trait in the same direction, but with significantly different magnitudes of effect (Supplementary Figure 15). This novel POE pattern may relate to the concept of incomplete imprinting, where both parental alleles are expressed but at different levels.

We also explored POEs within additive regions with a less stringent approach, analyzing each trait independently to reduce the multiple testing burden. Although these findings have

higher false discovery rate, they suggest novel associations worth further investigation. For example, two POEs were identified on IGF-1 levels, each supported by biological evidence. The first lead variant is located within *MLXIPL*, a gene involved in glucose metabolism and type 2 diabetes. The second is located within the *IGF2* gene, which supports a role for the locus in insulin regulation pathways.

Regulatory mechanism behind bi-polar dominant effects

Our imprinted region-focused scan underscored the complexity and prevalence of bi-polar POEs, where maternal and paternal alleles influence a trait in opposite directions. These effects were observed across a wide range of traits, including SHBG, triglycerides, HDL-C, HbA1c, glucose, standing height, cystatin C, creatinine, basal metabolic rate, leg and trunk fat-free mass, whole-body water mass, total protein, and various measures of fat percentage. Notably, while bi-polar effects have been reported previously, their mechanisms have often remained unclear. Our findings offer new insights that help clarify the genetic basis of these intriguing effects.

At the 7q32.2 imprinted region, we uncovered novel bi-polar POEs on triglycerides, HDL-C, and SHBG. These associations are particularly notable in the context of bi-polar dominance, as the lead variants act as eQTLs for both maternally expressed genes (*KLF14* and *CPA4*) and the paternally expressed *MEST*. The pleiotropic nature of these variants provides a compelling explanation for the observed bi-polar effects, with opposing parental influences arising from their simultaneous impact on genes exhibiting opposite imprinting patterns. This interplay between maternally and paternally expressed genes exemplifies the intricate regulatory mechanisms underlying bi-polar POEs.

Additionally, we uncovered examples of bi-polar POEs that are not directly explained by both paternal and maternal imprinted genes, suggesting the involvement of more complex regulatory networks.This includes for example a bi-polar effect on standing height at 11p15.5, with a lead variant splicing QTL for the maternally expressed *H19* gene and eQTL for *TNNT3*, a gene required for normal growth in mice[30].

Multi-trait integration reveals broader parental contributions

One of the key advantages of our method is its scalability and applicability to biobank-scale datasets, providing access to a vast array of phenotypes. Such phenotype-rich biobanks allow in-depth POE pheWAS follow-up, which can pinpoint pleiotropic mechanisms underlying multi-trait associations and opens new avenues to follow-up, such as colocalization and Mendelian Randomization to distinguish vertical and horizontal pleiotropy.

For example, we identified POEs associated with standing height and basal metabolic rate at 11p15.5. To better understand the genetic signal at this locus, we explored its associations with several related traits, including weight, waist and hip circumference, and detailed body composition measures such as fat, fat-free, and water mass. Interestingly, while the lead variant showed no significant association with fat percentage across different body regions (arm, leg, trunk, or whole body), it was strongly associated with fat-free traits, such as fat-free mass and water mass. This pattern suggests that the genetic signal at 11p15.5 is more likely driven by height and fat-free body mass, which are closely related to lean tissue

and skeletal structure, rather than by weight alone.

Another illustrative example comes from the 11p15.5 locus, where we identified POEs on cystatin C, creatinine, and urate levels. Both cystatin C and creatinine are well-established markers of kidney function, and colocalization analyses provided strong evidence for a shared genetic basis for these traits at this locus, likely related to renal filtration capacity. In contrast, urate, a byproduct of purine metabolism that is also filtered by the kidneys, exhibited lower colocalization probabilities with cystatin C and creatinine. This finding suggests that urate regulation, while partly overlapping with GFR-related traits, likely involves additional distinct pathways. Together, these three POEs link this locus to renal functions.

Lastly, we observed POEs on triglycerides (TG), HDL-C, and SHBG at the 7q32.2 region. These traits are established indicators of metabolic health and are closely tied to insulin resistance and metabolic syndrome. Insulin resistance typically raises TG levels while lowering HDL-C and SHBG levels, a pattern that aligns with the observed POEs. Despite the known associations of these traits with T2D risk, no significant associations were detected between the identified variants and T2D, pointing to independent regulatory mechanisms, likely specific to lipid and hormonal pathways.

Evolutionary insights supporting the parental conflict hypothesis

Analyzing POEs at a biobank scale enables us to move beyond investigating contrasting parental effects on the same trait at a single locus, such as bi-polar effects. While we can explore contrasting effects on the same trait across different loci, a more comprehensive approach leverages the vast range of available phenotypes to examine contrasting parental effects across both traits and loci. This broader perspective allows us to identify overarching patterns and gain deeper insights into the evolutionary dynamics of imprinted genes.

For example, IGF-1 levels exhibited contrasting POEs at two distinct loci. At 6q24.2, we identified a paternal effect decreasing IGF-1 level driven by a variant within the paternally expressed gene *PLAGL1*, which is implicated in transient neonatal diabetes mellitus[31,32]. The role of *PLAGL1* in glucose metabolism and insulin sensitivity[33] underscores the importance of this locus in regulating IGF-1 levels and metabolic pathways. At 16p13.3, we observed a maternal effect increasing IGF-1 levels driven by a variant that acts as eQTL for two maternally expressed genes, *ZNF597* and *NAA60*, as well as for *TRAP1*, a gene linked to mitochondrial function and metformin use[34]. Together, these findings illustrate how contrasting maternal and paternal effects at different loci collectively shape the genetic architecture of IGF-1 levels, offering valuable insights into the broader evolutionary dynamics underlying imprinted loci.

Notably, such findings align with the parental conflict theory, which posits that paternal alleles are selected to enhance resource extraction from the mother, promoting offspring growth and increasing the father's genetic success. In this framework, paternally expressed imprinted genes often drive growth and resource acquisition. In contrast, maternally inherited alleles are selected to conserve maternal resources for future reproduction and offspring survival, with maternally expressed genes acting as growth suppressors to counterbalance paternal effects. At the genetic association level, this dynamic is reflected by differential paternal and maternal effects on traits related to resource allocation, often across different

loci and in opposing directions, exemplifying bi-polar patterns. This pattern is evident at other loci too, for traits related to resource allocation: at 7q32.2 for SHBG, triglycerides and HDL-cholesterol; at 11p15.5 for T2D, HbA1c, glucose and height, but also for basal metabolic rate, whole body water mass, leg and trunk fat-free masses, and creatinine and cystatine C ; at 15q12 for total protein levels, and finally at 20q13.32 for fat percentage in the arms, legs, trunk, and whole body. These findings underscore the role of imprinted genes in balancing maternal and paternal interests across traits linked to resource allocation, fat storage, and energy usage. Their strong presence among our findings (across multiple loci and traits) may support the conflict hypothesis and likely represent footprints of the evolutionary forces shaping the genetic architecture of complex traits.

Differential parental contributions to SNP heritability

To examine genome-wide parental contributions to complex traits, as well as those within imprinted regions, we estimated SNP heritability separately for paternal, maternal, and POEs. This analysis revealed notable differences in the contribution of maternal and paternal haplotypes to certain traits, particularly those related to resource allocation, in line with the parental conflict hypothesis. For example, type 2 diabetes and arm fat percentage exhibited higher SNP heritability from maternal alleles. Conversely, traits such as birth weight, glucose levels, and basophil count showed stronger heritability from paternal haplotypes. These differences likely reflect distinct parental contributions to biological processes associated with growth, metabolic regulation, and immune function. Interestingly, some traits, such as IGF-1 and triglycerides, exhibited no significant differences between maternal and paternal heritability estimates but showed substantial PofO-specific heritability (h^2_{POE}). This suggests that maternal and paternal-specific genetic contributions to these traits are distributed differently across the genome.

Protein QTLs, a new frontier for POEs

We further leveraged protein quantification data both to validate POEs at the protein level and to assess POEs at established protein QTLs (pQTLs). Although the available protein panel did not cover many of the genes located at our complex trait POE-variant, we identified a significant POE-pQTL for *CPA4* when testing variants initially linked to triglycerides, HDL-C, and SHBG. While this could initially suggest a causal relationship between *CPA4*, the lead variants, and these traits, further analysis revealed a much more significant POE-pQTL located approximately 75 kb away from the POE-variant and in moderate linkage disequilibrium ($r^2 > 0.05$). This finding indicates that the detected POEs on triglycerides, HDL-C, and SHBG are unlikely to be driven by *CPA4*, with the moderate significance observed at the POE variant likely arising from linkage disequilibrium with the true causal variant. Instead, other genes at this locus, such as *KLF14* and *MEST*, are more plausible candidates due to their established eQTL associations with the lead variants. In addition, the POE-variant exhibited a paternal effect on *CPA4* protein level, despite the gene being maternally expressed. This likely reflect influence of paternally expressed genes via shared protein network, such as *MEST*[35]. While this finding does not conclusively identify the gene responsible for the observed POEs, it allows us to refine our candidate list, excluding *CPA4*

and prioritizing other loci for further study.

Beyond testing complex trait POE-variant for POE-pQTLs, we also evaluated PofO specificity at established pQTLs[22] and identified four significant POE-pQTLs. Two of these were located within known imprinted regions and showed parental effects consistent with the parental expression of the respective genes. For instance, the protein product of the paternally expressed gene *DLK1* was predominantly associated with paternally inherited alleles, though a moderate maternal association was also observed. This biparental influence likely reflects the interconnected nature of imprinted gene networks, where maternally expressed genes can indirectly modulate the expression or activity of paternally expressed genes. For example, the imprinting regulation of *DLK1* is also dependent on two differentially methylated regions (DMRs), including the *MEG3* DMR[36], a maternally expressed gene. This highlights the complex epigenetic mechanisms that drive *DLK1* expression and its imprinting pattern. In contrast, the protein product of *CPA4* exhibited a strong maternal association, consistent with its preferential maternal expression[37]. Interestingly, a significant - but moderate - paternal association was also observed for *CPA4*, potentially reflecting network-level interactions with paternally expressed genes such as *MEST*, which may modulate *CPA4* protein levels through shared pathways[35].

The remaining two POE-pQTLs were identified for genes outside known imprinted regions: *ADAM23* and *PER3*, both of which exhibited paternal effects, albeit demonstrating "asymmetric polar" effect. Although *ADAM23* is not currently classified as imprinted, it is located near two paternally expressed genes, *ZDBF2* and *GPR1*, and a recent study reported a paternal bias in its expression[38], suggesting incomplete imprinting. Similarly, *PER3* has been documented to show paternal-biased expression[39], consistent with the paternal effect observed in our study. These findings strengthen the case for these genes as candidates for incomplete or context-dependent imprinting and point to broader PofO specific mechanisms that extend beyond imprinting and involve rearing effects.

Interestingly, no significant POE-pQTLs were detected for several other known imprinted genes. This absence may indicate that protein levels do not always reflect RNA expression due to complex feedback mechanisms that could mask detectable PofO associations at the protein level. These results underscore the importance of complementary transcriptomic analyses to capture the full spectrum of POEs. Recent studies focusing on parental-specific eQTLs in parent-offspring trios have successfully validated known imprinted genes and identified novel candidates, emphasizing the value of integrating multi-omic approaches[40].

Replication analysis supports novel bi-polar dominant effects

Lastly, we validated several of our findings in the Estonian Biobank (EstBB), a cohort with an enrichment of familial relatedness, though limited in phenotype overlap with our detected POEs. Among the ten associations replicated in the EstBB, six were novel associations, while four corresponded to previously reported loci or variants in high linkage disequilibrium with known associations. Specifically, we confirmed our newly identified bipolar effect of rs7105710 on standing height, rs62471721 on triglycerides, rs4731690 on HDL cholesterol, and rs4264135 on creatinine. Additionally, we validated the effects of rs4417225 on glucose levels and rs10838787 on HbA1c. While the latter locus had been previously associated with T2D, its link to glucose-related traits provides further, albeit less novel,

insights. Notably, among the replicated associations were bi-polar effects driven by variants acting as eQTLs for distinct genes with contrasting parental expression (for HDL cholesterol and triglycerides). This finding further supports the hypothesis that pleiotropic effects may offer a mechanistic explanation for bi-polar dominant phenomena. Not all POEs identified in the UKBB were replicated in the EstBB, which could reflect differences in statistical power, cohort characteristics, or environmental factors. For instance, while two of the POEs on standing height at 11p15.5 were successfully replicated, the third association of the same locus was not. This discrepancy could arise from cohort-specific imprinting or parental nurturing effects.

Summary and future directions

Overall, this study and its replication efforts provide critical insights into the genetic and evolutionary mechanisms underlying POEs, with several key points. First, we established the largest cohort to date with available PofO information, enabling us to perform the largest and most comprehensive study of POEs across diverse traits, diseases, and protein levels. By employing a focused analytical approach to reduce the multiple testing burden, we successfully identified POEs that might not have reached genome-wide significance in a genome-wide scan.

Second, our study sheds light on the prevalence of bi-polar POEs, which we found to be far more common than previously recognized across imprinted loci. We provided a plausible explanation for these effects, particularly in cases where lead variants act as eQTLs for both maternally and paternally expressed genes, such as *KLF14* and *MEST* at the 7q32.2 locus.

Third, we characterized a novel type of POE, termed "asymmetric polar" parental effects, where both parental alleles affect a trait in the same direction, but one exerts a significantly stronger influence. This adds an important dimension to the understanding of imprinting mechanisms with potential link to incomplete imprinting mechanism, such as illustrated with *ADAM23* and *PER3*.

Fourth, although not replicated in the Estonian Biobank, we report the first observed sex-specific POE, found on glucose levels. While this finding highlights the potential complexity of sex-dependent imprinting, we acknowledge that it could be influenced by cohort-specific biases, such as differences in sample collection or sex-specific participation patterns[41].

Fifth, many of our results, both at the single-locus level (e.g., POE-GWAS hits) and the multi-trait or multi-locus level (e.g., cross-trait POE-GWAS analyses and heritability studies), align with the parental conflict hypothesis. This evolutionary framework suggests that paternally and maternally inherited alleles often exert opposing influences on traits related to resource allocation and offspring development.

Lastly, our validation efforts in the Estonian Biobank demonstrated that while some POEs are robustly replicated, others require larger sample sizes to achieve significance (e.g, sex-specific POE on glucose). This underscores the need for continued efforts to expand sample sizes through meta-analyses across multiple biobanks enriched for familial data, such as the MoBa cohort, Finngen, and the HUNT cohort. These efforts will be crucial for fully uncovering the genetic architecture of POEs and their implications for complex traits.

Methods

UK Biobank genotype processing

We used the UK Biobank Axiom Array data provided in PLINK format[42] and converted it to VCF format using PLINK v1.90b5[43]. We then used the UK biobank SNPs QC file (UK Biobank resource 1955) to keep only variants used for the official phasing of the original UK Biobank data release[42], resulting in 670,741 variant sites across the 22 autosomes and 16,601 variant sites on chromosome X. We then used the SHAPEIT5 phase_common tool[14] with default parameters and no filter on allele frequency to perform an initial phasing of autosomes. For chromosome X, we proceed as described in the official phasing report of the UK Biobank whole genome sequencing data, interim release of 200,031 samples[44]. Briefly, we removed pseudoautosomal regions (PAR), identified males as genetically determined, forced reference allele homozygosity at heterozygotes sites in males, and finally we provided the list of male individuals as input in the *–haploid* option of SHAPEIT5. Female individuals were phased as autosomes.

Close relative clustering

We use pairwise kinship estimates computed using the KING software[45] to identify related individuals up to the 4th degree in the UK Biobank cohort. We identified parent-offspring duos and trios as having kinship between 0.1767 and 0.3535, IBS0 below 0.0012 and age difference greater than 15 years[3,42], resulting in 1,071 trios and 4,136 duos (Supplementary Figures 1A-B). We used Mendel error rate to ensure the accuracy of the identified parent-offspring trios (Supplementary Figure 1C).

We next identified sibling pairs as those with kinship between 0.1767 and 0.3535, IBS0 above 0.0012 and age difference smaller than 15 years[3], resulting in 22,751 pairs for 41,661 unique individuals (Supplementary Figures 1A-B).

For individuals with more distant relatives (up to 4th degree), we utilized a clustering approach to segregate relatives by parental sides using the *igraph* package in R, as done previously[3]. Through this method, we identified 274,525 UK Biobank participants whose relatives could be clustered into parental groups based on their relatedness (Supplementary Figure 1D). In our analysis we refer to those close relatives as "surrogate parents".

We finally identified individuals who have both available parental genomes and inferred surrogate parents, which are utilized for validating our method. This allows us to perform the entire analysis using surrogate parents and excluding parental genomes, effectively simulating the remaining individuals without available parental genomes, and later reintroduce the parental genomes solely for validation and accuracy estimation. In subsequent sections we refer to those as the "validation cohort". A total of 2,141 individuals met these criteria, resulting in 3,160 target-relative pairs (Supplementary Figure 2A). For each target-relative pair, we used KING pairwise kinship estimates between the target's relative and the target's parents to assign the relative to a parental side (Supplementary Figure 2B). This validation cohort was subsequently used to assess the accuracy of our inferences and to derive probabilities for PofO assignments.

Inter-chromosomal phasing from available parental genomes

For individuals with available parental genomes (1,071 trios and 4,136 duos), we performed inter-chromosomal phasing using the *–pedigree* option of SHAPEIT5[14]. This method requires a three-column pedigree file listing offspring, fathers, and mothers. In cases where one parent is unavailable, the missing parent is indicated by *"NA"*. This procedure results in phased genotype data (i.e, haplotypes). The order of the haplotypes correspond to the order of parents in the pedigree file (here, first haplotypes are paternally inherited; second haplotypes are maternally inherited). Consequently, this method allows direct inference of the PofO of haplotypes from statistical phasing when parental genomes are available. The key advantage of using pedigree-based statistical phasing over traditional Mendelian logic is its ability to infer the PofO of alleles even when both parents are heterozygous. This is accomplished by leveraging haplotype information from the broader population, providing more robust and accurate results, such as done in traditional statistical phasing. In this study, the PofO inferred from parental genomes serves as the ground truth. This ground truth is critical for validating the accuracy of PofO inference derived from surrogate parents in the validation cohort (see subsequent sections).

Inter-chromosomal phasing from surrogate parents

Identity-by-descent (IBD) mapping is a powerful approach for identifying haplotype segments co-inherited from a common ancestor among pairs of relatives. By analyzing haplotype segments shared IBD with the same set of surrogate parents across the 22 autosomes for a given target individual, we can determine which haplotype segments are inherited from the same parent. This enables the construction of partial parental haplotype sets, which can then be used to perform inter-chromosomal phasing—segregating haplotypes inherited from each parent across the genome. This approach goes beyond traditional phasing methods, which are limited to resolving haplotypes within individual chromosomes (intra-chromosomal phasing).

For 274,525 individuals with identified surrogate parents, we used the THORIN tool[3] to map haplotype segments shared IBD between the target individuals and their surrogate parents. These IBD-shared segments served as the foundation for both intra- and inter-chromosomal phasing, building on prior methodologies[3]. The key principle here is that haplotypes shared IBD with the same surrogate parents originate from the same parent. Consequently, these haplotypes should consistently appear on the same parental haplotype across autosomes.

In practice, we filtered for shared haplotype segments longer than 3 centimorgans (cM), which we incorporated into a scaffold file. This scaffold was then used as input for the SHAPEIT5 phase_common tool. This step allowed us to refine and re-estimate haplotypes from genotype data, while simultaneously correcting intra-chromosomal phasing switch errors and performing inter-chromosomal phasing by assigning all haplotypes shared with the same surrogate parents to the same parental haplotype (e.g., first or second) across all 22 autosomes.

This approach was applied to 274,525 individuals from the UK Biobank. Accuracy assessments (Supplementary Figure 3) demonstrated the robustness and reliability of our inter-chromosomal phasing method in segregating parental haplotype sets with high precision.

Surrogate parents' parental side determination

Chromosome X

Identity-by-descent (IBD) mapping on chromosome X has been shown as an accurate approach to identify maternal relatives for male target individuals[3]. Here, we build upon this previous approach to probabilistically infer close relatives' parental side. To do so, we utilized the THORIN tool to map IBD segments between a target individual and its surrogate parents. When a target individual has several surrogate parents from the same family side, we combined them into a single surrogate parent set, which allow the THORIN tool to merge overlapping IBD segment from different relatives within the same set. We then retained only the largest IBD segment (size computed in Morgans) between the target and each surrogate parent set. Unlike the previous approach that only determine maternal relationships using a strict threshold in the chromosome X IBD[3], we probabilistically determined the surrogate parents' parental side. We used the validation cohort to derive probabilities of a surrogate parents set being on the paternal or maternal side based on the length of the chr X IBD haplotype segment shared with the target individual. This method effectively maximizes the number of surrogate parents with determined parental status.

Let l be the length in cM of the longest haplotype segment shared between the chrX of a focal target and that of its surrogate parent(s). In addition, we define l_i as the length of chrX haplotype sharing of an individual i with its surrogate parents, in the training set. Let I_{pat} refer to the set of N_{pat} target individuals with paternal relatives and I_{mat} to those N_{mat} targets with maternal relatives in the training set. We derive the probability of the surrogate parent of a target individual (in the test set), sharing l cM chrX with its surrogate parent, being on the paternal and maternal side as follows:

$$Pr_{pat}(l) = \frac{\frac{1}{N_{mat}} \sum_{i \in I_{pat}} I(l_i > l)}{\frac{1}{N_{pat}} \sum_{i \in I_{mat}} I(l_i > l) + \frac{1}{N_{pat}} \sum_{i \in I_{mat}} I(l_i > l)} \tag{1}$$

$$Pr_{mat}(l) = \frac{\frac{1}{N_{pat}} \sum_{i \in I_{pat}} I(l_i < l)}{\frac{1}{N_{pat}} \sum_{i \in I_{pat}} I(l_i < l) + \frac{1}{N_{mat}} \sum_{i \in I_{mat}} I(l_i < l)} \tag{2}$$

where

$$I(l_i < l) = \begin{cases} 1 & \text{if } l_i < l \\ 0 & \text{otherwise} \end{cases} \tag{3}$$

We initially applied this approach on the males individuals subset of the validation cohort (N=857). We found that all surrogate fathers share IBD haplotype segments smaller than 11.3 cM, and 99% share segments smaller than 3 cM (Supplementary Figure 4A). We then evaluated the accuracy of our probabilistic assignment. To do so, we proceeded with a "Leave One Sample Out" approach: we remove a given individual from the training set and

predicted its paternal and maternal sides by deriving probabilities using the $N-1$ individuals of training set (Supplementary Figure 4B). We repeated this for the N individuals of the training set. To compute accuracy at a given maternal probability p, we defined true positives (TP) as the number of surrogate mothers with probability $> p$ and false positive (FP) as the number of surrogate fathers with probability $> p$. We then computed accuracy as $TP/(TP+FP)$ (Supplementary Figure 4C).

Applying this method to the UK Biobank male individuals with available surrogate parents and unknown parental assignment, we were able to probabilistically assign parental sides to surrogate parents for a total of 115,027 male individuals. Notably, 34% of these individuals (N=39,100) achieved the highest possible parental assignment probability, indicating a robust and reliable classification (Supplementary Figure 4D).

Mitochondrial DNA

Mitochondrial DNA (mtDNA), which is exclusively inherited from the mother, serves as a valuable tool for identifying maternal relatives. However, the UK Biobank Axiom array data proved inadequate for this purpose due to the limited availability of genotyped variants (N=265). To overcome this limitation, we used the whole-genome sequencing GraphTyper cram file available on the UK Biobank Research and Analysis Platform (RAP) for 500,000 individuals. We called variants from the mtDNA whole-genome sequencing (WGS) cram files for 274,525 UK Biobank individuals (those with inter-chromosomal phasing) and their surrogate parents using the MitoHPC software[46] with default parameters.

We then aimed at determining a surrogate parent's parental side using genetic similarities on the mtDNA. However, typical IBD mapping software are derived from the Li & Stephens Hidden Markov Model, which excels at modeling the human recombinant genomes architecture by accounting for mutation and recombination between haplotypes. Due to mtDNA's lack of recombination and its higher mutation rate compared to autosomes, these software proved unsuitable. As a result, we adopted an alternative approach to evaluate non-recombinant DNA sharing between pairs of individuals. This approach is inspired from the Jaccard index and termed here Minor Variant Sharing (MVS). It involves evaluating the proportion of shared minor alleles between relative pairs. This allows us to overcome the limitations of traditional IBD mapping software for mtDNA by basing our analysis on IBS (Identity-By-State) rather than IBD.

Let V_t be the set of variants in the target individual. Similarly, let V_r be the set of variant in the target's relative. Let 0 be the value of a major allele, and 1 be the value of a minor allele. Thus, we compute mtDNA MVS as:

$$MVS(t,r) = \frac{V_t \cap V_r}{V_t \cup V_r} \tag{4}$$

Using the validation cohort, we found that maternal relatives exhibit a higher average MVS compared to paternal relatives (Supplementary Figures 5-7A). The effectiveness of this metric depends on the degree of relatedness and is particularly precise for 2nd degree relatives.

For these relatives, MVS values strongly correlate with the probability of a maternal relationships. However, for more distant relatives (due to the possible presence of an intermediary male relative in the genetic lineage disrupting mtDNA inheritance from the maternal side), low MVS values do not translate to paternal relationship.

To predict the parental side of relatives from the mtDNA MVS, we adopted a perfectly analogous procedure to the one outlined for chrX sharing whereby we replaced chrX IBD segment length with the mtDNA MVS value. To evaluate the accuracy of this approach, we stratified target samples by their degree of relatedness to their closest relatives in the cohort 5-7C).

This methodology was applied to predict relative parental side for 19,022 2nd degree, 114,965 3rd degree, and 312,447 4th degree target-relative pairs (Supplementary Figures 5D-7D). For targets with multiple relatives of the same degree, we retained only the relative with the highest predicted accuracy, resulting in 17,625 2nd degree, 95,151 3rd degree, and 204,924 4th degree target-relative pairs. Notably, 69,580 of these pairs were assigned to a parental side with a probability greater than 0.99 (Supplementary Figure 8A). Additionally, parental side assignments were supported by multiple relatives for 9,948 individuals (Supplementary Figure 8B). Together, this indicates a reliable parental assignment from mtDNA MVS predictions.

Chromosome Y

Chromosome Y sharing between male relatives can indicate paternal lineage. Due to chromosome Y lack of recombination outside PAR regions, we did not employ IBD mapping. Instead, we calculated chromosome Y MVS, similar to our approach with mtDNA. Similarly, the effectiveness of this method depends heavily on the degree of relatedness, as an intermediary female in the genetic lineage interrupts chromosome Y transmission. We used chromosome Y whole-genome sequencing DRAGEN pVCFs files available on the UK Biobank RAP to compute MVS for male target-male relative pairs as described above for mtDNA. We stratified chromosome Y variants by variant type (SNV and Indels) and by Minor Allele Frequency (MAF). Since this can be done only for male target-relative pairs, we are practically limited to using only 3,907 2nd, 24,342 3rd and 66,124 4th degree relative pairs (72,730 unique total target individuals). To explore the potential of this approach, we analyzed 543 male target-male relative pairs from the validation cohort. We found that rare MVS on chromosome Y (MAF <1%) is a reliable predictor of both paternal and maternal sides for all 2nd degree relatives, a good predictor of paternal side for approximately 13% of 3rd degree relatives, but is inaccurate for 4th degree relatives (Supplementary Figure 9). However, since 2nd degree relatives can already be assigned parental sides with high accuracy using mtDNA, the practical utility of Chromosome Y MVS lies primarily in resolving ambiguous PofO assignments among 3rd degree relatives. Among 3rd degree relatives, 11,525 individuals had PofO probabilities below 0.95 when combining Chromosome X and mtDNA predictions. Based on the prediction rate of 13% for Chromosome Y MVS, this method could add approximately 1,500 individuals with improved parental assignments. While this novel approach effectively determines paternal lineage, its limited contribution to sample size—relative to the computational effort and cost of implementing it at scale on the UK Biobank RAP—led us to conclude that a broader application of this method was not justi-

fied. Despite its proven accuracy, we opted not to implement Chromosome Y MVS for all 3rd degree target-relative pairs.

Parent-of-Origin determination

From close relatives

We integrated inter-chromosomal phasing with inferred parental side information from relatives to determine the PofO for each parental haplotype set. Specifically, a haplotype set was classified as maternally inherited if its haplotypes shared IBD segments with maternal relatives, and paternally inherited if they shared IBD segments with paternal relatives. When the assignment was possible for only one of the two haplotypes in a target individual, we assumed the absence of uniparental disomy and inferred the parental origin of the second haplotype by exclusion.

From crossovers to PoO inference in siblings

By analyzing IBD segments shared by siblings, we can infer crossover (CO) locations in parental haplotypes. Together with sex-specific genetic recombination maps[7], Qiao *et al.*[8] have demonstrated that we can estimate the likelihood of a set of COs originating from either the mother or father, allowing us to determine the PofO of the haplotype carrying this set of COs. This method is reliable exclusively for sibling pairs, as they guarantee that the detected CO events occurred in the parents. With more distant relatives, the uncertainty increases significantly. For instance, CO events identified between second-degree relatives could have occurred in the parents or grandparents, resulting in a mix of male-specific and female-specific CO events on the same haplotype.
We identified haplotypes shared IBD between sibling pairs using the THORIN tool. We kept only haplotype segments larger than 3cM. We used IBD segment breakends as CO positions. However, we are very unlikely to pinpoint the exact CO positions using this approach. First, because we are restricted to genotyped markers. Second, due to the nature of the Li & Stephens Hidden Markov Model used to map IBD segments in the THORIN tool - which does not transition at homozygous sites - we identify COs at heterozygotes only. Therefore, we used a 1,000 base pair (bp) window around each CO position to increase chances of including the true position.
We then used recombination maps to extrapolate the probability of a CO occurring within this window based on the genetic distance in Morgans between the start and end positions of the window. We repeated this process for both the male-specific and the female-specific recombination maps for all the CO events identified on the same haplotype.

Let $D_f(p)$ be the distance between the CO position p and the nearest female-specific recombination map position in Morgan and $D_m(p)$ the distance to the nearest male-specific recombination map position. To determine the most likely parent giving rise to an observed CO at position p, we can compute the difference in Morgan between male and female recombination probability:

$$\Delta(p) = log10(D_f(p)) - log10(D_m(p)) \tag{5}$$

Assuming perfect intra-chromosomal phasing, we can deduce that all CO identified on a given haplotype are inherited from the same parent. We can therefore aggregate Morgan differences for the n_0 and n_1 CO positions of haplotype 0 and haplotype 1, respectively, and compute a global score per chromosome using both haplotypes as:

$$Score_{chr} = \sum_{i=1}^{n_0} \Delta_0(p(i)) - \sum_{i=1}^{n_1} \Delta_1(p(i)) \tag{6}$$

This approach can be sensitive to misidentified crossovers, which may arise from various sources, such as inaccuracies in IBD segment boundaries due to errors in the IBD mapper, genotyping errors, or consanguinity. These errors can inflate or deflate the global score. To mitigate this and remove confounders, we compared the observed number of CO $N_{obs}(CO)$ events to the expected number $N_{exp}(CO)$. $N_{exp}(CO)$ depends on the chromosome length in Morgan l_M. Since we aggregate crossovers across both siblings first and second haplotypes, we can observe COs that occurred on four haplotypes, and thus $N_{exp}(CO) = 4l_M$. However, CO positions shared between siblings are counted only once, therefore, $N_{exp}(CO)$ represents the theoretical maxima, and the number COs that is possible to identify is within the range $[0, 4l_M]$, where 0 corresponds to siblings in IBD2 or IBD0 for the entire chromosome. In practice, since artifacts from the IBD mapper can inflate this number and go beyond $4l_M$, we evaluated the distribution of observed CO for each chromosome. Individuals strongly deviating from this distribution (more than 10 times the interquartile range) are removed.
The accuracy of determining the PofO of haplotypes depends on the number of COs analyzed, which varies with chromosome length (in Morgans) (Supplementary Figure 10A). Using intra-chromosomal phasing, we could only determine the PofO for COs within individual chromosomes by computing $Score_{chr}$, requiring separate calculations for each chromosome. In contrast, inter-chromosomal phasing enabled us to group COs occurring across the entire genome on the same parental haplotype set, allowing us to infer the PofO for the entire set at once. This enabled the computation of a genome-wide score, thereby increasing the available genomic length and number of COs (Supplementary Figure 10B):

$$Score_{whole\ genome} = \sum_{chr=1}^{22} Score_{chr} \tag{7}$$

We initially assigned the PofO of haplotype using this score as follows: a negative score means that the first haplotype of the individual is paternally inherited, and a positive score means that it is maternally inherited. We evaluated the efficiency of our approach using a subset of the validation cohort that included 88 individuals with at least one sibling and available inter-chromosomal phasing from close relatives. Since inter-chromosomal phasing might not be available for all chromosomes, we simulated varying conditions by altering the number of chromosomes analyzed per individual, resulting in different numbers of inferred COs depending on the genomic length analyzed (Supplementary Figure 10B). We found that inter-chromosomal phasing significantly increases accuracy compared to single chromosome analysis (Supplementary Figures 10C-E). Moreover, the PofO of COs could be assigned

for 96.4% of individuals using inter-chromosomal phasing, versus only 51.3% with intra-chromosomal phasing (Supplementary Figure 10F).

To avoid relying on strict threshold, we utilized the validation cohort to derive probabilistic determinations of haplotypes' parental origin using inferred COs from inter-chromosomally phased data. Let us consider a score S_t for the target individual t that has been computed using a specific number of inter-chromosomally phased chromosomes. Taken altogether, these chromosomes have a genomic length in Morgan l_t. Since the number of observed COs $N_{obs}(CO)$ depends on l_t and that S_t depends on $N_{obs}(CO)$, we define $I_{pat}(t)$ as the set of individuals of the validation cohort for which H_0 is paternally inherited and for which l is within the window (l_t-3, l_t+3), and $I_{mat}(t)$ as the set of individuals of the validation cohort for which H_0 is maternally inherited and for which l is within the window $(l_t - 3, l_t + 3)$. The cardinality of these sets are denoted by $N_{pat}(t)$ and $N_{mat}(t)$, respectively. This allows us to compare our obtained score to a subset of the validation cohort that had a similar available genomic length as l_t.

Since we assigned negative scores to paternal side and positive scores to maternal side, we can then define the probability of paternal origin of a genome-wide haplotype of target sample t as follows

$$Pr_{pat}(t) = \frac{\frac{1}{N_{pat}(t)} \sum_{i \in I_{pat}(t)} I(S_i < S_t)}{\frac{1}{N_{pat}(t)} \sum_{i \in I_{pat}(t)} I(S_i < S_t) + \frac{1}{N_{mat}(t)} \sum_{i \in I_{mat}(t)} I(S_i < S_t)} \tag{8}$$

We evaluated the accuracy of this approach using the validation cohort. We simulated varying conditions by altering the number of chromosomes analyzed per individual, ranging from only 1 chromosome used, to the full set of inter-chromosomally phased chromosomes for each individual. We observed better accuracy for scores strongly deviating from zero (Supplementary Figure 11A). In addition, we observed that larger available genomic lengths (i.e, more chromosomes) resulted in less errors, and that no errors were detected when using more than 10 Morgan (Supplementary Figure 11B). Notably, when using the full set of available inter-chromosomally phased chromosomes per individual in the validation cohort (i.e the most realistic scenario), we achieved 100% accuracy (Supplementary Figures 11A-B).

We applied this approach on 26,635 individuals with available inter-chromosomal phasing and at least one sibling. The specific configurations of our sample set (genomic length and number of COs) matched the highest accuracy (Supplementary Figures 11C,D).

Since inter-chromosomal phasing is not available for all siblings, we additionally use 14,695 individuals without inter-chromosomal phasing available and at least one sibling. We applied the single-chromosome approach using strict threshold at scores of -2 and 2 to determine the PofO of each target haplotypes separately, and assessed the different parameters of this approach (Supplementary Figure 12).

Accuracy of combined parent-of-origin predictors

A given individual can have several predictors of its haplotype PofO: chromosome X IBD, mtDNA MVS from different relatives, and sib-score. For each individual, we kept the predictor with the probability yielding the highest accuracy at determining paternal or maternal

side. As a result, we could unambiguously determine the relatives' parental side for 99.1% of the target individuals (N=267,831). For ambiguous cases (N=2,491), we then prioritize predictors in the order indicated by overall accuracy of the predictor: chromosome X, sib-score, MVS for second-degree relatives. We obtained 209 individuals with parental sides undetermined because of conflicting mtDNA-based PoO predictions from different (third- and fourth-degree) relatives in the same surrogate parent cluster. In addition, we also had 14,596 individuals with PofO inferred from single-chromosome sibling-score. As a result, we obtained a final set of 284,709 individuals, of which more than 40% (N=125,202) have a probability between 0.99 and 1 (Supplementary Figure 13A). The vast majority of relatives' parental side (89.9%) is determined from a single predictor (Supplementary Figure 13B) while the rest is confirmed by multiple predictors (N=29,154), which strengthen our confidence in these parental assignments. By removing the validation cohort and combining with individuals having PofO inferred from available parental genomes, we assembled a final set of 286,666 individuals. We finally compared our PofO determination to the one obtained from parental genomes at each heterozygous site of the validation cohort, revealing an accuracy of 98% (Supplementary Figure 14).

Parental haplotypes imputation and encoding

To infer the PofO for untyped alleles, we used haploid imputation as done previously[3] to separately impute each parental haplotype using the *–out-ap-field* option of IMPUTE5 v1.2.1[47] and the Haplotype Reference Consortium as a reference panel. This provides an AP field indicating imputed paternal and maternal allele dosages. We then kept only variants with an INFO score greater than 0.8 and Minor Allele Frequency (MAF) greater than 1%. We encoded parental haplotype in separate files. For each target and at each variant, we weighted parental allele imputed dosage by the parental assignment probability. Let us consider an imputed variant v for a target individual t with haploid imputed dosages $AP_{mat}(t,v)$ and $AP_{pat}(t,v)$ for maternal and paternal haplotype, respectively. Let us also consider the parental assignment probability p_t for the target t given by combined predictors. We re-encoded our data as:

$$DS_{mat}(t,v) = AP_{mat}(t,v) * p_t + AP_{pat}(t,v) * (1 - p_t) \tag{9}$$

$$DS_{pat}(t,v) = AP_{pat}(t,v) * p_t + AP_{mat}(t,v) * (1 - p_t) \tag{10}$$

From this, we adapted a haploid genotype posterior probability field GP (probability triplets for the three possible genotypes) as:

$$GP_{mat}(t,v) = (1 - DS_{mat}(t,v), DS_{mat}(t,v), 0) \tag{11}$$

$$GP_{pat}(t,v) = (1 - DS_{pat}(t,v), DS_{pat}(t,v), 0) \tag{12}$$

Finally, we also combined maternal and paternal alleles at heterozygous only to directly test for differential effect (all homozygous sites are encoded as missing):

$$GP_{diff}(t,v) = (DS_{mat}(t,v)/DS_{dip}(t,v), DS_{pat}(t,v)/DS_{dip}(t,v), 0) \tag{13}$$

where

$$DS_{dip}(t,v) = DS_{mat}(t,v) + DS_{pat}(t,v) \tag{14}$$

Identification of Parent-of-origin effects

Parent-of-origin effects is a generic name that characterize many different type of genetic effect whose effect depends on the parental origin of the assessed allele, the most known probably being strict paternal and maternal effects. However, many other type of POE exists (Supplementary Figure 15). To increase our likelihood of detecting POE effect, we use the differential scan to directly assess the differential effect between paternal and maternal alleles among heterozygous individuals. To then infer the direction of the effect, we use a paternal-specific and maternal-specific GWAS scan, which separately evaluate the effect of each parental haplotype. To perform GWAS analysis, we used Regenie v3.2.9[48]. We performed the model fitting only on the genotyped variants as recommended (i.e regenie step1). We then tested paternal, maternal and differential haplotypes (i.e GP_{pat}, GP_{mat} and GP_{diff}) separately (i.e regenie step2). We denote the p-values resulting from these GWAS P_P, P_M and P_D for paternal, maternal and differential GWAS, respectivels. We used the first 20 Principal Components (PCs), age and sex as covariates. In addition, we restricted our association tests to individuals who self-identified as "White British" and have a similar genetic ancestry determined by principal components analysis (UK Biobank field 22006), and we restricted the differential scan to variants with imputed PofO dosages greater than 0.99, as done previously[3].

Given the complexity and diverse nature of POE effects, we employed a multi-faceted approach to identify novel putative associations. Beside a traditional genome-wide scan, we leveraged biological knowledge by focusing on known imprinted regions, which are more likely to exhibit POE. Second, recognizing that POE effects can also arise outside of these known regions, we expanded our analysis to perform a GWAS scan focusing on regions exhibiting additive association with the examined trait. For these analyses, we selected a total of 59 phenotypes, mostly from blood biomarkers and morphological traits. This comprehensive approach allowed us to maximize the potential for discovering novel POE signals across a broad spectrum of traits. To account for the number of traits tested, we computed phenotypic correlation between each pair of traits. We then used the function *simpleM* from the R package *hscovar* to compute the effective number of traits tested, which resulted in $N_{eff}(traits) = 48$. All associations were pruned using genetic distance smaller than 500kb and LD<0.01.

To identify POE genome-wide, we used a stringent POE significance threshold (i.e, differential P-value P_D) of $5 \times 10^{-8}/48 = 1 \times 10^{-9}$ to correct for the number of independent tests performed across our 59 selected traits.

To identify POE within additive regions, we first selected significant additive associations (p-value $< 5 \times 10^{-8}/48 = 1.04 \times 10^{-9}$), which we then tested for POE using the differential GWAS. We corrected our POE significance threshold for the number of identified additive association such that the differential p-value P_D threshold $= 0.05/N_a$, where N_a is the number of independent additive associations.

To identify POE within imprinted regions, we limited our analysis to variants within a 500kb window around known imprinted genes, as these regions are biologically predisposed to display differential effects based on parental origin. This targeted strategy enabled us to leverage prior biological knowledge to enhance the likelihood of identifying true POE effects. In practice, we use imprinted regions coordinates published previously[5]. To ensure statistical rigor while maintaining sensitivity, we adjusted the POE significance threshold by accounting for the LD structure within these regions. After calculating the number of effective independent tests, we applied a significance threshold of $P_D < 0.05/16,574 = 3.01 \times 10^{-6}$, where 16,574 is the number of independent tests performed within imprinted regions. Additionally, we verified whether the identified associations would pass the more stringent threshold of 6.27×10^{-8}, which corresponds to $3.01 \times 10^{-6}/48$, where 48 is the effective number of traits tested.

Replication of known parent-of-origin associations

We used publicly available summary data for height studies directly reporting POEs or reporting separate paternal and maternal GWAS estimates[3,4,5,9,10,11,12,13]. When differential GWAS coefficients were not directly available, we computed a differential scan similar to the one performed in our study:

$$Z_D = \frac{\widehat{\beta}_P - \widehat{\beta}_M}{\sqrt{SE_P^2 + SE_M^2}} \tag{15}$$

$$P_D = 2 \times (1 - \Phi(|Z_D|)) \tag{16}$$

where Φ is the cumulative distribution function of the standard normal distribution and $|Z_D|$ is the absolute value of the z-score.

Sex-specific differences in Parent-of-Origin effects

We performed a differential GWAS scan separately for males and females to obtain sex-specific coefficients. We then assessed significant differences of effects using a z-score approach:

$$Z_D = \frac{\widehat{\beta}_{D_{males}} - \widehat{\beta}_{D_{females}}}{\sqrt{SE^2_{D_{males}} + SE^2_{D_{females}}}} \tag{17}$$

$$P_{Z_D} = 2 \times (1 - \Phi(|Z_{comp}|)) \tag{18}$$

SNPs heritability

We used the software LD Score Regression[49] to compute SNPs heritability (h^2) from our GWAS summary data. We used the publicly available LD scores from 1000 Genome Project (KGP). We munged GWAS summary data and estimated heritability as recommended by the authors of the software and with default parameters. For h^2 computed on subsets of data (i.e within- and outside imprinted regions), we weighted the estimates by the proportion of variants included in the data subset. To assess difference between heritability estimates, we combined estimates into a z-score :

$$Z_{h^2} = \frac{h^2_a - h^2_b}{\sqrt{SE^2_a + SE^2_b}} \tag{19}$$

$$P_{h^2} = 2 \times (1 - \Phi(|Z_{h^2}|)) \tag{20}$$

where a and b are (i) paternal and maternal estimates (Figures 7A,B), or (ii) differential estimates within imprinted regions and outside imprinted regions (Figure 7C).

Estonian Biobank genotype processing

We used the Quality Controlled (QC) genotype data genome built GRCh38 in Variant Call Format (vcf) provided by the Estonian Biobank team[23]. Similar to when processing the UKBB data, we used SHAPEIT5[14] to phase autosomes and chromosome X, and KING[45] to estimate relatedness. To impute the EstBB genotype data, we use the Estonian Biobank WGS reference panel, including 2,695 individuals. We performed phasing of the reference panel using the two steps process of SHAPEIT5[14]. We used the resulting reference panel to impute the data SNP array data using IMPUTE5[47]. For all the remaining analysis, we proceed as for the UK Biobank. To infer the PofO of haplotypes for individuals without available parental genomes, we used only IBD sharing on chromosome X and sibling score, since chromosome Y WGS and mtDNA WGS were not available to compute MVS. To perform association analysis, we focused on traits for which we had at least 20,000 individuals in the Estonian Biobank. This resulted in 10 traits, namely standing height, glucose, type 2 diabetes, glycated haemoglobin, HDL cholesterol, triglycerides, hip circumference, creatinine, cystatin C and platelet count. We derived phenotypes from electronic health records (EHR), unless NMR metabolomics measurements were available[50], which were available in greater

sample size compared to blood biomarkers (for glucose, triglycerides, HDL cholesterol and creatinine).

Data availability

The summary data will be publicly accessible for download upon publication through our database (http://poedb.dcsr.unil.ch/, currently hosting data from our previous study). Prior to publication, data can be obtained by contacting the corresponding authors. The UK Biobank genetic data are available under restricted access. Access can be obtained by application via the UK Biobank Access Management System (https://www.ukbiobank.ac.uk/enable-your-research/apply-for-access). The Estonian Biobank data is also available under restricted access. The access to the Estonian Biobank data must be approved by the Scientific Advisory Committee of the Estonian Biobank and by the Estonian Committee on Bioethics and Human Research. More details are available at https://genomics.ut.ee/en/content/estonian-biobank#dataaccess. Data produced as part of this study (i.e inter-chromosomally phased data and PofO information) will be returned to their respective biobanks. Access will be granted upon publication to approved researchers.

Code availability

The phasing software SHAPEIT5 and parent-of-origin IBD mapping software THORIN are available under MIT license at https://github.com/odelaneau/shapeit5 and https://github.com/RJHFMSTR/PofO_inference/tree/master/step4_pofo_inference/THORIN. Custom scripts, pipeline and updated documentation will be made available upon publication on github and deposited in the a Zenodo repository.

Acknowledgments

We thank all biobanks participants for sharing their data. The Estonian Biobank data analysis was carried out in part in the High-Performance Computing Center of University of Tartu, Estonia. The UK Biobank data analysis was carried out in part in the High-Performance Computing Center of University of Lausanne, Switzerland. Metabolomics data of the Estonian Biobank has been generated by as part of a collaboration between Nightingale Health Plc and Institute of Genomics, University of Tartu. The development of quality-controlled dataset was supported by the Estonian Research Council grant no PRG1291.

Ethics statement

The activities of the EstBB are regulated by the Human Genes Research Act, which was adopted in 2000 specifically for the operations of the EstBB. Individual level data analysis in the EstBB was carried out under ethical approval 1.1-12/295 from the Estonian Committee on Bioethics and Human Research (Estonian Ministry of Social Affairs), using data according to release application nr T38 from the Estonian Biobank. This research has been conducted using the UK Biobank Application Number 16389 and 66995, and funded by the Swiss National Science Foundation (SNSF) project grant SNSF 310030-189147.

Authors information

Authors contributions

R.J.H. and Z.K. designed the study and wrote the manuscript. R.J.H. performed all experiments. O.D. contributed to statistical phasing and sex chromosomes integration. S.R. contributed to imputation experiments. T.C. contributed to the implementation of the sibling model. A.V.D.G. contributed to optimizing haplotype data encoding. L.M., R.M. and F.D.P contributed to the analyses in the Estonian Biobank cohort. The Estonian Biobank research team performed data collection, genotyping and QC of the Estonian Biobank genetic data. J.K. and N.T. developed quality control criteria for the Estonian Biobank metabolite data. All authors reviewed the final manuscript. The project has been supervised by Z.K.

Corresponding authors

Correspondence to Robin J. Hofmeister (robin.j.hofmeister@gmail.com) and Zoltán Kutalik (zoltan.kutalik@unil.ch).

Competing interests

O.D is a current employee of Regeneron Genetics Center. The others authors declare no competing interests.

Additional authors affiliations

Estonian Biobank research team

Andres Metspalu[1], Lili Milani[1], Tõnu Esko[1], Reedik Mägi[1], Mari Nelis[1] and Georgi Hudjashov[1]
[1] Estonian Genome Centre, Institute of Genomics, University of Tartu

References

[1] T. Moore and D. Haig. "Genomic imprinting in mammalian development: a parental tug-of-war". In: *Trends in genetics: TIG* 7.2 (Feb. 1991), pp. 45–49. ISSN: 0168-9525. DOI: 10.1016/0168-9525(91)90230-N.

[2] Juan F Macias-Velasco et al. "Parent-of-origin effects propagate through networks to shape metabolic traits". In: *eLife* 11 (), e72989. ISSN: 2050-084X. DOI: 10.7554/eLife.72989. URL: https://www.ncbi.nlm.nih.gov/pmc/articles/PMC9075957/ (visited on 08/08/2024).

[3] Robin J. Hofmeister et al. "Parent-of-Origin inference for biobanks". In: *Nature Communications* 13.1 (Nov. 5, 2022). Publisher: Nature Publishing Group, p. 6668. ISSN: 2041-1723. DOI: 10.1038/s41467-022-34383-6. URL: https://www.nature.com/articles/s41467-022-34383-6 (visited on 08/07/2024).

[4] Hye In Kim et al. "Genome-wide survey of parent-of-origin-specific associations across clinical traits derived from electronic health records". In: *Human Genetics and Genomics Advances* 2.3 (June 11, 2021), p. 100039. ISSN: 2666-2477. DOI: 10.1016/j.xhgg.2021.100039. URL: https://www.ncbi.nlm.nih.gov/pmc/articles/PMC8756508/ (visited on 08/08/2024).

[5] Augustine Kong et al. "Parental origin of sequence variants associated with complex diseases". In: *Nature* 462.7275 (Dec. 2009). Publisher: Nature Publishing Group, pp. 868–874. ISSN: 1476-4687. DOI: 10.1038/nature08625. URL: https://www.nature.com/articles/nature08625 (visited on 08/07/2024).

[6] Neil M. Davies et al. "The importance of family-based sampling for biobanks". In: *Nature* 634.8035 (Oct. 2024). Publisher: Nature Publishing Group, pp. 795–803. ISSN: 1476-4687. DOI: 10.1038/s41586-024-07721-5. URL: https://www.nature.com/articles/s41586-024-07721-5 (visited on 10/25/2024).

[7] Claude Bhérer, Christopher L. Campbell, and Adam Auton. "Refined genetic maps reveal sexual dimorphism in human meiotic recombination at multiple scales". In: *Nature Communications* 8.1 (Apr. 25, 2017). Publisher: Nature Publishing Group, p. 14994. ISSN: 2041-1723. DOI: 10.1038/ncomms14994. URL: https://www.nature.com/articles/ncomms14994 (visited on 11/22/2024).

[8] Ying Qiao et al. *Reconstructing parent genomes using siblings and other relatives*. Pages: 2024.05.10.593578 Section: New Results. May 14, 2024. DOI: 10.1101/2024.05.10.593578. URL: https://www.biorxiv.org/content/10.1101/2024.05.10.593578v1 (visited on 08/08/2024).

[9] Einat Granot-Hershkovitz et al. "Searching for parent-of-origin effects on cardiometabolic traits in imprinted genomic regions". In: *European Journal of Human Genetics* 28.5 (May 2020). Publisher: Nature Publishing Group, pp. 646–655. ISSN: 1476-5438. DOI: 10.1038/s41431-019-0568-1. URL: https://www.nature.com/articles/s41431-019-0568-1 (visited on 10/25/2024).

[10] Thorhildur Juliusdottir et al. "Distinction between the effects of parental and fetal genomes on fetal growth". In: *Nature Genetics* 53.8 (Aug. 2021), pp. 1135–1142. ISSN: 1546-1718. DOI: 10.1038/s41588-021-00896-x.

[11] Robin N. Beaumont et al. "Genome-wide association study of placental weight identifies distinct and shared genetic influences between placental and fetal growth". In: *Nature Genetics* 55.11 (Nov. 2023). Publisher: Nature Publishing Group, pp. 1807–1819. ISSN: 1546-1718. DOI: 10.1038/s41588-023-01520-w. URL: https://www.nature.com/articles/s41588-023-01520-w (visited on 10/25/2024).

[12] Magdalena Zoledziewska et al. "Height-reducing variants and selection for short stature in Sardinia". In: *Nature Genetics* 47.11 (Nov. 2015). Publisher: Nature Publishing Group, pp. 1352–1356. ISSN: 1546-1718. DOI: 10.1038/ng.3403. URL: https://www.nature.com/articles/ng.3403 (visited on 10/25/2024).

[13] Stefania Benonisdottir et al. "Epigenetic and genetic components of height regulation". In: *Nature Communications* 7.1 (Nov. 16, 2016). Publisher: Nature Publishing Group, p. 13490. ISSN: 2041-1723. DOI: 10.1038/ncomms13490. URL: https://www.nature.com/articles/ncomms13490 (visited on 10/25/2024).

[14] Robin J. Hofmeister et al. "Accurate rare variant phasing of whole-genome and whole-exome sequencing data in the UK Biobank". In: *Nature Genetics* 55.7 (July 2023). Publisher: Nature Publishing Group, pp. 1243–1249. ISSN: 1546-1718. DOI: 10.1038/s41588-023-01415-w. URL: https://www.nature.com/articles/s41588-023-01415-w (visited on 08/08/2024).

[15] Xiaoying Wang et al. "Diabetes knowledge predicts HbA1c levels of people with type 2 diabetes mellitus in rural China: a ten-month follow-up study". In: *Scientific Reports* 13.1 (Oct. 25, 2023). Publisher: Nature Publishing Group, p. 18248. ISSN: 2045-2322. DOI: 10.1038/s41598-023-45312-y. URL: https://www.nature.com/articles/s41598-023-45312-y (visited on 11/18/2024).

[16] Heather A. Lawson, James M. Cheverud, and Jason B. Wolf. "Genomic imprinting and parent-of-origin effects on complex traits". In: *Nature reviews. Genetics* 14.9 (Sept. 2013), pp. 609–617. ISSN: 1471-0056. DOI: 10.1038/nrg3543. URL: https://www.ncbi.nlm.nih.gov/pmc/articles/PMC3926806/ (visited on 08/08/2024).

[17] Jason B. Wolf et al. "Genome-wide analysis reveals a complex pattern of genomic imprinting in mice". In: *PLoS genetics* 4.6 (June 6, 2008), e1000091. ISSN: 1553-7404. DOI: 10.1371/journal.pgen.1000091.

[18] THE GTEX CONSORTIUM. "The GTEx Consortium atlas of genetic regulatory effects across human tissues". In: *Science* 369.6509 (Sept. 11, 2020). Publisher: American Association for the Advancement of Science, pp. 1318–1330. DOI: 10.1126/science.aaz1776. URL: https://www.science.org/doi/10.1126/science.aaz1776 (visited on 10/25/2024).

[19] Urmo Võsa et al. "Large-scale cis- and trans-eQTL analyses identify thousands of genetic loci and polygenic scores that regulate blood gene expression". In: *Nature Genetics* 53.9 (Sept. 2021). Publisher: Nature Publishing Group, pp. 1300–1310. ISSN:

1546-1718. DOI: 10.1038/s41588-021-00913-z. URL: https://www.nature.com/articles/s41588-021-00913-z (visited on 10/25/2024).

[20] Eleonora Porcu et al. "Limited evidence for blood eQTLs in human sexual dimorphism". In: *Genome Medicine* 14.1 (Aug. 11, 2022), p. 89. ISSN: 1756-994X. DOI: 10.1186/s13073-022-01088-w. URL: https://doi.org/10.1186/s13073-022-01088-w (visited on 11/01/2024).

[21] Elena Bernabeu et al. "Sex differences in genetic architecture in the UK Biobank". In: *Nature Genetics* 53.9 (Sept. 2021). Publisher: Nature Publishing Group, pp. 1283–1289. ISSN: 1546-1718. DOI: 10.1038/s41588-021-00912-0. URL: https://www.nature.com/articles/s41588-021-00912-0 (visited on 10/31/2024).

[22] Benjamin B. Sun et al. "Plasma proteomic associations with genetics and health in the UK Biobank". In: *Nature* 622.7982 (Oct. 2023). Publisher: Nature Publishing Group, pp. 329–338. ISSN: 1476-4687. DOI: 10.1038/s41586-023-06592-6. URL: https://www.nature.com/articles/s41586-023-06592-6 (visited on 10/25/2024).

[23] Lili Milani et al. *From Biobanking to Personalized Medicine: the journey of the Estonian Biobank*. Pages: 2024.09.22.24313964. Sept. 24, 2024. DOI: 10.1101/2024.09.22.24313964. URL: https://www.medrxiv.org/content/10.1101/2024.09.22.24313964v1 (visited on 10/25/2024).

[24] Veryan Codd et al. "Polygenic basis and biomedical consequences of telomere length variation". In: *Nature Genetics* 53.10 (Oct. 5, 2021), p. 1425. DOI: 10.1038/s41588-021-00944-6. URL: https://pmc.ncbi.nlm.nih.gov/articles/PMC8492471/ (visited on 10/31/2024).

[25] Petar N. Grozdanov et al. "SHQ1 is required prior to NAF1 for assembly of H/ACA small nucleolar and telomerase RNPs". In: *RNA* 15.6 (June 2009), p. 1188. DOI: 10.1261/rna.1532109. URL: https://pmc.ncbi.nlm.nih.gov/articles/PMC2685518/ (visited on 10/31/2024).

[26] Andrew S. Venteicher et al. "Identification of ATPases pontin and reptin as telomerase components essential for holoenzyme assembly". In: *Cell* 132.6 (Mar. 21, 2008), p. 945. DOI: 10.1016/j.cell.2008.01.019. URL: https://pmc.ncbi.nlm.nih.gov/articles/PMC2291539/ (visited on 10/31/2024).

[27] Katarina Nordfjäll et al. "Telomere length and heredity: Indications of paternal inheritance". In: *Proceedings of the National Academy of Sciences* 102.45 (Nov. 8, 2005). Publisher: Proceedings of the National Academy of Sciences, pp. 16374–16378. DOI: 10.1073/pnas.0501724102. URL: https://www.pnas.org/doi/10.1073/pnas.0501724102 (visited on 10/25/2024).

[28] Qiao Weng et al. "The known genetic loci for telomere length may be involved in the modification of telomeres length after birth". In: *Scientific Reports* 6.1 (Dec. 8, 2016). Publisher: Nature Publishing Group, p. 38729. ISSN: 2045-2322. DOI: 10.1038/srep38729. URL: https://www.nature.com/articles/srep38729 (visited on 10/25/2024).

[29] Jessica L. Buxton et al. "Human leukocyte telomere length is associated with DNA methylation levels in multiple subtelomeric and imprinted loci". In: *Scientific Reports* 4.1 (May 14, 2014). Publisher: Nature Publishing Group, p. 4954. ISSN: 2045-2322. DOI: 10.1038/srep04954. URL: https://www.nature.com/articles/srep04954 (visited on 10/25/2024).

[30] Yawen Ju et al. "Troponin T3 expression in skeletal and smooth muscle is required for growth and postnatal survival: Characterization of Tnnt3 mice". In: *genesis* 51.9 (2013). _eprint: https://onlinelibrary.wiley.com/doi/pdf/10.1002/dvg.22407, pp. 667–675. ISSN: 1526-968X. DOI: 10.1002/dvg.22407. URL: https://onlinelibrary.wiley.com/doi/abs/10.1002/dvg.22407 (visited on 11/19/2024).

[31] M. Kamiya et al. "The cell cycle control gene ZAC/PLAGL1 is imprinted–a strong candidate gene for transient neonatal diabetes". In: *Human Molecular Genetics* 9.3 (Feb. 12, 2000), pp. 453–460. ISSN: 0964-6906. DOI: 10.1093/hmg/9.3.453.

[32] Deborah Mackay et al. "Clinical utility gene card for: Transient Neonatal Diabetes Mellitus, 6q24-related". In: *European Journal of Human Genetics* 22.9 (Sept. 2014). Publisher: Nature Publishing Group, pp. 1153–1153. ISSN: 1476-5438. DOI: 10.1038/ejhg.2014.27. URL: https://www.nature.com/articles/ejhg201427 (visited on 10/30/2024).

[33] Hao Hong et al. "Central IGF1 improves glucose tolerance and insulin sensitivity in mice". In: *Nutrition & Diabetes* 7.12 (Dec. 19, 2017). Publisher: Nature Publishing Group, pp. 1–10. ISSN: 2044-4052. DOI: 10.1038/s41387-017-0002-0. URL: https://www.nature.com/articles/s41387-017-0002-0 (visited on 11/01/2024).

[34] D. S. Matassa et al. "Oxidative metabolism drives inflammation-induced platinum resistance in human ovarian cancer". In: *Cell Death & Differentiation* 23.9 (Sept. 2016). Publisher: Nature Publishing Group, pp. 1542–1554. ISSN: 1476-5403. DOI: 10.1038/cdd.2016.39. URL: https://www.nature.com/articles/cdd201639 (visited on 10/25/2024).

[35] Damian Szklarczyk et al. "The STRING database in 2023: protein-protein association networks and functional enrichment analyses for any sequenced genome of interest". In: *Nucleic Acids Research* 51 (D1 Jan. 6, 2023), pp. D638–D646. ISSN: 1362-4962. DOI: 10.1093/nar/gkac1000.

[36] Wende Zhu et al. "Meg3-DMR, not the Meg3 gene, regulates imprinting of the Dlk1-Dio3 locus". In: *Developmental Biology* 455.1 (Nov. 1, 2019), pp. 10–18. ISSN: 1095-564X. DOI: 10.1016/j.ydbio.2019.07.005.

[37] Tomohiko Kayashima et al. "The novel imprinted carboxypeptidase A4 gene (CPA4) in the 7q32 imprinting domain". In: *Human Genetics* 112.3 (Mar. 2003), pp. 220–226. ISSN: 0340-6717. DOI: 10.1007/s00439-002-0891-3.

[38] Bharati Jadhav et al. "RNA-Seq in 296 phased trios provides a high-resolution map of genomic imprinting". In: *BMC Biology* 17.1 (June 24, 2019), p. 50. ISSN: 1741-7007. DOI: 10.1186/s12915-019-0674-0. URL: https://doi.org/10.1186/s12915-019-0674-0 (visited on 10/25/2024).

[39] Florian Zink et al. "Insights into imprinting from parent-of-origin phased methylomes and transcriptomes". In: *Nature Genetics* 50.11 (Nov. 2018). Publisher: Nature Publishing Group, pp. 1542–1552. ISSN: 1546-1718. DOI: 10.1038/s41588-018-0232-7. URL: https://www.nature.com/articles/s41588-018-0232-7 (visited on 10/25/2024).

[40] Yongtao Guan and Daniel Levy. *Abundant Parent-of-origin Effect eQTL in Humans: The Framingham Heart Study*. Pages: 2024.06.05.597677 Section: New Results. June 10, 2024. DOI: 10.1101/2024.06.05.597677. URL: https://www.biorxiv.org/content/10.1101/2024.06.05.597677v1 (visited on 11/15/2024).

[41] Nicola Pirastu et al. "Genetic analyses identify widespread sex-differential participation bias". In: *Nature Genetics* 53.5 (May 2021). Publisher: Nature Publishing Group, pp. 663–671. ISSN: 1546-1718. DOI: 10.1038/s41588-021-00846-7. URL: https://www.nature.com/articles/s41588-021-00846-7 (visited on 11/20/2024).

[42] Clare Bycroft et al. "The UK Biobank resource with deep phenotyping and genomic data". In: *Nature* 562.7726 (Oct. 2018). Publisher: Nature Publishing Group, pp. 203–209. ISSN: 1476-4687. DOI: 10.1038/s41586-018-0579-z. URL: https://www.nature.com/articles/s41586-018-0579-z (visited on 08/08/2024).

[43] Shaun Purcell et al. "PLINK: A Tool Set for Whole-Genome Association and Population-Based Linkage Analyses". In: *American Journal of Human Genetics* 81.3 (Sept. 2007), pp. 559–575. ISSN: 0002-9297. URL: https://www.ncbi.nlm.nih.gov/pmc/articles/PMC1950838/ (visited on 08/08/2024).

[44] Diogo M Ribeiro et al. *Phasing report*. Google Docs. URL: https://docs.google.com/document/d/1EJmh-JcR8HBvu3rjBtREw_50kDIW-sOW2EcC6zweuTc/edit?usp=embed_facebook (visited on 08/08/2024).

[45] Ani Manichaikul et al. "Robust relationship inference in genome-wide association studies". In: *Bioinformatics* 26.22 (Nov. 15, 2010), pp. 2867–2873. ISSN: 1367-4811, 1367-4803. DOI: 10.1093/bioinformatics/btq559. URL: https://academic.oup.com/bioinformatics/article/26/22/2867/228512 (visited on 08/08/2024).

[46] Stephanie L Battle et al. "A bioinformatics pipeline for estimating mitochondrial DNA copy number and heteroplasmy levels from whole genome sequencing data". In: *NAR Genomics and Bioinformatics* 4.2 (June 1, 2022), lqac034. ISSN: 2631-9268. DOI: 10.1093/nargab/lqac034. URL: https://doi.org/10.1093/nargab/lqac034 (visited on 08/08/2024).

[47] Simone Rubinacci, Olivier Delaneau, and Jonathan Marchini. "Genotype imputation using the Positional Burrows Wheeler Transform". In: *PLOS Genetics* 16.11 (Nov. 16, 2020). Publisher: Public Library of Science, e1009049. ISSN: 1553-7404. DOI: 10.1371/journal.pgen.1009049. URL: https://journals.plos.org/plosgenetics/article?id=10.1371/journal.pgen.1009049 (visited on 08/08/2024).

[48] Joelle Mbatchou et al. "Computationally efficient whole-genome regression for quantitative and binary traits". In: *Nature Genetics* 53.7 (July 2021). Publisher: Nature Publishing Group, pp. 1097–1103. ISSN: 1546-1718. DOI: 10.1038/s41588-021-00870-

7. URL: https://www.nature.com/articles/s41588-021-00870-7 (visited on 10/25/2024).

[49] Brendan K. Bulik-Sullivan et al. "LD Score regression distinguishes confounding from polygenicity in genome-wide association studies". In: *Nature Genetics* 47.3 (Mar. 2015). Publisher: Nature Publishing Group, pp. 291–295. ISSN: 1546-1718. DOI: 10.1038/ng.3211. URL: https://www.nature.com/articles/ng.3211 (visited on 10/28/2024).

[50] Ralf Tambets et al. *Genome-wide association study for circulating metabolites in 619,372 individuals*. Pages: 2024.10.15.24315557. Oct. 31, 2024. DOI: 10.1101/2024.10.15.24315557. URL: https://www.medrxiv.org/content/10.1101/2024.10.15.24315557v2 (visited on 11/26/2024).

Figures

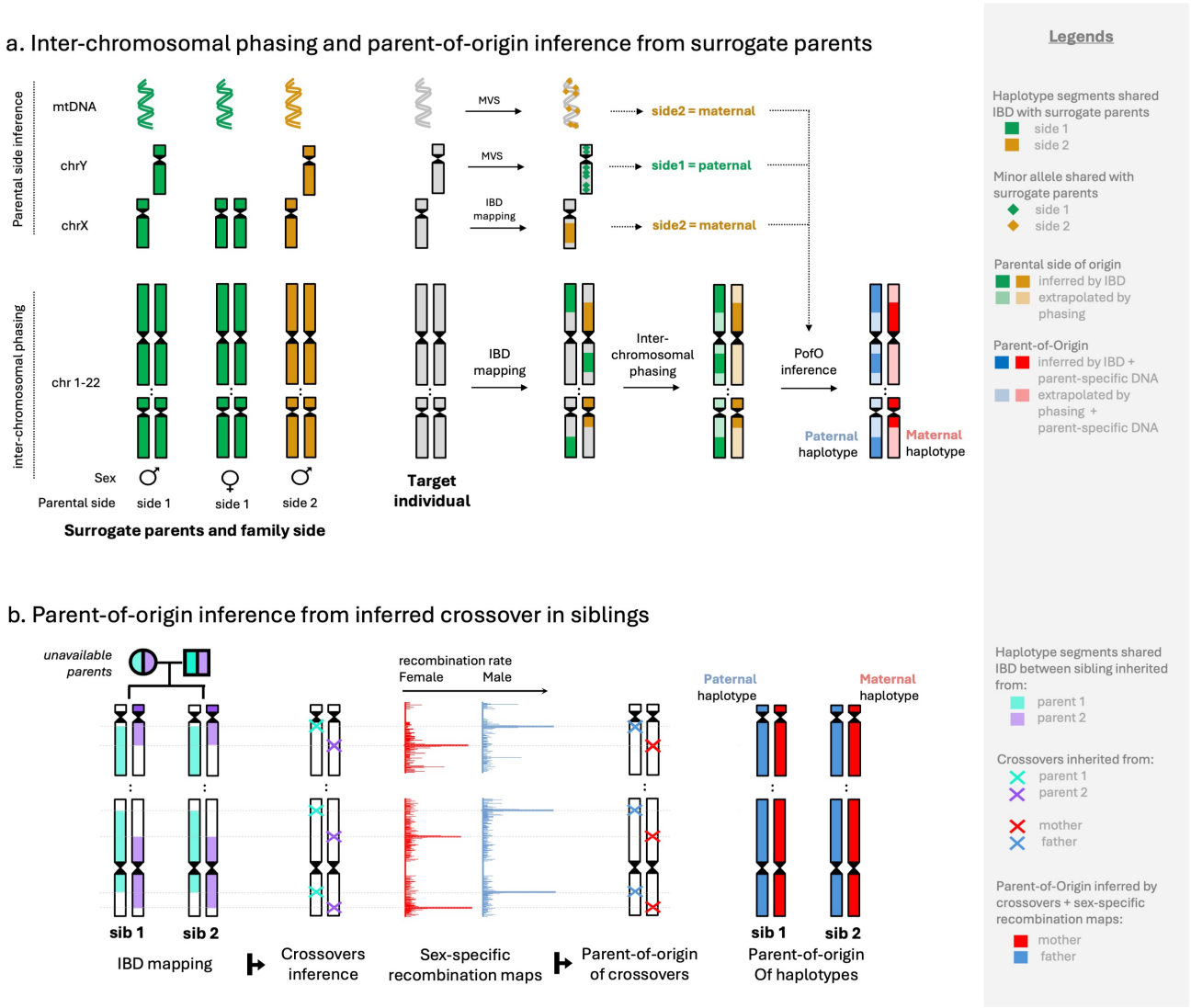

Fig. 1 | Inter-chromosomal phasing and parent-of-origin methods overview. a) Inter-chromosomal phasing and parent-of-origin inference. We initially clustered relatives (2nd, 3rd and 4th degree) into surrogate parent groups, segregating the relatives into "one family side" (green) *vs* "the other family side" (orange). We then combined two steps to infer the PofO of a focal individual: on the one hand, we leveraged IBD sharing with surrogate parent groups to perform inter-chromosomal phasing. For instance, green IBD tracks were forced to align on the first haplotype, simultaneously correcting for intra-chromosomal phasing errors; on the other hand, we examined genetic similarities on chromosome X, Y and mtDNA between the focal individual and its surrogate parents, to assign surrogate parent groups to a parental side. Finally, we deduce the PofO of inter-chromosomally phased haplotypes from the parental side of the surrogate parent in IBD (see Methods for details). **b**) To determine the PofO of siblings, we first inferred crossover events using IBD haplotypes. We then overlapped inferred crossovers with sex-specific genetic map to derive the likelihood of a crossover originating from the mother of the father. This subsequently allowed us to deduce the PofO of the haplotype carrying the crossover.

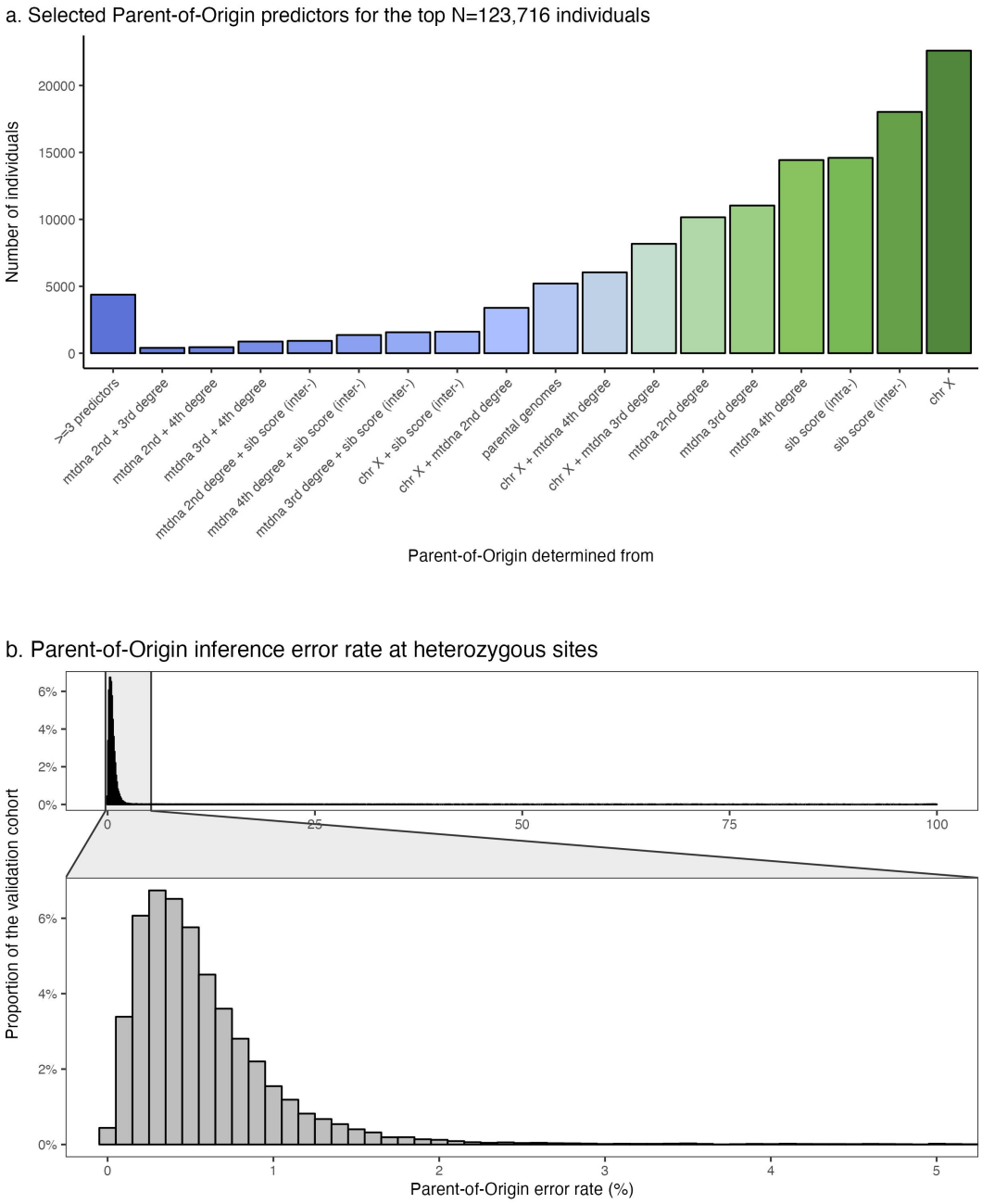

Fig. 2 | Selected parent-of-origin predictors and error rate. **a**) Distribution of selected PofO predictors for individuals having a PofO probability greater than 0.99 (see Supplementary Figure 13 for full distribution). **b**) Distribution of the PofO error rate. Errors were computed at heterozygous site only by comparing the PofO determined using our approach to the one obtained from parental genomes. There are on average 2.06% of errors. This is inflated by individuals for which entire haplotypes are incorrect, resulting from inter-chromosomal phasing errors, totaling 64 haplotypes (in the validation cohort). These are likely due to the presence of relatives sharing both paternal and maternal IBD segments, which may be due to consanguinity, and were not filtered out during the construction of the validation cohort. As a result, only a few individuals' haplotypes inflate the global error rate and most of them have a PofO correctly assigned. Indeed, the majority of haplotypes (83.9%) exhibit error rates below 1%, and half of the haplotypes have less than 0.48% of errors.

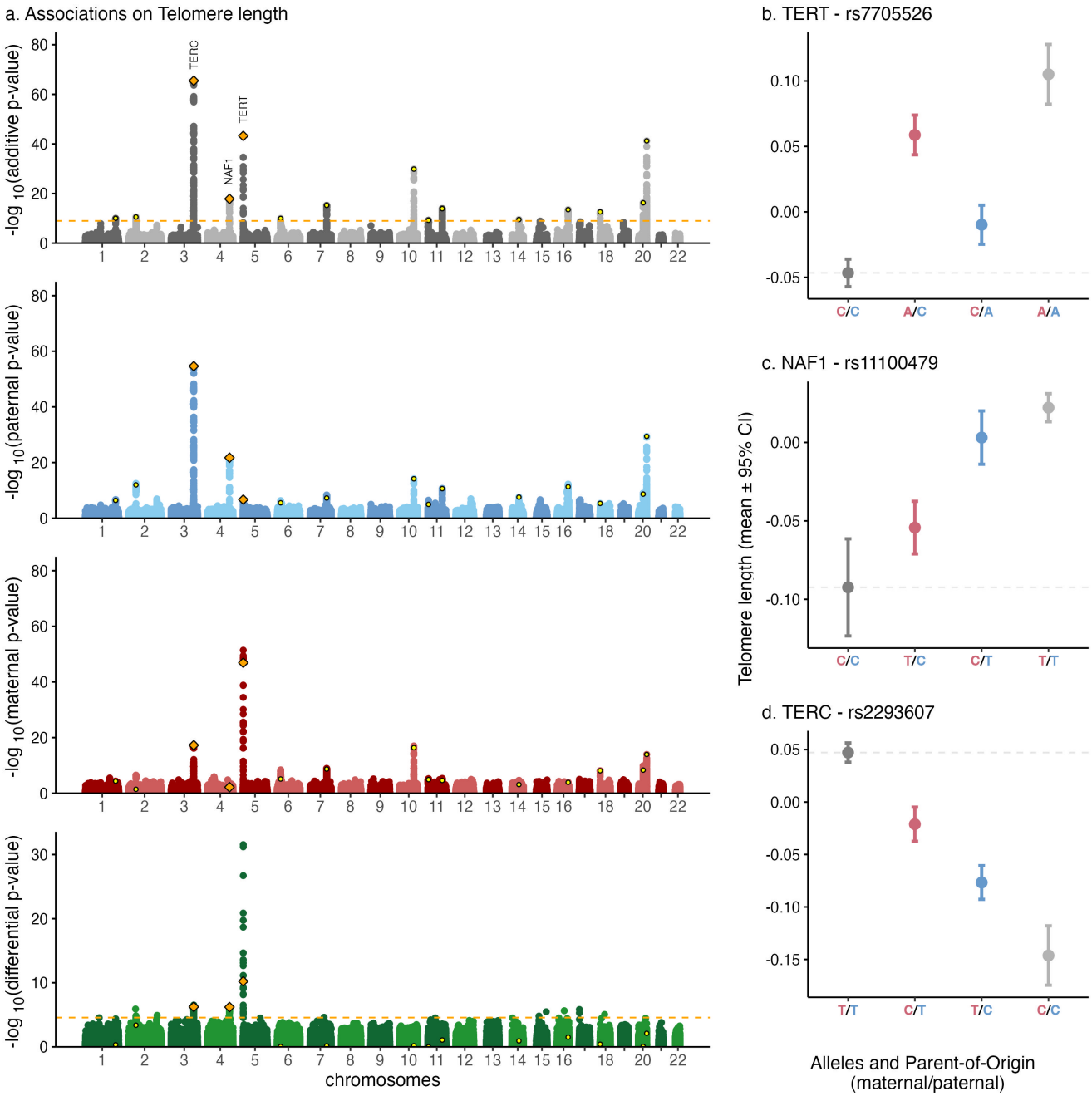

Fig. 3 | Parent-of-origin associations on telomere length. a) Genome-wide associations for additive (grey), paternal (blue), maternal (red) and differential (green) effects represented as association strength ($-log_{10}(p-value)$, y-axis) along genomic position (x-axis). Each point represent a genetic variants. Yellow dots indicate additive genome-wide significant variants (those then tested for POE). Orange diamond indicate variant exhibiting significant POE among the lead additive effect variants. Orange dashed lines indicate significant thresholds (1×10^{-9} for the additive effects and 3.1×10^{-6} for POEs). **b-d**) Genotypes and PofO of alleles (x-axis) effects on telomere length (y-axis). Red and blue alleles indicate maternal and paternal alleles, respectively. Dots show mean values, error bars show 95% confidence intervals. Grey dashed line represent the mean value of individual carrying no alternative allele (i.e genotype 0).

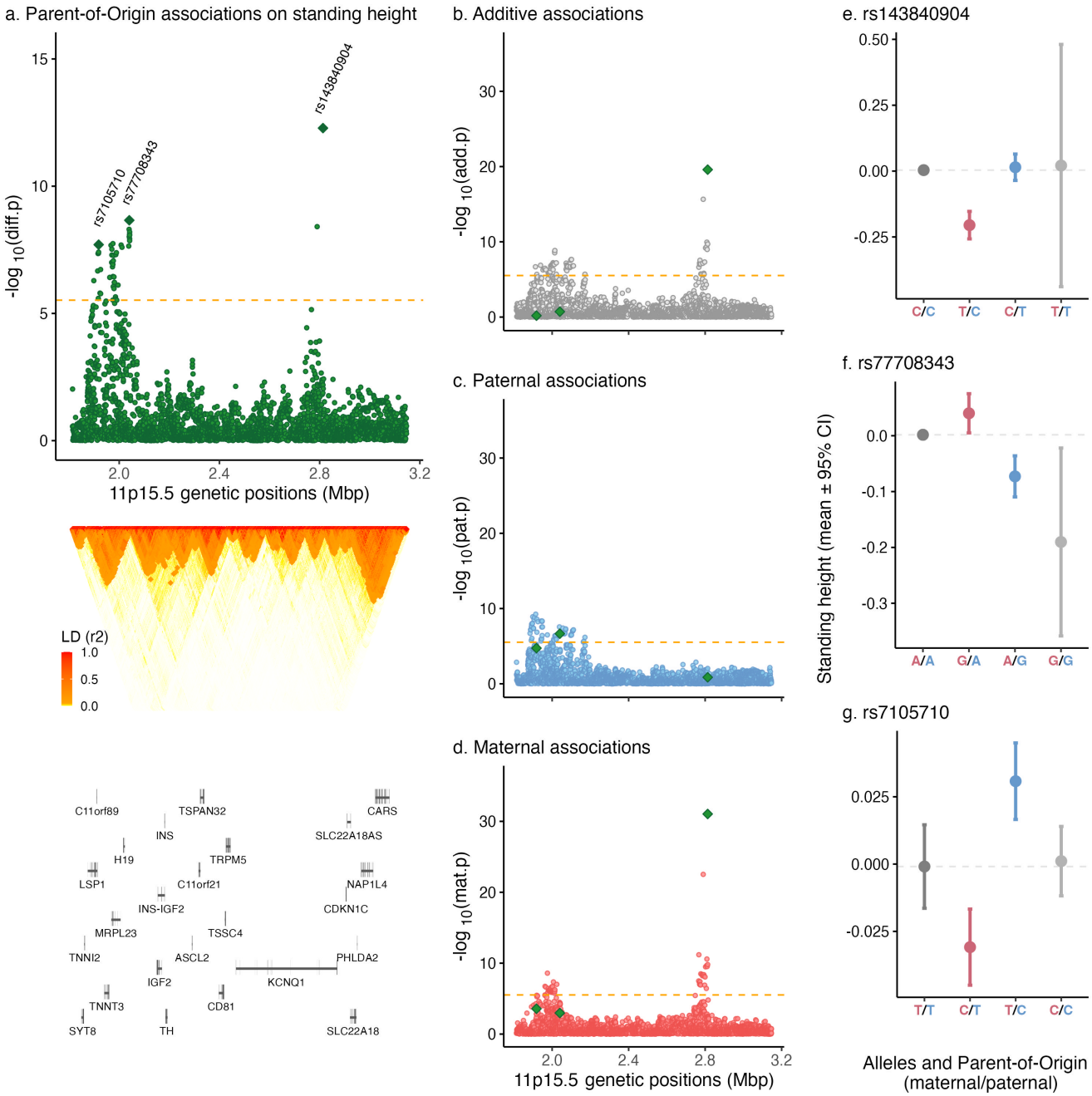

Fig. 4 | Parent-of-Origin associations on standing height. **a**) Differential GWAS (top) shows the association strength ($-log_{10}(p-value)$, y-axis) along genomic position (x-axis). Each point represent a genetic variants. Diamonds indicate variants with independent POE on standing height found in this study. Linkage Disequilibrium (LD) pattern (middle) ranges from LD=0 (white) to LD=1 (red). Gene positions (bottom) along the 11p15.5 imprinted region (x-axis). Horizontal lines show the gene start and end positions. Vertical lines show the exons start and end positions. Gene names are shown below the corresponding gene coordinates. **b-d**) Additive (b, grey), Paternal (c, blue) and Maternal (d, red) associations on standing height shown as association strength ($-log_{10}(p-value)$, y-axis) along genomic position (x-axis). Green diamonds indicate POEs selected in the differential scan. **e-g**) Genotypes and PofO of alleles (x-axis) effects on standing height (y-axis). Red and blue alleles indicate maternal and paternal alleles, respectively. Dots show mean values, error bars show 95% confidence intervals. Grey dashed line represent the mean value of individual carrying no alternative allele (i.e genotype 0).

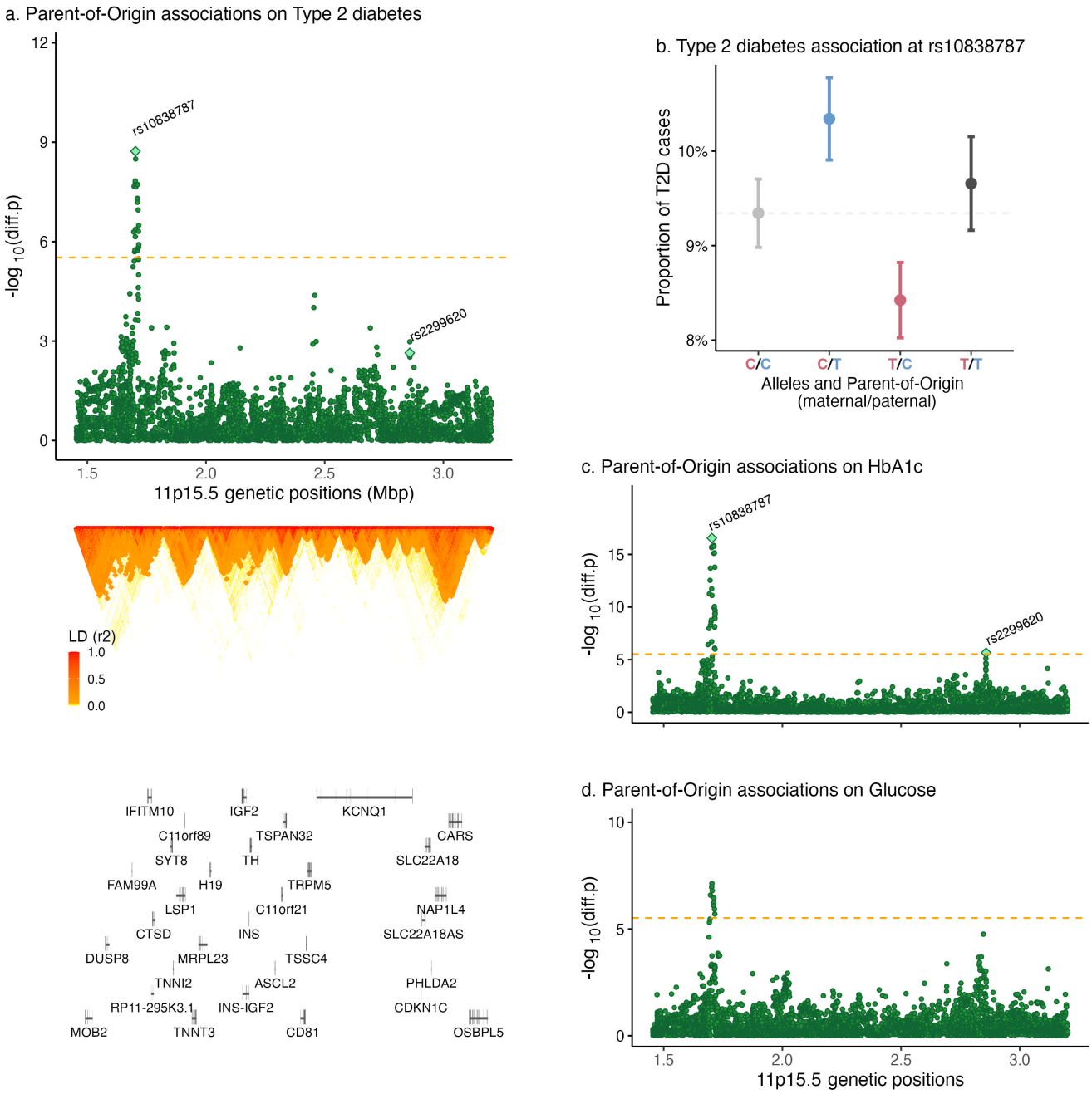

Fig. 5 | Parent-of-origin associations on type 2 diabetes and blood biomarkers at 7q32.3. a) Differential GWAS (top) shows the association strength ($-log_{10}(p-value)$, y-axis) along genomic position (x-axis). Each point represent a genetic variants. Diamonds indicate lead POE variants reported in the results section. Dashed orange line represents the significance threshold used in this study when focusing on imprinted regions (3.1×10^{-06}). Linkage Disequilibrium (LD) pattern (middle) range from LD=0 (white) to LD=1 (red). Gene positions (bottom) along the 11p15.5 imprinted region (x-axis). Horizontal lines show the gene start and end positions. Vertical lines show the exons start and end positions. Gene names are shown below the corresponding gene coordinates. **b**) Proportion of type-2-diabetes cases and 95% confidence intervals (y-axis) per genotype and PofO groups (x-axis). Red and blue alleles indicate maternal and paternal alleles, respectively. Dots show mean values, error bars show 95% confidence intervals. Grey dashed line represent the mean value of individual carrying no alternative allele (i.e genotype 0). **c-d**) Differential GWAS for (**c**) glycated haemoblogin (HbA1c), and (**d**) glucose. Association strength ($-log_{10}(p-value)$, y-axis) along genomic position (x-axis). Each point represent a genetic variants. Dashed orange line represents the significance threshold used in this study when focusing on imprinted regions (3.1×10^{-6}). Diamonds indicate lead POE variants reported in the results section.

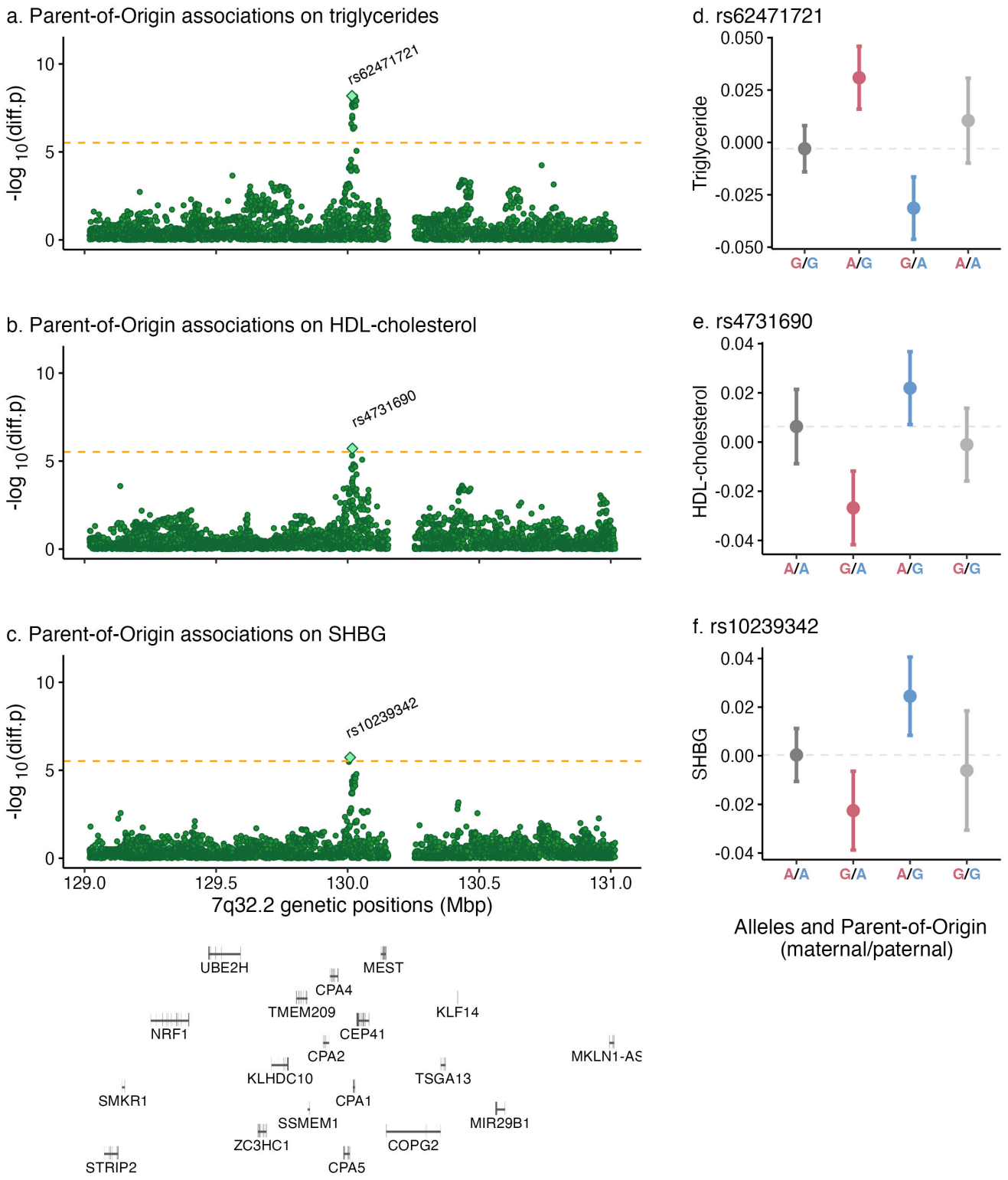

Fig. 6 | Parent-of-Origin associations on Triglyceride, HDL-cholesterol and SHBG at 11p15.5. a-c) Differential GWAS show the association strength ($-log_{10}(p-value)$, y-axis) along genomic position (x-axis) for (**a**) triglycerides, (**b**) HDL-cholesterol, and (**c**) SHBG. Each point represent a genetic variants. Diamonds indicate lead POE variants. Dashed orange line represents the significance threshold used in this study when focusing on imprinted regions (3.1×10^{-6}). Bottom panel shows gene positions along the genomic positions (x-axis). **d-f**) Genotypes and PofO of alleles (x-axis) effects on traits (y-axis). Red and blue alleles indicate maternal and paternal alleles, respectively. Dots show mean values, vertical bars show 95% confidence intervals. Grey dashed line represent the mean value of individual carrying no alternative allele (i.e genotype 0).

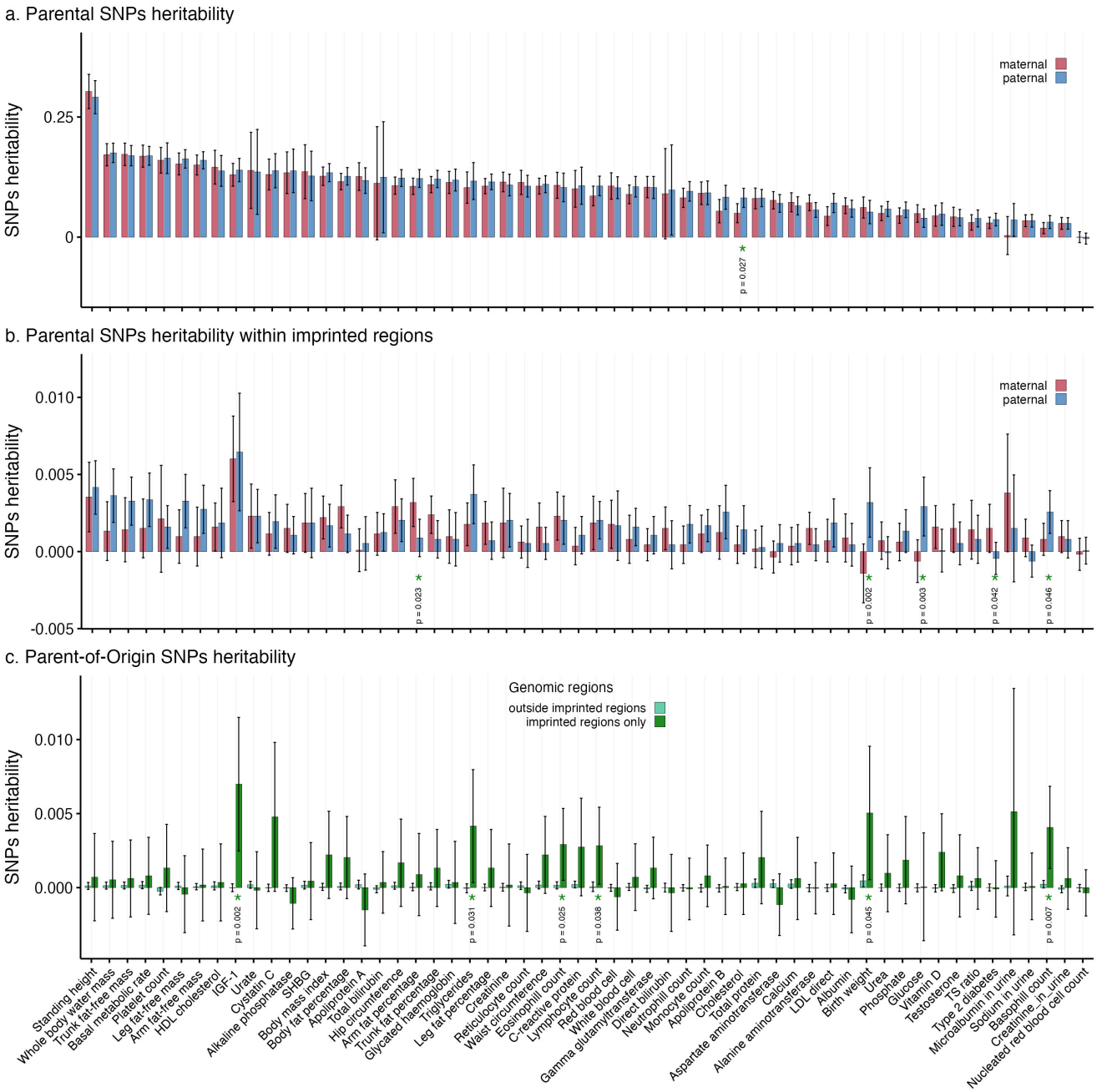

Fig. 7 | SNPs heritability. SNPs heritability (h^2, y-axis) across 56 traits tested (x-axis). Paternal (blue) and maternal (red) h^2 was estimated (**a**) genome-wide and (**b**) within imprinted regions. Stars and p-value indicate nominal significant differences between paternal and maternal h^2. **c**) h^2_{POE} was estimated within and outside imprinted regions. Stars and p-value indicate nominal significant differences between h^2_{POE} within imprinted regions *vs* outside imprinted regions. Three out of the 59 selected traits were not represented here due to disproportionate standard errors: lipoprotein A, rheumatoid factor and oestradiol.

Tables

CHR	GENPOS	ID	A0	A1	A1FREQ	BETA PAT	SE PAT	P PAT	BETA MAT	SE MAT	P MAT	BETA DIFF	SE DIFF	P DIFF	BETA ADD	SE ADD	P ADD	PHENAME	Status	Locus
3	169482335	rs2293607	T	C	0.245	-0.122	0.008	2.26E-55	-0.068	0.008	5.36E-18	-0.055	0.011	5.70E-07	-0.095	0.006	3.34E-66	TS ratio	novel	TERC
4	164012901	rs11100479	C	T	0.778	0.079	0.008	1.82E-22	0.022	0.008	6.61E-03	0.057	0.012	6.25E-07	0.050	0.006	1.46E-18	TS ratio	novel	NAF1
5	1285974	rs7705526	C	A	0.323	0.038	0.007	2.09E-07	0.106	0.007	1.27E-47	-0.068	0.010	5.82E-11	0.072	0.005	5.78E-44	TS ratio	known	TERT
11	2813322	rs143840904	C	T	0.019	-0.023	0.015	1.37E-01	-0.183	0.016	9.13E-32	0.152	0.021	5.21E-13	-0.100	0.011	2.56E-20	Standing height	known	*KCNQ1*
11	2857194	rs2237895	A	C	0.418	0.012	0.007	7.54E-02	0.051	0.007	8.34E-15	-0.040	0.009	2.16E-05	0.031	0.005	1.79E-11	Glycated haemoglobin	novel (tags known T2D)	*KCNQ1*
14	101176212	rs12881545	G	C	0.675	0.015	0.007	3.41E-02	0.086	0.007	9.44E-36	-0.072	0.010	2.34E-13	0.050	0.005	8.60E-25	Platelet count	known	MEG3

Table 1 | Significant Parent-of-origin effects within additive regions.
CHR: chromosome; GENPOS: genetic position (hg19); ID: variant rs id; A0: reference allele; A1: assessed allele; A1FREQ: A1 allele frequency. BETA, SE and P denote effect sizes, standard errors and P-values; PAT, MAT, DIFF and ADD denote paternal, maternal, differential and additive tests; PHENAME: phenotype name.

CHR	GENPOS	ID	A0	A1	A1FREQ	BETA PAT	SE PAT	P PAT	BETA MAT	SE MAT	P MAT	BETA DIFF	SE DIFF	P DIFF	BETA ADD	SE ADD	P ADD	PHENAME	STATUS	Locus
11	1918083	**rs7105710**	T	C	0.545	0.017	0.004	1.84E-05	-0.014	0.004	2.65E-04	0.032	0.005	1.98E-08	0.001	0.002	0.18	Standing height*	novel	H19, MRPL23, TNNT3
11	2040272	**rs77708343**	A	G	0.039	-0.055	0.011	2.21E-07	0.034	0.010	1.07E-03	-0.088	0.015	2.18E-09	-0.010	0.007	1.92E-01	Standing height*	known	IGF2, H19
11	2813322	rs143840904	C	T	0.019	-0.023	0.015	1.37E-01	-0.183	0.016	9.13E-32	0.152	0.021	5.21E-13	-0.100	0.011	2.56E-20	Standing height*	known	KCNQ1
11	2040272	**rs77708343**	A	G	0.040	-0.048	0.011	1.25E-05	0.035	0.011	1.33E-03	-0.083	0.015	7.53E-08	-0.006	0.008	4.34E-01	Basal metabolic rate	novel	IGF2, MRLP32, TNNI2
11	2040272	**rs77708343**	A	G	0.040	-0.052	0.011	1.28E-06	0.033	0.011	2.06E-03	-0.085	0.015	1.80E-08	-0.009	0.008	2.29E-01	Leg fat-free mass*	novel	IGF2, MRLP32, TNNI2
11	2040272	**rs77708343**	A	G	0.040	-0.044	0.010	3.08E-05	0.033	0.010	1.23E-03	-0.077	0.015	1.63E-07	-0.005	0.007	5.32E-01	Whole body water mass	novel	IGF2, MRLP32, TNNI2
11	2041348	**rs78507815**	G	T	0.053	-0.031	0.009	7.03E-04	0.033	0.009	1.86E-04	-0.065	0.013	3.61E-07	0.002	0.006	7.68E-01	Trunk fat-free mass	novel	IGF2, MRLP32, TNNI2
11	1703564	**rs4417225**	C	T	0.426	0.029	0.008	9.26E-05	-0.028	0.008	2.04E-04	0.057	0.011	7.40E-08	0.001	0.005	8.85E-01	Glucose	novel (tags known T2D)	H19, IGF2
11	1702929	**rs10838787**	G	A	0.425	0.136	0.027	3.88E-07	-0.091	0.027	7.55E-04	0.228	0.038	1.87E-09	0.023	0.019	2.26E-01	Type 2 diabetes	known	H19, IGF2
11	1702929	**rs10838787**	G	A	0.425	0.050	0.007	2.34E-14	-0.028	0.007	1.80E-05	0.078	0.009	2.77E-17	0.011	0.005	1.76E-02	Glycated haemoglobin*	novel (tags known T2D)	H19, IGF2
11	2858295	rs2299620	C	T	0.036	-0.011	0.018	5.22E-01	-0.129	0.017	1.50E-13	0.116	0.024	2.23E-06	-0.072	0.013	9.05E-09	Glycated haemoglobin	novel (tags known T2D)	KCNQ1
11	1920285	rs4264135	A	G	0.293	-0.033	0.006	1.83E-07	0.014	0.006	3.31E-02	-0.046	0.009	2.22E-07	-0.010	0.005	2.90E-02	Urate	novel	MRLP23, H19, IGF2
11	1998031	**rs170102**	G	A	0.346	-0.041	0.006	5.96E-11	0.026	0.006	3.19E-05	-0.067	0.009	5.98E-14	-0.007	0.004	9.47E-02	Cystatin C*	novel	MRLP23, H19, IGF2
11	2003944	**rs217215**	T	G	0.656	0.030	0.006	2.53E-07	-0.024	0.006	2.68E-05	0.054	0.008	4.94E-11	0.003	0.004	5.04E-01	Creatinine*	novel	MRLP23, H19, IGF2
7	130009312	**rs10239342**	T	G	0.309	0.022	0.007	1.36E-03	-0.024	0.007	4.15E-04	0.045	0.009	1.87E-06	-0.001	0.005	8.17E-01	SHBG	novel	KLF14, MEST, COPG2
7	130016470	**rs62471721**	G	A	0.351	-0.023	0.007	9.70E-04	0.033	0.007	1.57E-06	-0.057	0.010	6.51E-09	0.005	0.005	2.85E-01	Triglycerides*	novel	KLF14, MEST, CPA4, COPG2
7	130017940	**rs4731690**	A	G	0.503	0.019	0.006	1.97E-03	-0.022	0.006	2.76E-04	0.041	0.009	1.92E-06	-0.002	0.004	7.01E-01	HDL cholesterol	novel	MEST, CPA4, COPG2
7	130463192	rs6467315	C	G	0.509	0.001	0.006	9.02E-01	-0.042	0.006	5.81E-11	0.043	0.009	2.20E-06	-0.021	0.005	5.72E-06	Hip circumference	novel (tags known T2D)	KLF14
20	57216538	**rs80116540**	A	G	0.075	0.035	0.010	4.38E-04	-0.043	0.010	2.04E-05	0.078	0.014	3.39E-08	-0.004	0.007	6.09E-01	Arm fat percentage*	novel	GNAS, STX16, CTSZ
20	57216538	**rs80116540**	A	G	0.075	0.037	0.010	2.65E-04	-0.037	0.010	2.27E-04	0.074	0.014	2.06E-07	0.000	0.007	9.90E-01	Body fat percentage	novel	GNAS, STX16, CTSZ
20	57226079	**rs6026426**	C	G	0.070	0.045	0.012	3.08E-04	-0.040	0.012	1.37E-03	0.085	0.018	1.29E-06	0.003	0.009	7.64E-01	Trunk fat percentage	novel	GNAS, STX16, CTSZ
20	57484934	**rs3730173**	C	T	0.052	0.036	0.010	3.18E-04	-0.035	0.010	3.95E-04	0.071	0.014	5.32E-07	0.000	0.007	9.95E-01	Leg fat percentage	novel	GNAS, CTSZ
6	144274210	rs12528876	T	C	0.171	-0.036	0.009	2.58E-05	0.021	0.009	1.60E-02	-0.057	0.012	2.96E-06	-0.008	0.006	1.96E-01	IGF-1	novel	PLAGL1
16	3412861	rs7188903	A	G	0.703	-0.012	0.007	1.03E-01	0.041	0.007	5.35E-08	-0.053	0.011	6.14E-07	0.014	0.005	7.24E-03	IGF-1	novel	ZNF597, NAA60
15	25983333	**rs146982369**	C	G	0.014	0.101	0.032	1.88E-03	-0.106	0.032	9.99E-04	0.208	0.044	2.59E-06	-0.003	0.023	8.82E-01	Total protein	novel	ATP10A
14	101185187	rs59228823	G	C	0.245	-0.010	0.008	2.04E-01	-0.092	0.008	3.87E-34	0.082	0.011	1.92E-14	-0.051	0.005	2.36E-21	Platelet count*	known	MEG3

Table 2 | Significant Parent-of-origin effect within imprinted regions.

CHR: chromosome; GENPOS: genetic position (hg19); ID: variant rs id; A0: reference allele; A1: assessed allele; A1FREQ: A1 allele frequency. BETA, SE and P denote effect sizes, standard errors and P-values; PAT, MAT, DIFF and ADD denote paternal, maternal, differential and additive tests. PHENAME: phenotype name; *: robust when correcting for the number of phenotype tested; bold ID: bi-polar POEs. Highlighted colors denote clusters of POEs associated with traits sharing substantial similarities.

CHR	GENPOS	ID	A0	A1	A1FREQ	BETA PAT	SE PAT	P PAT	BETA MAT	SE MAT	P MAT	BETA DIFF	SE DIFF	P DIFF	BETA ADD	SE ADD	P ADD	PHENAME	STATUS
14	101176212	rs12881545	G	C	0.668	0.826	0.023	2.26E-274	0.187	0.023	1.24E-15	0.642	0.033	3.03E-84	0.505	0.016	2.34E-206	DLK1	primary pQTL and POE-pQTL
7	129938598	rs34587586	G	T	0.404	-0.434	0.024	2.77E-71	-0.634	0.024	4.44E-149	0.201	0.034	5.60E-09	-0.532	0.017	1.53E-210	CPA4	primary pQTL
7	129940561	rs12538292	G	A	0.327	-0.432	0.025	4.85E-65	-0.667	0.025	2.32E-151	0.238	0.036	3.51E-11	-0.548	0.018	7.76E-205	CPA4	primary POE-pQTL
2	207311349	rs72933203	T	A	0.104	1.017	0.035	1.45E-190	0.723	0.034	9.02E-102	0.293	0.048	1.29E-09	0.865	0.024	1.01E-281	ADAM23	primary pQTL
2	207413625	rs13429599	G	A	0.270	0.719	0.024	5.93E-204	0.457	0.024	9.30E-84	0.263	0.034	4.34E-15	0.576	0.017	4.18E-267	ADAM23	primary POE-pQTL
1	7914177	rs228647	G	A	0.570	0.506	0.023	6.87E-110	0.241	0.023	4.13E-26	0.264	0.032	1.95E-16	0.375	0.016	7.50E-120	PER3	primary pQTL
1	7856346	rs228682	T	C	0.401	0.540	0.023	4.34E-121	0.241	0.023	1.09E-25	0.297	0.032	5.41E-20	0.395	0.016	4.32E-128	PER3	primary POE-pQTL

Table 3 | Significant Parent-of-Origin protein QTLs.

CHR: chromosome; GENPOS: genetic position (hg19); ID: variant rs id; A0: reference allele; A1: assessed allele; A1FREQ: A1 allele frequency. BETA, SE and P denote effect sizes, standard errors and P-values; PAT, MAT, DIFF and ADD denote paternal, maternal, differential and additive tests. PHENAME: phenotype name.

Supplementary Figures

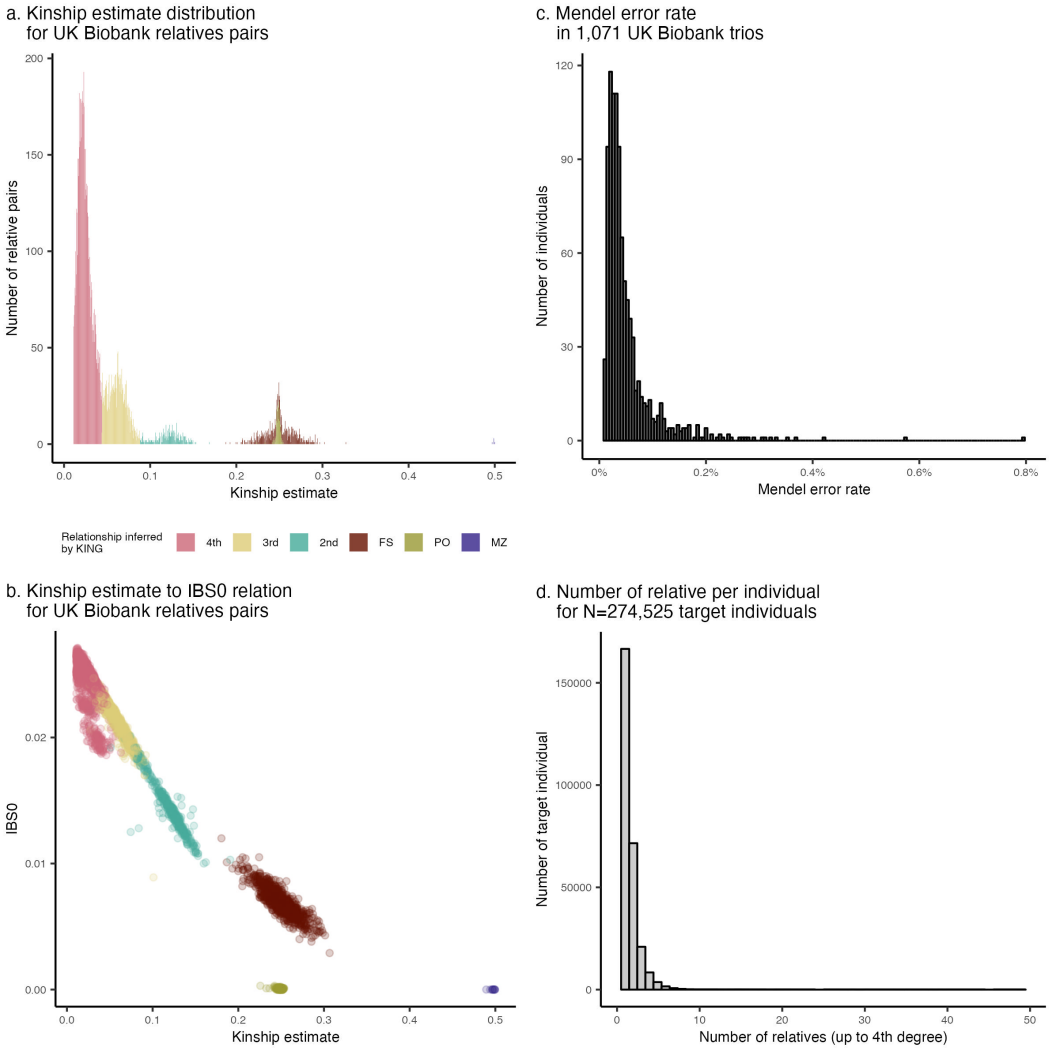

Supplementary Fig. 1 | Relatedness inference and close relative clustering in the UK Biobank. a) Kinship estimates distribution and **b**) Kinship estimates versus IBS0 estimates across all UK Biobank monozygotic twins (MZ), first siblings (FS), parent-offspring (PO), second-, third-, and fourth-degree relative pairs. **c**) Mendel error rate distribution across 1,071 UK Biobank parent-offspring trios. None of the trios exhibited a high error rate that would necessitate exclusion. **d**) Distribution of the number of close relatives (up to the fourth degree) per individual across 274,252 UK Biobank individuals with available surrogate parent cluster(s). We found on average 1.65 relatives per individual.

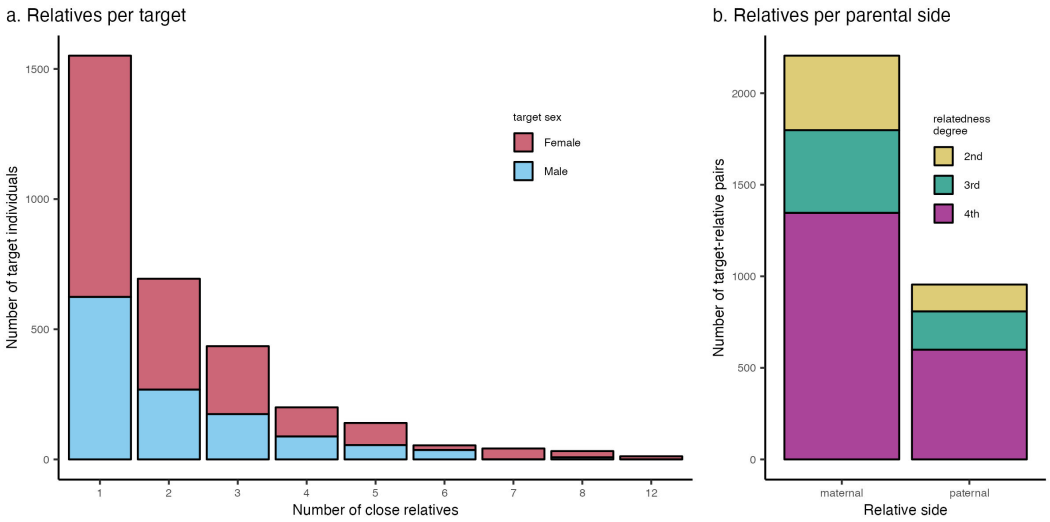

Supplementary Fig. 2 | Validation cohort structure. **a**) Distribution of the number of close relatives (up to the fourth degree) per individual across 2,141 UK Biobank individuals with both available surrogate parent cluster(s) and available parental genomes. Most target individuals are females (60.3%) and have a single surrogate parent (49%). **b**) Distribution of surrogate mother and surrogate father stratified by relatedness degree for 3,160 target-relative pairs. Approximately 70% of surrogate parents in the validation cohort are on the maternal side (i.e., surrogate mothers), and the majority are fourth-degree relatives pairs (61.5%).

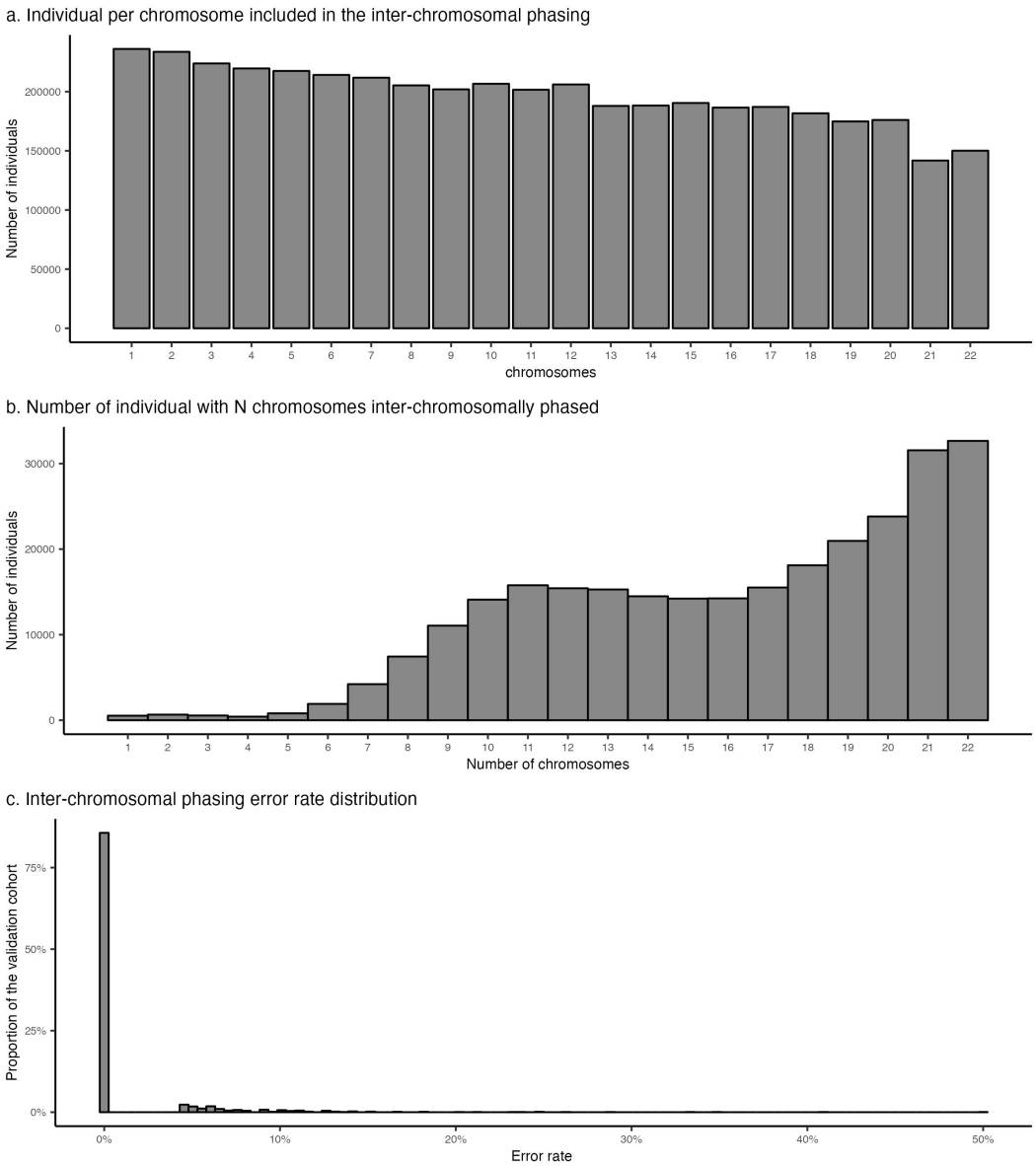

Supplementary Fig. 3 | Inter-chromosomal phasing from close relative groups. **a**) Distribution of the number of individuals with a given chromosome included in the inter-chromosomal phasing. The sample sizes vary across chromosomes, as inter-chromosomal phasing requires at least one IBD segment shared with a surrogate parent on the chromosome. Larger chromosomes are more frequently included, likely due to a higher likelihood of containing at least one IBD segment. **b**) Distribution of the number of individuals with N chromosomes (x-axis) successfully included in the inter-chromosomal phasing. Only 12% of individuals (32,651) had all 22 autosomes phased inter-chromosomally. On average, individuals had 16 chromosomes included in inter-chromosomal phasing. **c**) Distribution of inter-chromosomal phasing error rates across individuals in the validation cohort. Error rates were calculated by comparing phasing results based on surrogate parents to the ground truth obtained from available parental genomes. Most individuals (85.6%) were perfectly phased, with an average error rate of only 1.06% for flipped haplotypes, underscoring the robustness and reliability of the inter-chromosomal phasing method in accurately resolving parental haplotype sets.

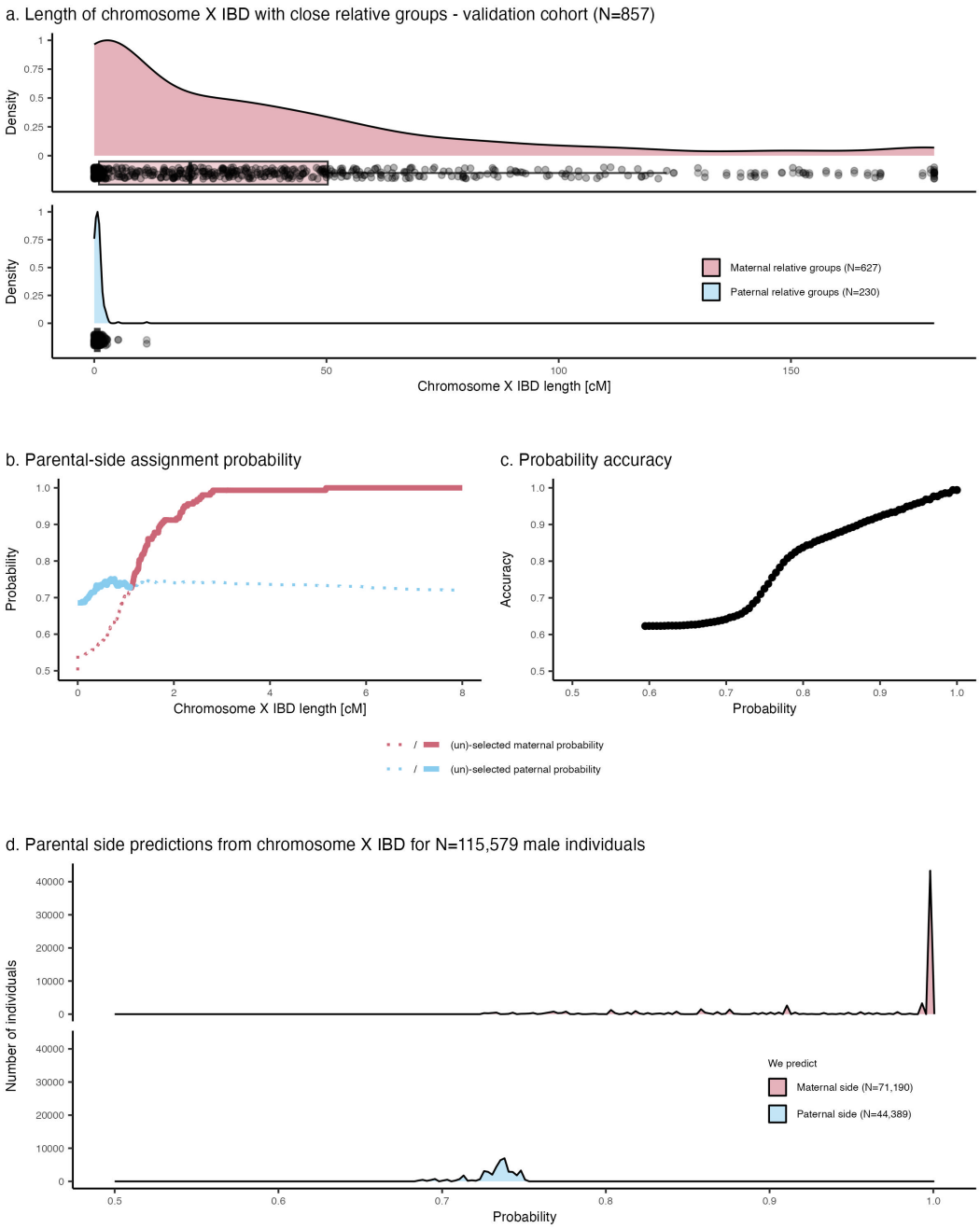

Supplementary Fig. 4 | Parental side assignment from chromosome X IBD analysis in male individuals. a) Density distribution of chromosome X IBD segment length in centimorgan (cM) between targets and surrogate father (blue) and targets and surrogate mother (red) across the validation cohort's male individuals. Boxes indicate the interquartile range (IQR), with the bottom and top of the box representing the 25th (Q1) and 75th (Q3) percentiles, respectively. The horizontal line within the box represents the median (50th percentile). Whiskers extend to the smallest and largest values within $Q1-1.5 \times IQR$ and $Q3 + 1.5 \times IQR$. Each point represent a target-relative pair. **b**) Parental side probabilities depending on chromosome X IBD segment length derived from the validation cohort. Selected and unselected maternal (red) and paternal (blue) probabilities for a given x-axis value are indicated by solid and dotted lines, respectively. **c**) Accuracy of parental side predictions (y-axis) as a function of the parental side probability (x-axis). **d**) Distribution of maternal (red) and paternal (blue) side assignment probabilities derived chromosome X IBD across 115,579 UK Biobank male individuals.

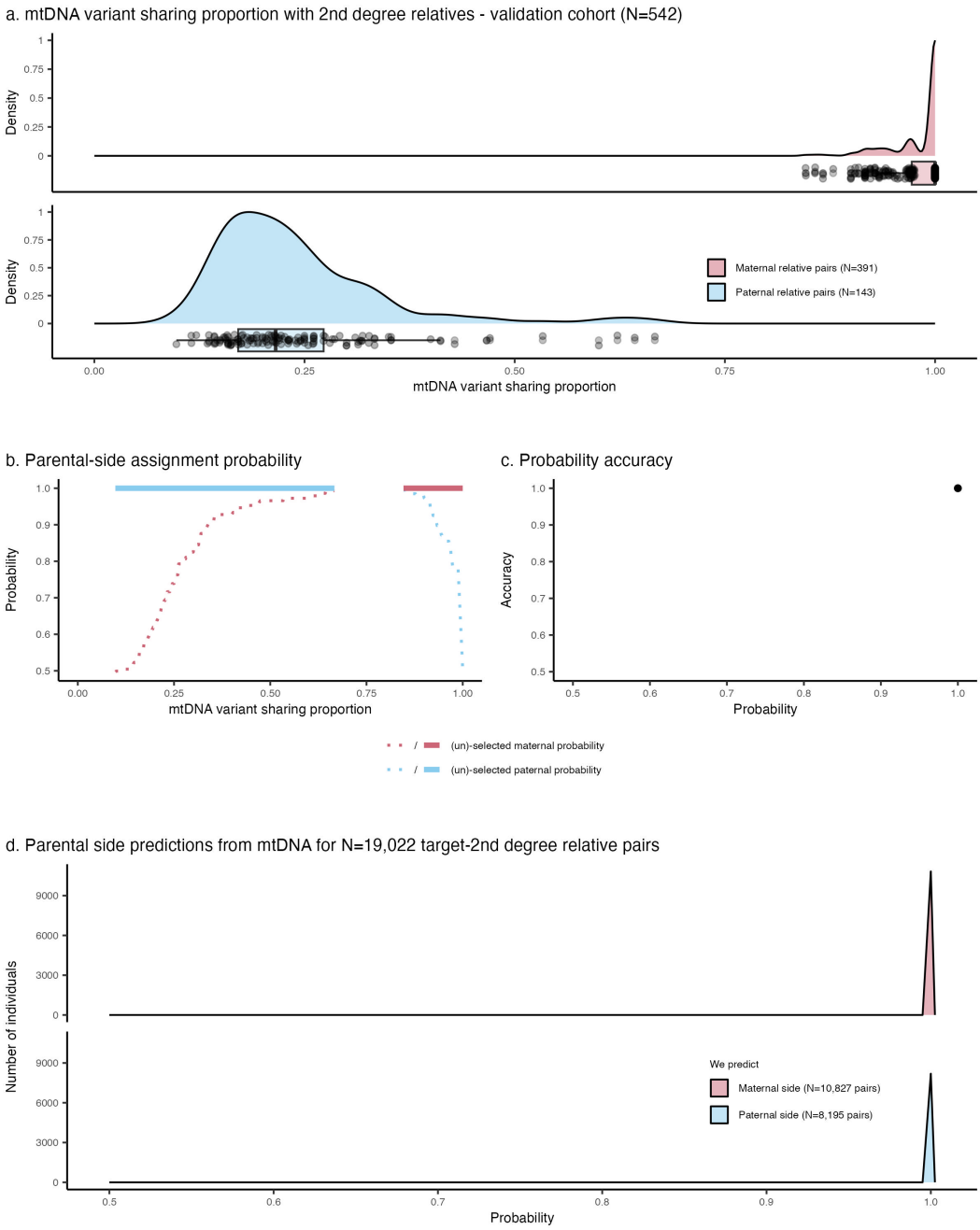

Supplementary Fig. 5 | Parental side assignment from mitochondrial DNA Minor Variant Sharing (MVS) analysis in 2nd degree relative pairs. a) Density distribution of mtDNA Minor Variant Sharing (MVS) between targets and 2nd degree surrogate father (blue) and targets and 2nd degree surrogate mother (red) across the validation cohort's individuals. Boxes indicate the interquartile range (IQR), with the bottom and top of the box representing the 25th (Q1) and 75th (Q3) percentiles, respectively. The horizontal line within the box represents the median (50th percentile). Whiskers extend to the smallest and largest values within $Q1-1.5 \times IQR$ and $Q3 + 1.5 \times IQR$. Each point represent a target-relative pair. **b**) Parental side probabilities depending on mtDNA MVS derived from the validation cohort. Selected and unselected maternal (red) and paternal (blue) probabilities for a given x-axis value are indicated by solid and dotted lines, respectively. **c**) Accuracy of parental side predictions (y-axis) as a function of the parental side probability (x-axis). **d**) Distribution of maternal (red) and paternal (blue) side assignment probabilities derived from mtDNA MVS across 19,022 UK Biobank 2nd degree relative pairs.

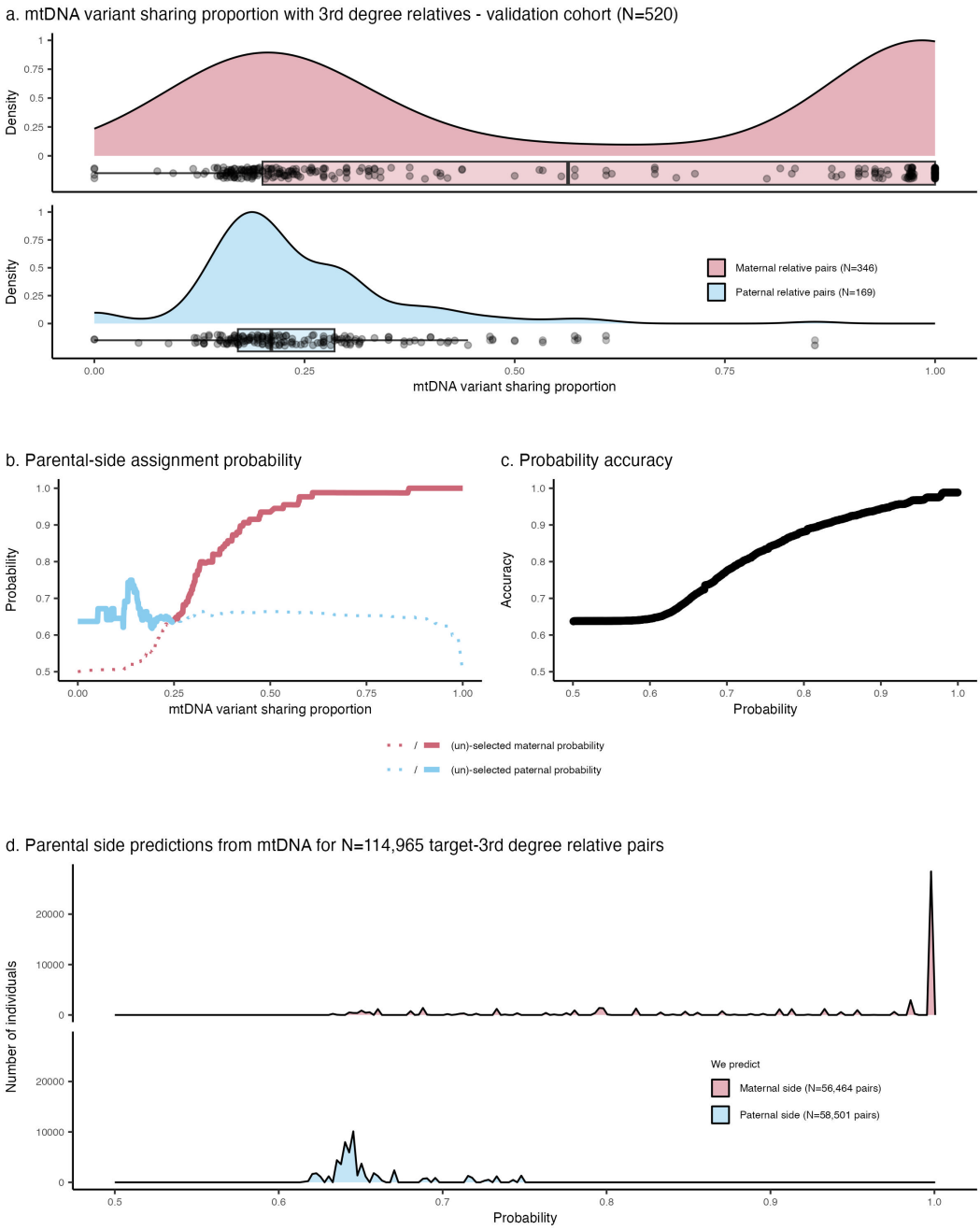

Supplementary Fig. 6 | Parental side assignment from mitochondrial DNA Minor Variant Sharing (MVS) analysis in 3rd degree relative pairs. a) Density distribution of mtDNA Minor Variant Sharing (MVS) between targets and 3rd degree surrogate father (blue) and targets and 3rd degree surrogate mother (red) across the validation cohort's individuals. Boxes indicate the interquartile range (IQR), with the bottom and top of the box representing the 25th (Q1) and 75th (Q3) percentiles, respectively. The horizontal line within the box represents the median (50th percentile). Whiskers extend to the smallest and largest values within $Q1-1.5 \times IQR$ and $Q3 + 1.5 \times IQR$. Each point represent a target-relative pair. **b**) Parental side probabilities depending on mtDNA MVS derived from the validation cohort. Selected and unselected maternal (red) and paternal (blue) probabilities for a given x-axis value are indicated by solid and dotted lines, respectively. **c**) Accuracy of parental side predictions (y-axis) as a function of the parental side probability (x-axis). **d**) Distribution of maternal (red) and paternal (blue) side assignment probabilities derived from mtDNA MVS across 114,965 UK Biobank 3rd degree relative pairs.

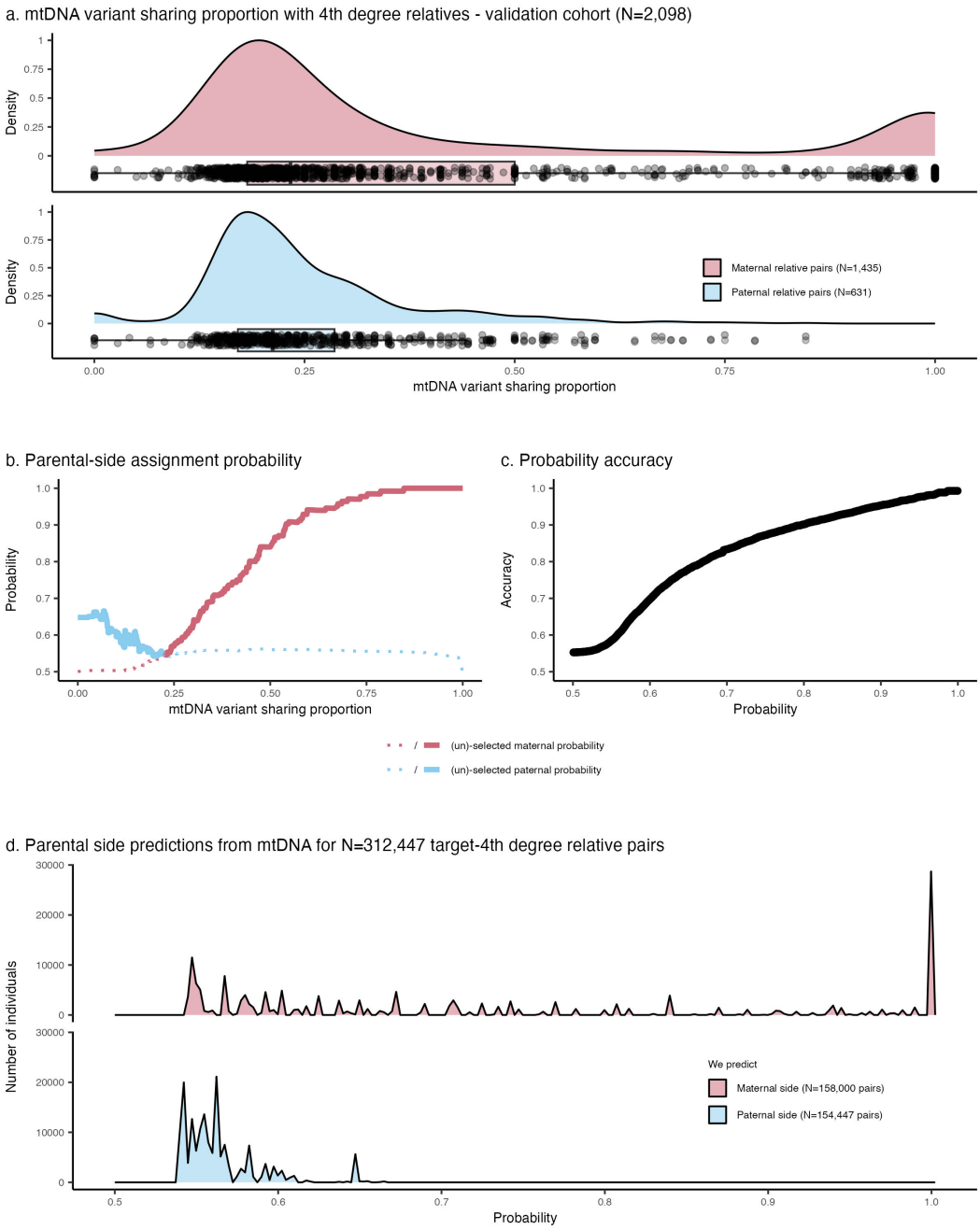

Supplementary Fig. 7 | Parental side assignment from mitochondrial DNA Minor Variant Sharing (MVS) analysis in 4th degree relative pairs. a) Density distribution of mtDNA Minor Variant Sharing (MVS) between targets and 4th degree surrogate father (blue) and targets and 4th degree surrogate mother (red) across the validation cohort's individuals. Boxes indicate the interquartile range (IQR), with the bottom and top of the box representing the 25th (Q1) and 75th (Q3) percentiles, respectively. The horizontal line within the box represents the median (50th percentile). Whiskers extend to the smallest and largest values within $Q1-1.5 \times IQR$ and $Q3+1.5 \times IQR$. Each point represent a target-relative pair. **b**) Parental side probabilities depending on mtDNA MVS derived from the validation cohort. Selected and unselected maternal (red) and paternal (blue) probabilities for a given x-axis value are indicated by solid and dotted lines, respectively. **c**) Accuracy of parental side predictions (y-axis) as a function of the parental side probability (x-axis). **d**) Distribution of maternal (red) and paternal (blue) side assignment probabilities derived from mtDNA MVS across 312,447 UK Biobank 4th degree relative pairs.

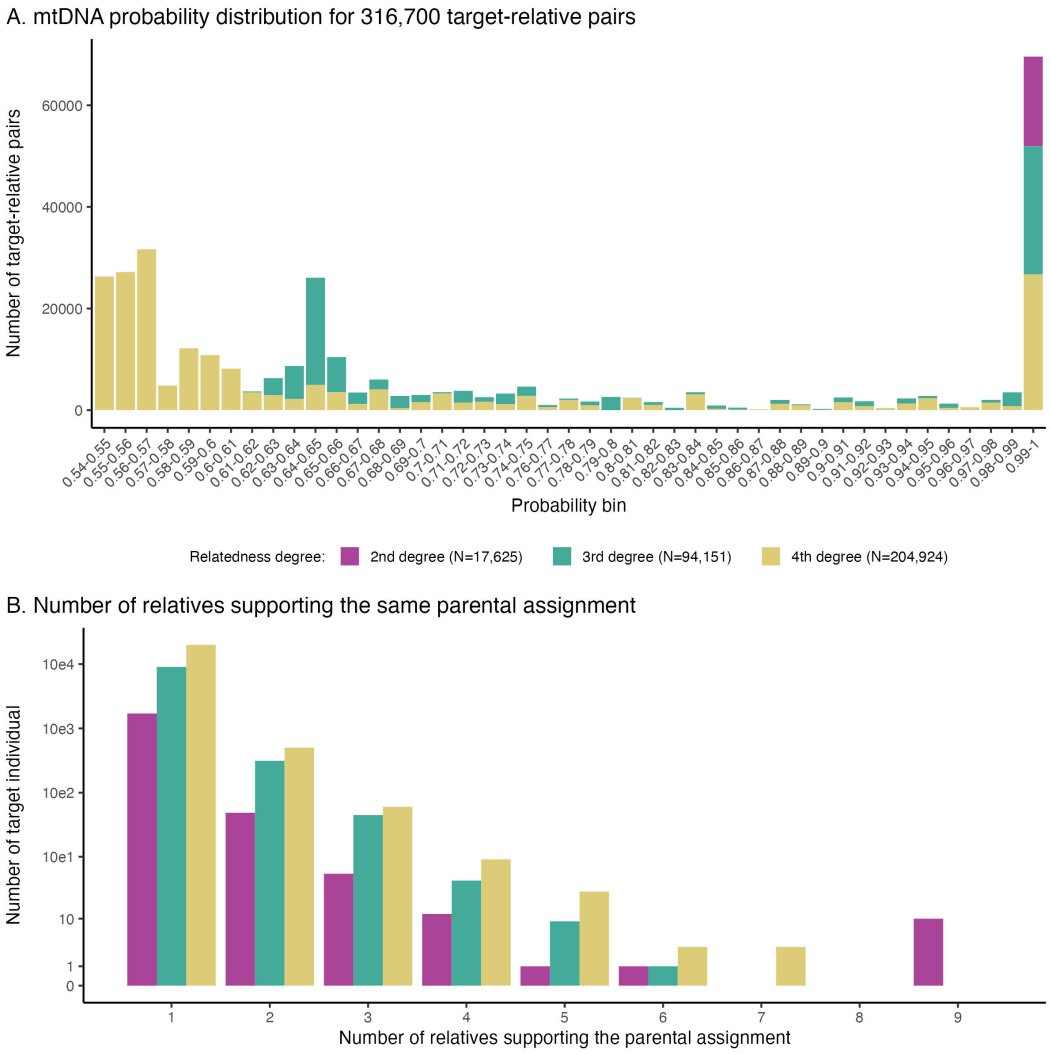

Supplementary Fig. 8 | Selection of mitochondrial DNA (mtDNA) Minor Variant Sharing (MVS) predictors for parental side assignments. a) Distribution of parental side assignment probabilities for 316,700 target-relative pairs, stratified by relatedness degree (2nd, 3rd, and 4th degree). For individuals with multiple relatives of the same degree, only the relative with the highest predicted accuracy was retained. Probabilities are binned at intervals of 0.01 for visualization. **b**) Log-scale distribution of the number of target individuals (y-axis) based on the number of relatives (x-axis) supporting the same parental side assignment, further stratified by degree of relatedness.

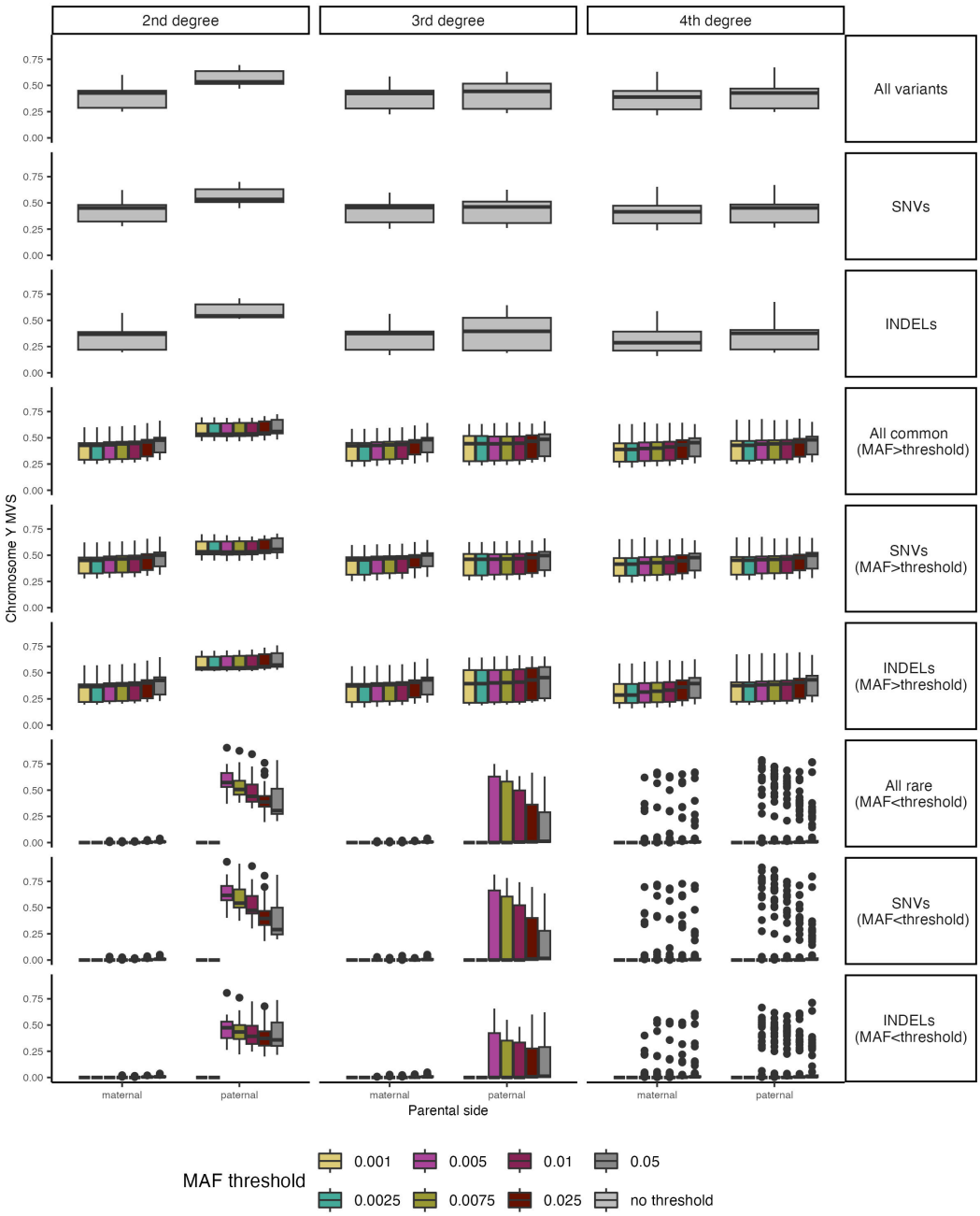

Supplementary Fig. 9 | Chromosome Y Minor Variant Sharing (MVS) analysis. The y-axis represents the proportion of chromosome Y minor variants shared (MVS), stratified by parental side assignments (maternal or paternal, x-axis), relatedness degrees (columns: 2nd, 3rd, and 4th degree), variant categories (rows), and minor allele frequency (MAF) thresholds (color-coded). Categories include all variants, single nucleotide variants (SNVs), insertions/deletions (INDELs), common variants (MAF > threshold), and rare variants (MAF < threshold). The MAF thresholds are denoted in the legend for clearer distinction of variant frequencies.

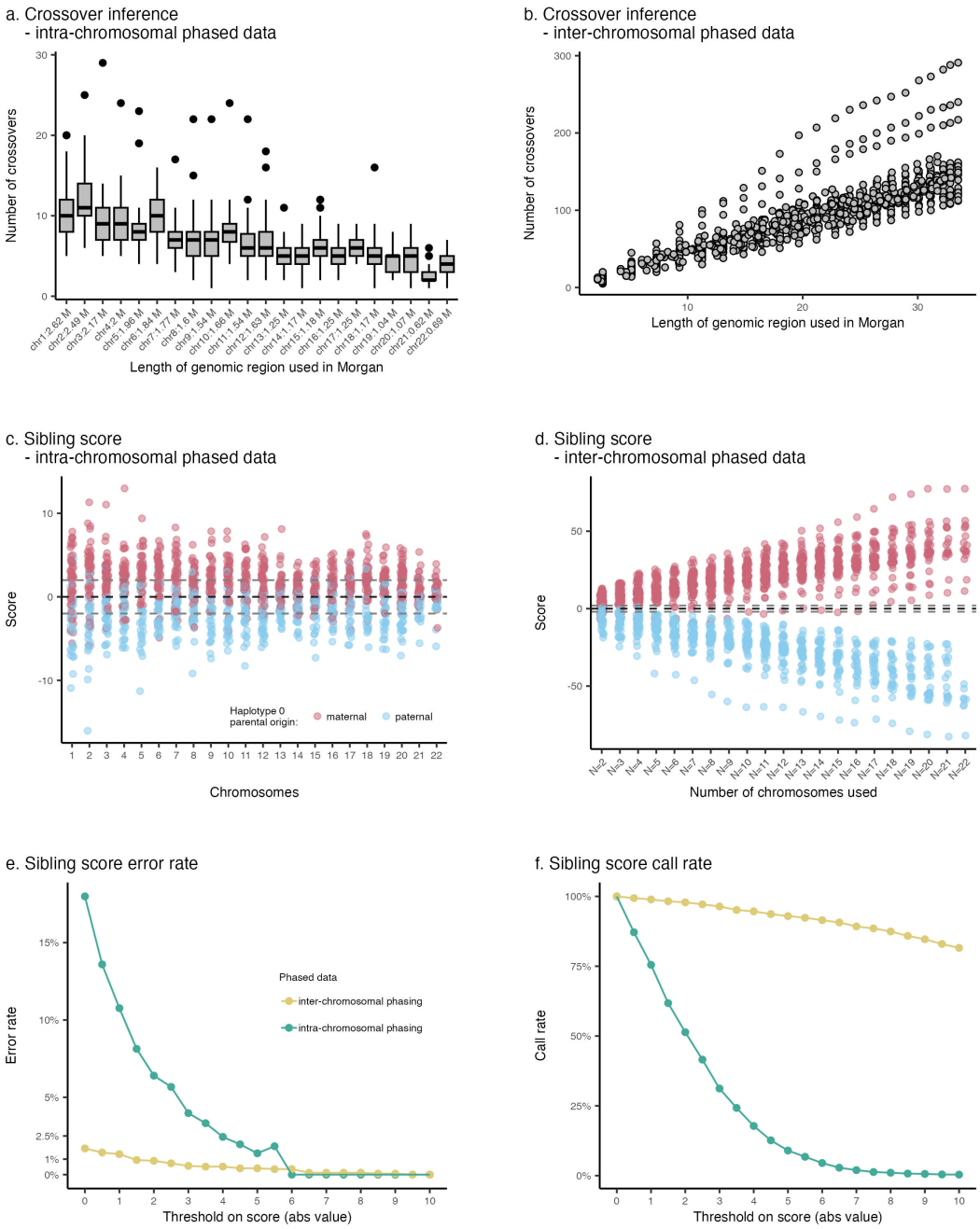

Supplementary Fig. 10 | Evaluation of sibling scores from intra- and inter-chromosomal phasing in N=88 individuals of the validation cohort. **a**) Distribution of the number of inferred crossovers (y-axis) per chromosome (x-axis) derived from intra-chromosomally phased data. **b**) Distribution of the number of inferred crossovers (y-axis) relative to the genomic length used (in Morgans, x-axis) derived from inter-chromosomally phased data. **c**) Distribution of sibling scores (y-axis) per chromosome (x-axis) using intra-chromosomally phased data. Maternal and paternal haplotypes are color-coded in red and blue, respectively. **d**) Distribution of sibling scores (y-axis) relative to the number of chromosomes included in inter-chromosomally phased data (x-axis). **e**) Error rates (y-axis) of sibling scores for varying score thresholds (absolute values, x-axis). For example, excluding ambiguous scores between -2 and 2 reduced error rates to 1.4% with inter-chromosomal phasing, compared to 6.4% with intra-chromosomal phasing. **f**) Call rates (y-axis) of sibling scores for varying score thresholds (absolute values, x-axis), showing the proportion of individuals meeting the threshold criteria.

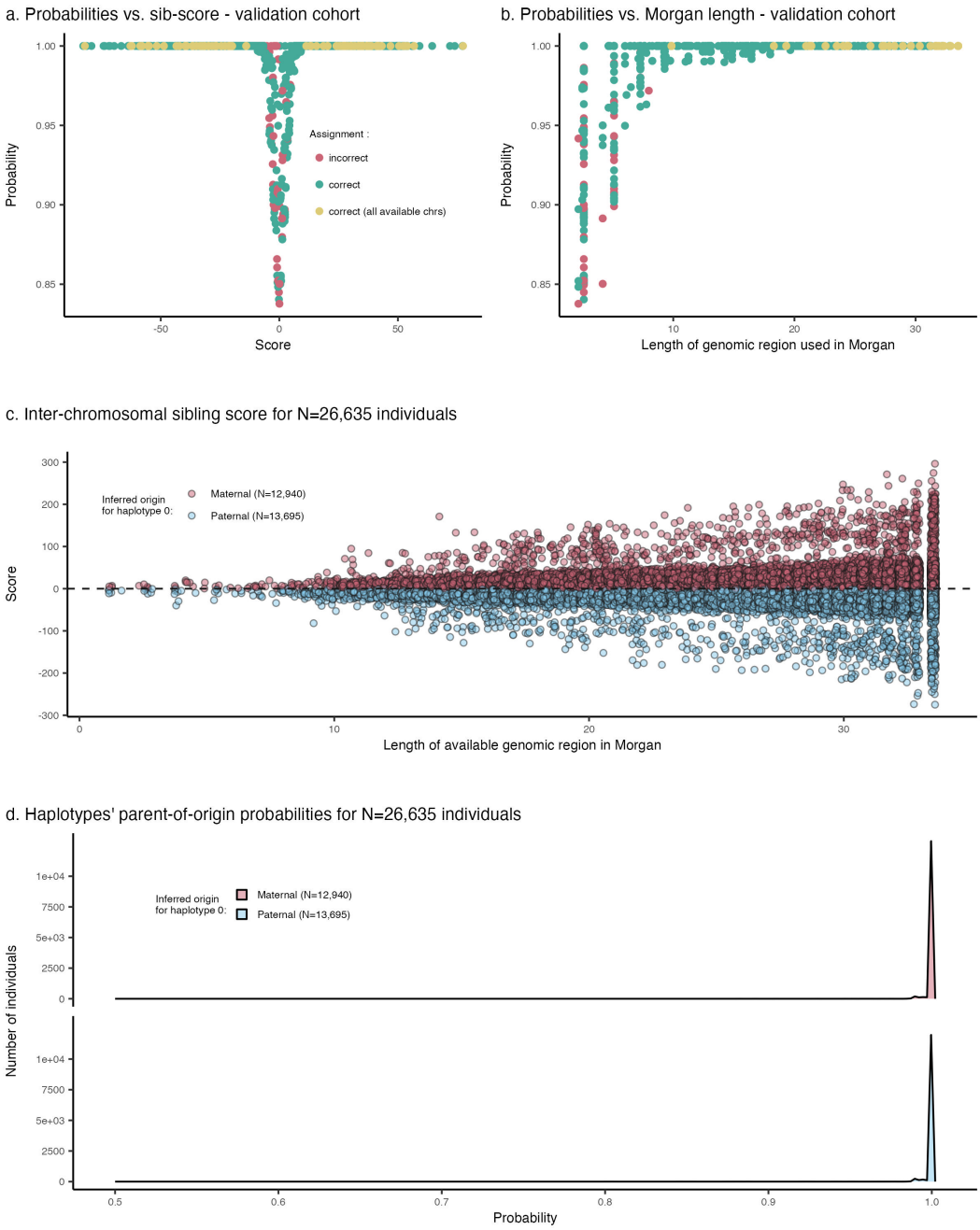

Supplementary Fig. 11 | Validation and derivation of parent-of-origin probabilities using sibling scores from inter-chromosomal phased data. **a**) PofO probabilities (y-axis) as a function of sibling scores (x-axis) in the validation cohort. Each dot represents a specific configuration (an individual with a given number of chromosomes used). We varied the number of chromosome used per individual to assess the accuracy of different configurations (see Supplementary Figure 10D). Red dots indicate incorrect parental assignments, green dots indicate correct assignments, and yellow dots denote correct assignments using the maximum available chromosomes (N_{max}, corresponds to the full set of inter-chromosomally phased chromosome for a given individual). No errors were observed when N_{max} chromosomes were used. **b**) PofO probabilities (y-axis) plotted against the total available genomic length in Morgans (x-axis) for sibling score calculation in the validation cohort. Each configuration is represented as a dot (color-coded as in panel a). Increasing genomic length results in higher assignment accuracy, with perfect accuracy achieved at N_{max} (yellow dots). **c**) Sibling scores (y-axis) derived for N=26,635 individuals across available genomic lengths (x-axis). Most configurations (99.5%) cover more than 10 Morgans and include over 30 inferred crossover events, ensuring high assignment accuracy (as indicated in the validation panels a and b). **d**) Distribution of PofO probabilities for 26,635 individuals. A majority of individuals (>95%) exhibit probabilities of 1, resulting in perfect accuracy within the validation cohort (see yellow dots in panel a).

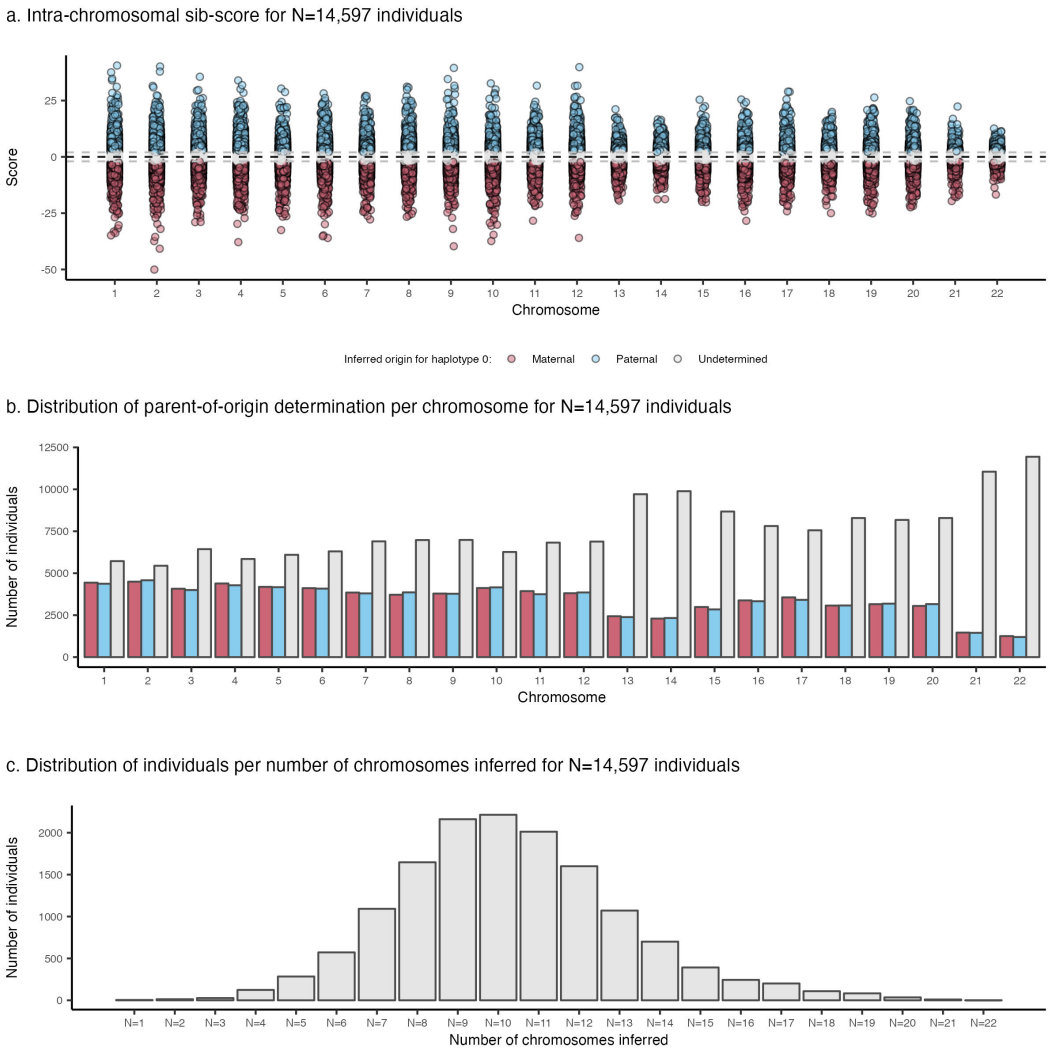

Supplementary Fig. 12 | Derivation of parent-of-origin probabilities using sibling scores from intra-chromosomal phased data. **a**) Sibling scores calculated for each chromosome independently (x-axis). Each dot corresponds to a single chromosome, with blue and red dots indicating paternal and maternal assignment, respectively, for the first haplotype. Undetermined assignments are shown in gray. **b**) Distribution of the number of individuals (y-axis) with inferred PofO for each chromosome (x-axis). Larger chromosomes exhibit higher numbers of PofO inference (e.g., 8,811 individuals for chromosome 1), while smaller chromosomes show fewer inferences (e.g., 2,450 individuals for chromosome 22), reflecting the increased likelihood of crossovers on larger chromosomes. **c**) Distribution of the number of chromosomes with inferred PofO per individual (x-axis), with counts shown on the y-axis. On average, individuals have 10.3 chromosomes with PofO inferred. This is lower compared to the average of 16 chromosomes inferred using inter-chromosomal phasing (see Supplementary Figure 3B).

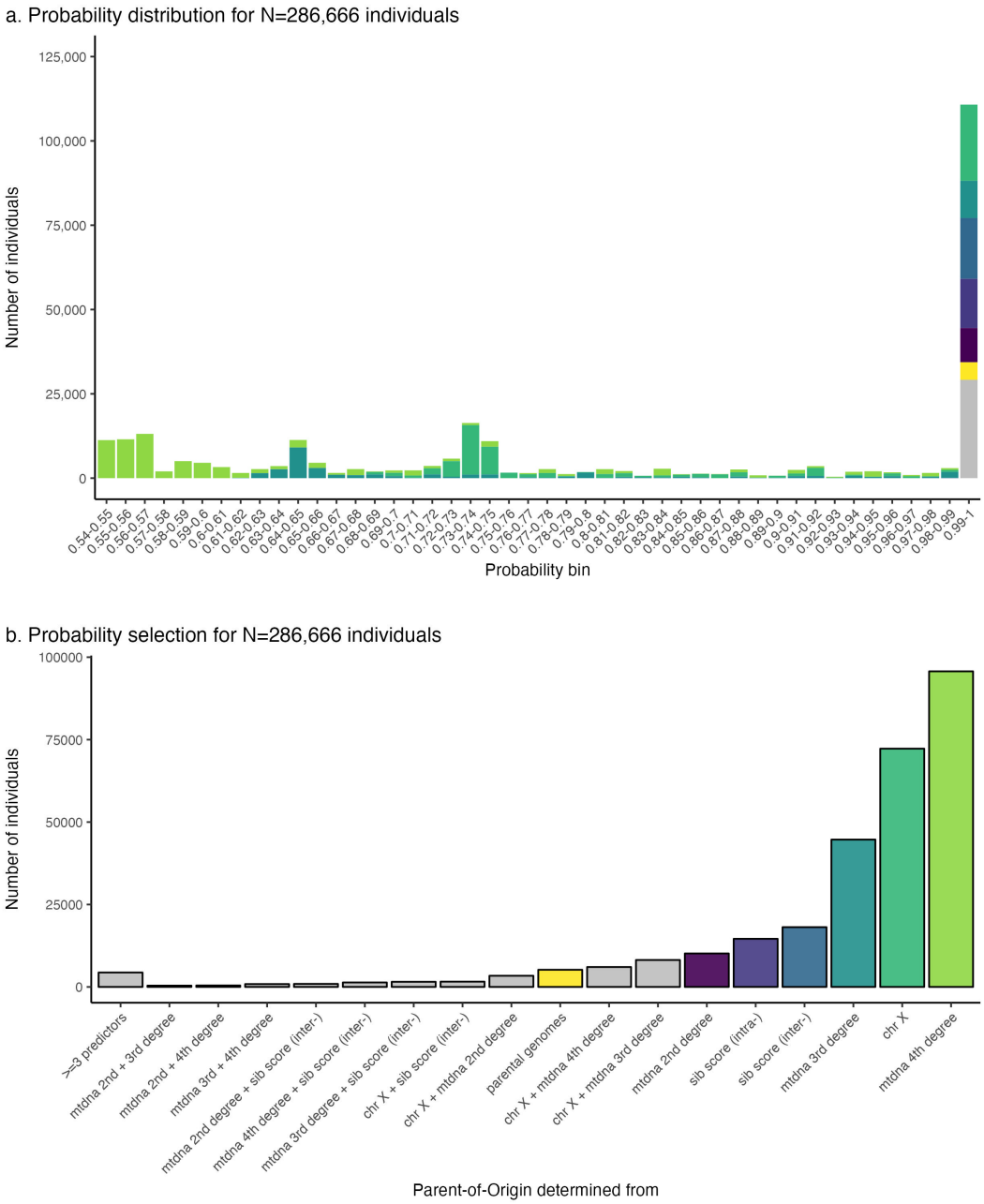

Supplementary Fig. 13 | Selection of parent-of-origin predictors. **a**) Distribution of PofO probabilities for N=286,666 individuals. The x-axis represents probability bins, and the y-axis shows the number of individuals. Colors correspond to the predictors used for PofO determination, as indicated in panel (b). **b**) Number of individuals (y-axis) with PofO inferred from various predictors (x-axis). Predictors include parental genomes, mtDNA MVS, chromosome X, sibling scores using either intra- or inter-chromosomal phasing, and combinations of these metrics across different degrees of relatedness. The largest contributions to PofO inference come from 4th degree relatives via mtDNA (light green).

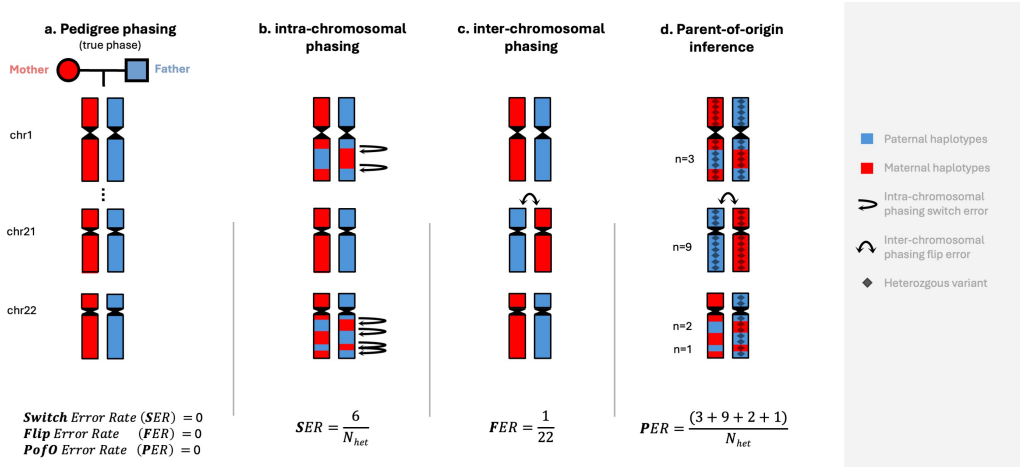

Supplementary Fig. 14 | Illustration of errors in statistical methods. a) A perfectly phased individual (both intra- and inter-chromosomally). Phasing is performed using the parental genomes: maternal (red) and paternal (blue). In this scenario, the PofO is directly inferred alongside the phasing process without errors. **b**) An individual with intra-chromosomal phasing errors introduced by traditional phasing software (e.g., SHAPEIT5[14]). These errors are represented as switches between parental haplotypes within the same chromosome (horizontal arrows), with 6 switches shown here. Since switches occur only at heterozygous sites, the switch error rate (SER) is calculated as $SER = 6/N_{het}$, where N_{het} is the total number of heterozygous sites. **c**) An individual with inter-chromosomal phasing errors but assumed perfect intra-chromosomal phasing (no switches within the same chromosome). Errors in this case are represented as flips of entire parental haplotypes across chromosomes (vertical arrow), with one flip shown here. The flip error rate (FER) is calculated as the proportion of chromosomes flipped relative to the majority, ranging from 0% to 50%. **d**) An individual with combined intra- and inter-chromosomal phasing errors. PofO inference errors aggregate contributions from both switch and flip errors. The PofO error rate (PER) is computed as the proportion of heterozygous sites (grey diamonds) incorrectly assigned. For example, in this scenario, assigning the first haplotype as maternal and the second as paternal results in a total of 15 errors.

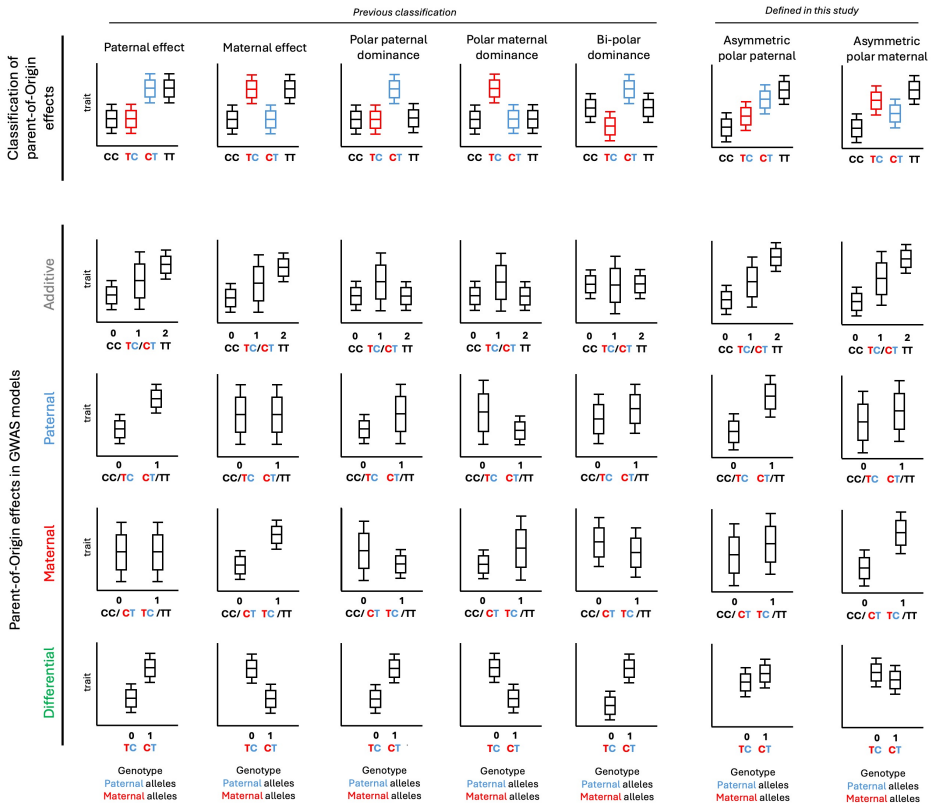

Supplementary Fig. 15 | Classification and detection of parent-of-origin effects in GWAS. Top panel illustrates the classification of POEs[16] and shows the variation in trait values (y-axis) across genotypes and parental origin of alleles (x-axis). Maternal alleles are shown in red, and paternal alleles are shown in blue. Boxplots represent the distribution of trait values for different genotypes: black boxes for homozygotes, red boxes for maternal heterozygotes, and blue boxes for paternal heterozygotes. Each boxplot includes the 25th, 50th (median), and 75th percentiles, with whiskers extending to the minimum and maximum values. **Bottom panels** show the interpretation of the different POEs (x-axis) using various GWAS models (y-axis), including additive, paternal, maternal, and differential models. In this study, we identified POEs using the differential GWAS model.

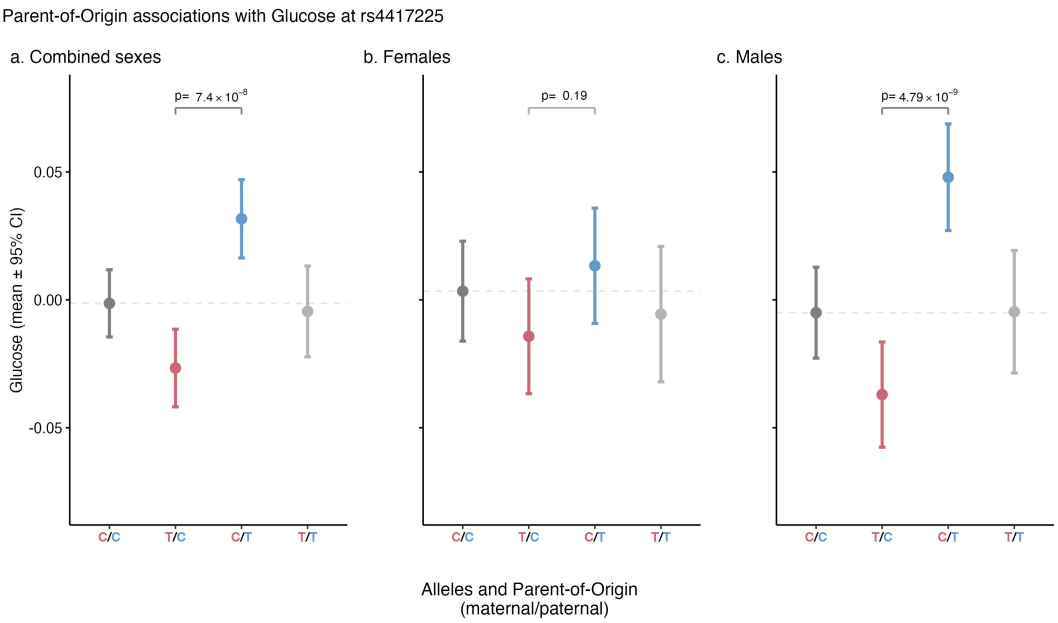

Supplementary Fig. 16 | Sex-specificity of glucose associations at rs4417225. Effects of genotypes and PofO of alleles (x-axis) on glucose level (y-axis) for (**a**) both sexes combined, (**b**) males only, and (**c**) females only. Red markers represent maternal alleles, while blue markers represent paternal alleles. The data points show the mean glucose levels, with error bars indicating the 95% confidence intervals. A grey dashed line represents the mean glucose level for individuals with the reference genotype (C/C). Significance values from the differential GWAS tests are annotated within each panel.

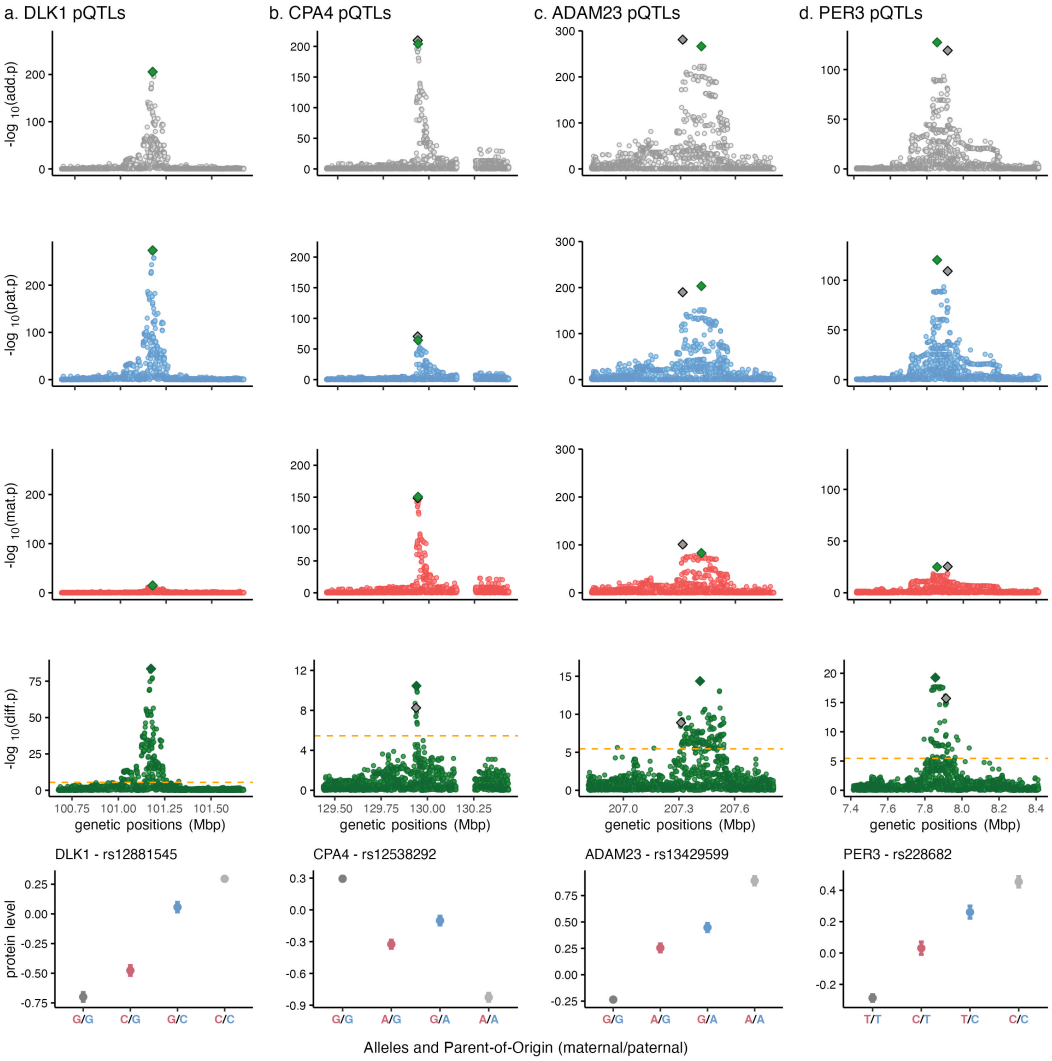

Supplementary Fig. 17 | Significant Parent-of-Origin pQTLs. Association strength ($-log_{10}(p - value)$, y-axis) along genomic position (x-axis) for additive (grey), paternal (blue), maternal (red) and differential (green) GWAS on (**a**) DLK1, (**b**) CPA4, (**c**) ADAM23 and (**d**) PER3. Diamonds show the primary additive association previously reported[22] (grey) and the primary POE-pQTL detected in this study (green). Orange dashed line indicate the significance threshold ($P_D < 0.05/14285 = 3.5 \times 10^{-6}$). **Bottom panel** show the effects of alleles and PofO on normalized protein levels.

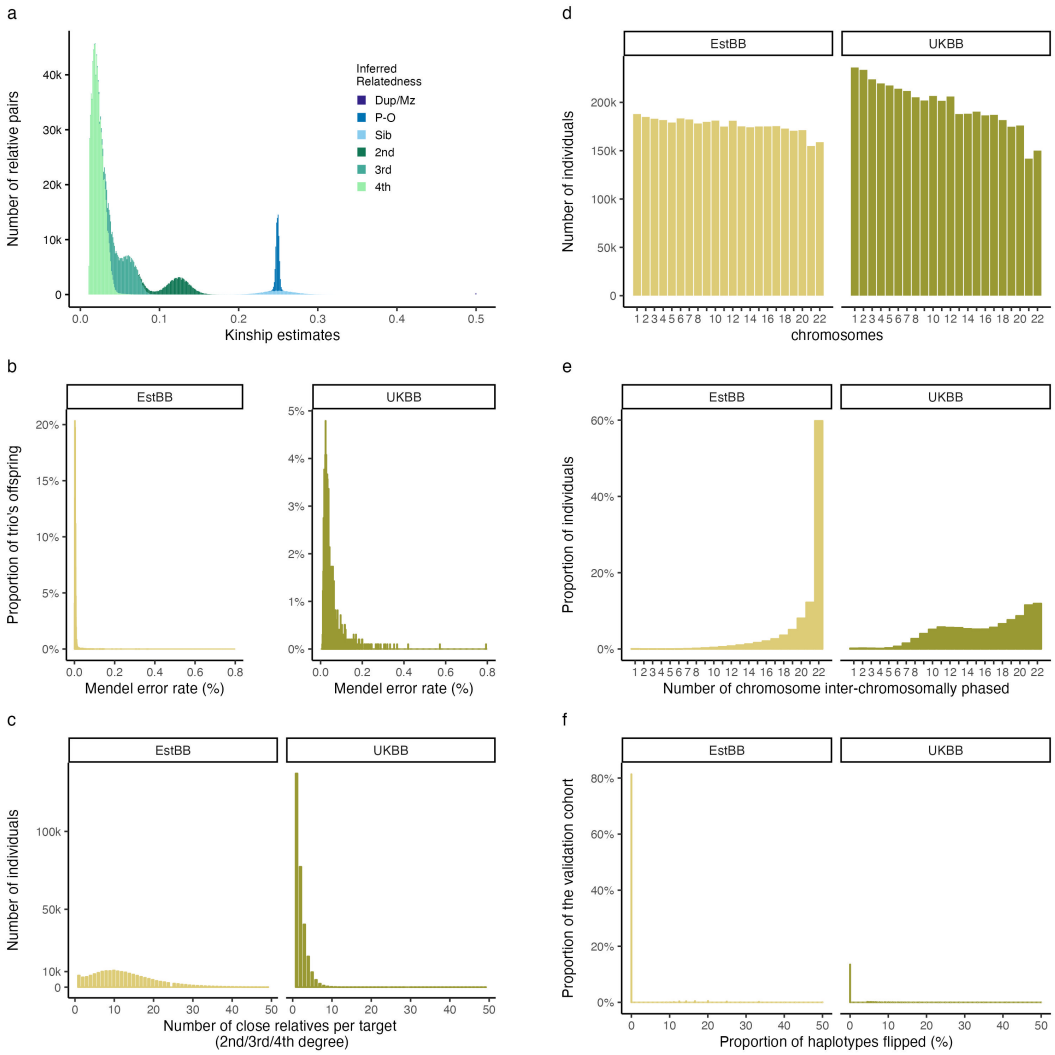

Supplementary Fig. 18 | Overview of relatedness metrics and inter-chromosomal phasing in the Estonian Biobank (EstBB), with comparisons to the UK Biobank (UKBB). a) Distribution of inferred relatedness across the EstBB cohort. Dup/MZ=monozygotic twins; P-O=parent-offspring; Sib=sibling; 2nd=2nd degree relative pairs; 3rd=3rd degree relative pairs; 4th=4th degree relative pairs. Relatedness was inferred using the KING software v2.2.7[45]. **b**) Distribution of Mendel error in trio's offspring for both the EstBB and UKBB cohorts. **c**) Distribution of the number of close relative per individual. **d**) Distribution of the number of individuals (y-axis) with a given chromosome (x-axis) successfully included in the inter-chromosomal phasing. **e**) Distribution of the number of individuals with N chromosomes (x-axis) successfully included in the inter-chromosomal phasing. **f**) Distribution of inter-chromosomal phasing error rate in the validation cohorts, calculated by comparing phasing results from surrogate parents to those obtained using parental genomes as the ground truth.

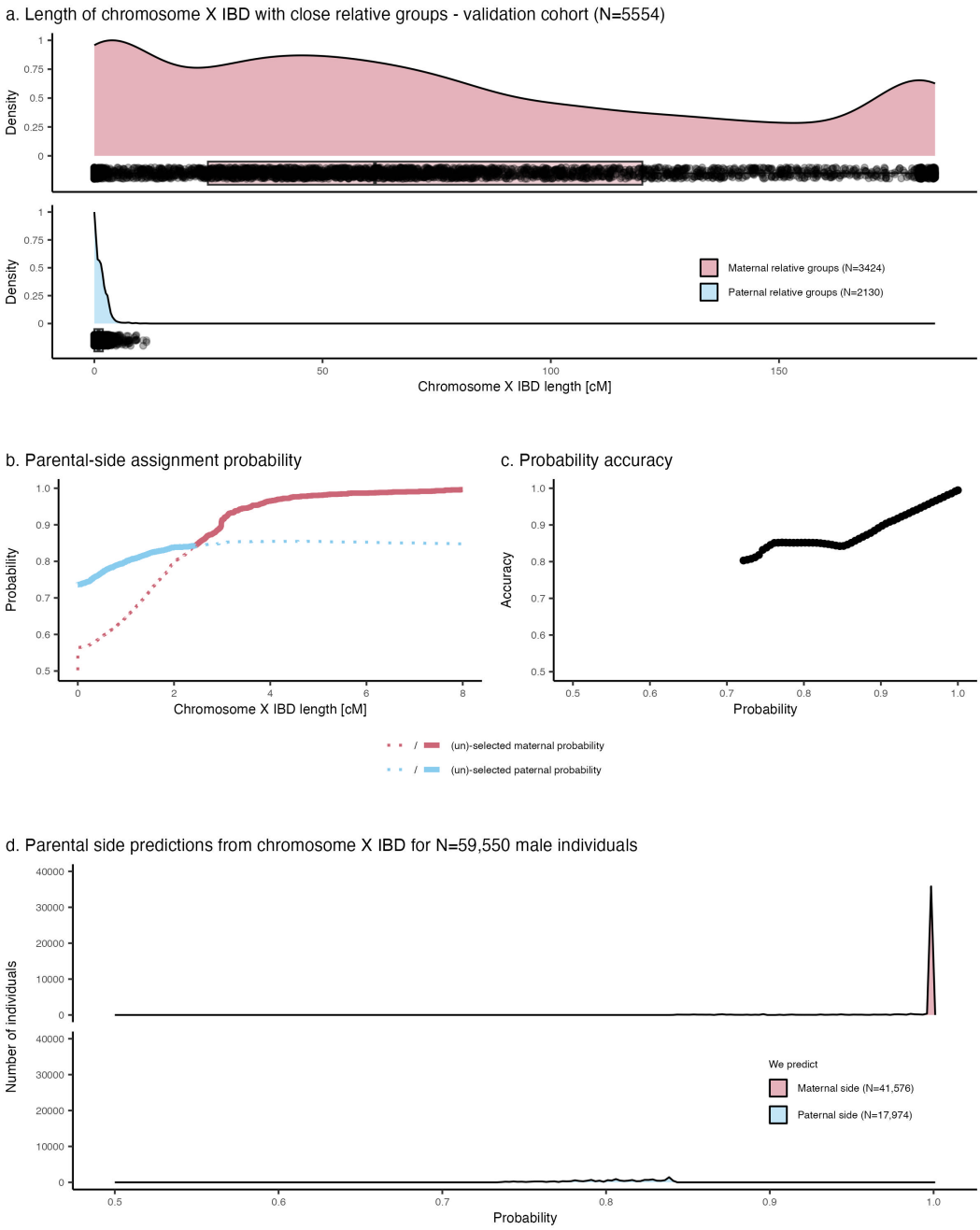

Supplementary Fig. 19 | Parental side assignment from chromosome X IBD analysis in male individuals in the Estonian Biobank. **a**) Density distribution of chromosome X IBD segment length in centimorgan (cM) between targets and surrogate father (blue) and targets and surrogate mother (red) across the validation cohort's male individuals. Boxes indicate the interquartile range (IQR), with the bottom and top of the box representing the 25th (Q1) and 75th (Q3) percentiles, respectively. The horizontal line within the box represents the median (50th percentile). Whiskers extend to the smallest and largest values within $Q1-1.5 \times IQR$ and $Q3+1.5 \times IQR$. Each point represent a target-relative pair. **b**) Parental side probabilities depending on chromosome X IBD segment length derived from the validation cohort. Selected and unselected maternal (red) and paternal (blue) probabilities for a given x-axis value are indicated by solid and dotted lines, respectively. **c**) Accuracy of parental side predictions (y-axis) as a function of the parental side probability (x-axis). **d**) Distribution of maternal (red) and paternal (blue) side assignment probabilities derived chromosome X IBD across 59,550 Estonian Biobank male individuals.

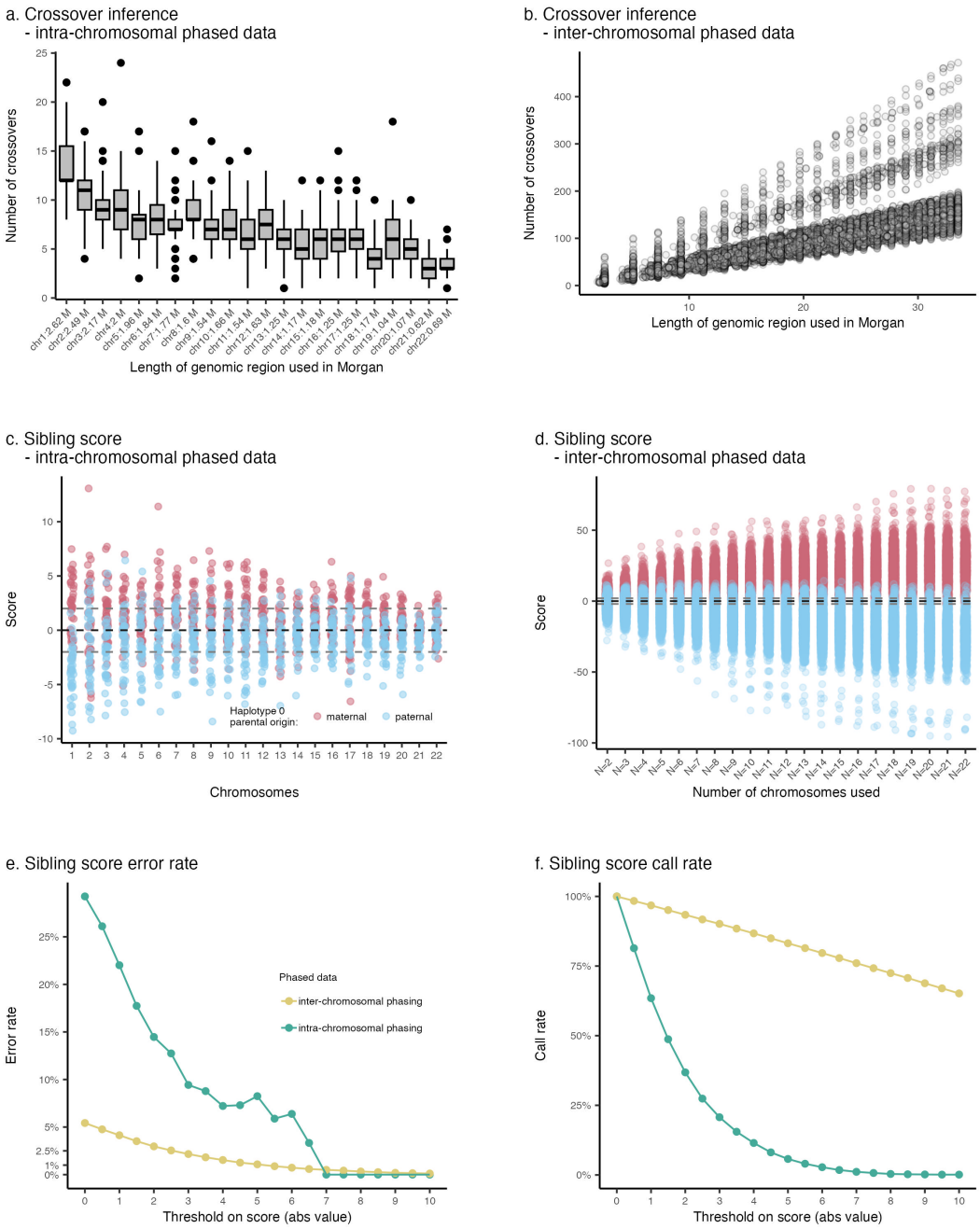

Supplementary Fig. 20 | Evaluation of sibling scores from intra- and inter-chromosomal phasing in the Estonian Biobank validation cohort. **a**) Distribution of the number of inferred crossovers (y-axis) per chromosome (x-axis) derived from intra-chromosomally phased data. **b**) Distribution of the number of inferred crossovers (y-axis) relative to the genomic length used (in Morgans, x-axis) derived from inter-chromosomally phased data. **c**) Distribution of sibling scores (y-axis) per chromosome (x-axis) using intra-chromosomally phased data. Maternal and paternal haplotypes are color-coded in red and blue, respectively. **d**) Distribution of sibling scores (y-axis) relative to the number of chromosomes included in inter-chromosomally phased data (x-axis). **e**) Error rates (y-axis) of sibling scores for varying score thresholds (absolute values, x-axis). **f**) Call rates (y-axis) of sibling scores for varying score thresholds (absolute values, x-axis), showing the proportion of individuals meeting the threshold criteria.

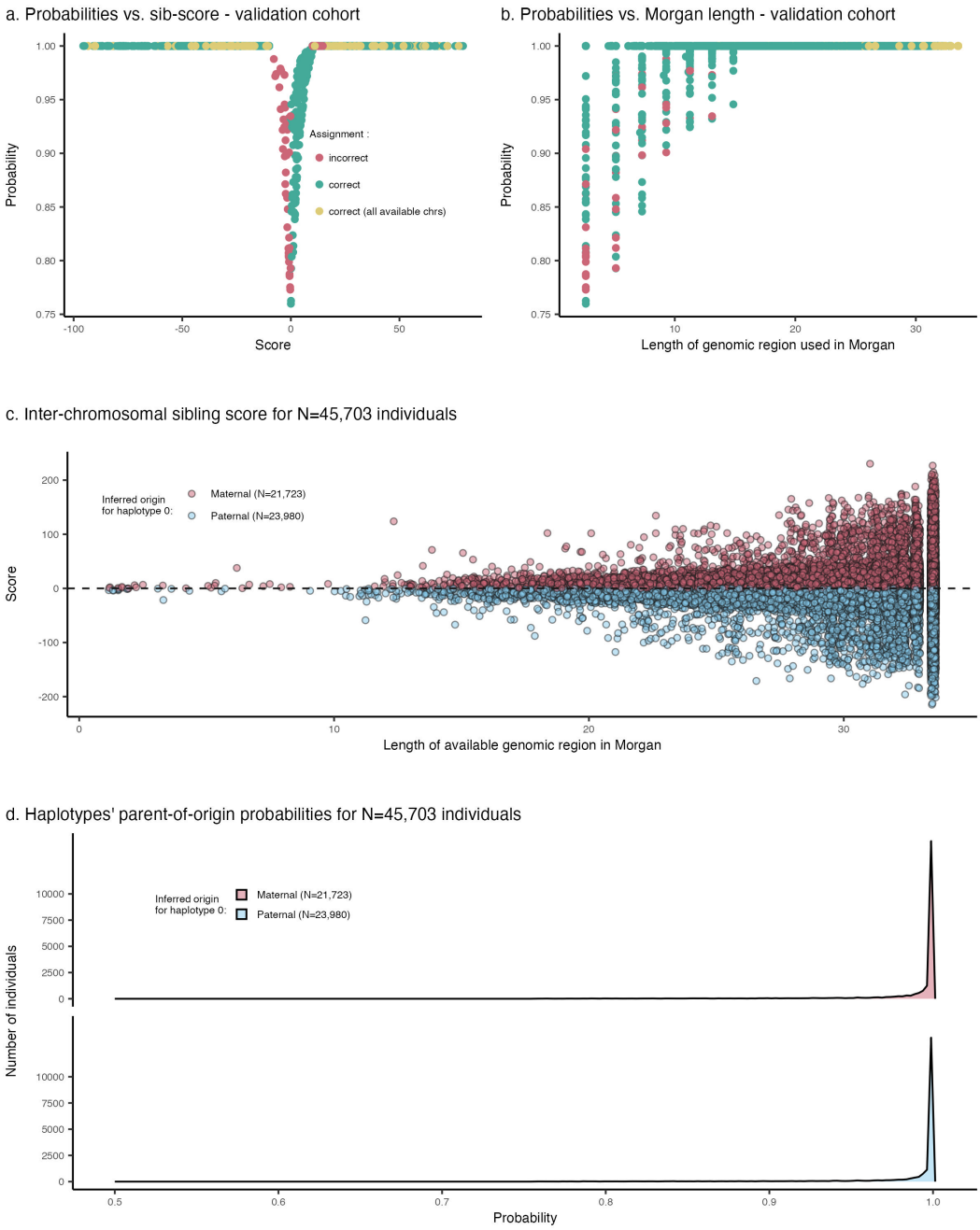

Supplementary Fig. 21 | Validation and derivation of parent-of-origin probabilities using sibling scores from inter-chromosomal phased data in the Estonian Biobank. a) PofO probabilities (y-axis) as a function of sibling scores (x-axis) in the validation cohort. Each dot represents a specific configuration (an individual with a given number of chromosomes used). We varied the number of chromosome used per individual to assess the accuracy of different configurations. Red dots indicate incorrect parental assignments, green dots indicate correct assignments, and yellow dots denote correct assignments using the maximum available chromosomes (N_{max}, corresponds to the full set of inter-chromosomally phased chromosome for a given individual). No errors were observed when N_{max} chromosomes were used. **b**) PofO probabilities (y-axis) plotted against the total available genomic length in Morgans (x-axis) for sibling score calculation in the validation cohort. Each configuration is represented as a dot (color-coded as in panel a). Increasing genomic length results in higher assignment accuracy, with perfect accuracy achieved at N_{max} (yellow dots). **c**) Sibling scores (y-axis) derived for N=45,703 individuals across available genomic lengths (x-axis). **d**) Distribution of PofO probabilities for 45,703 Estonian Biobank individuals.

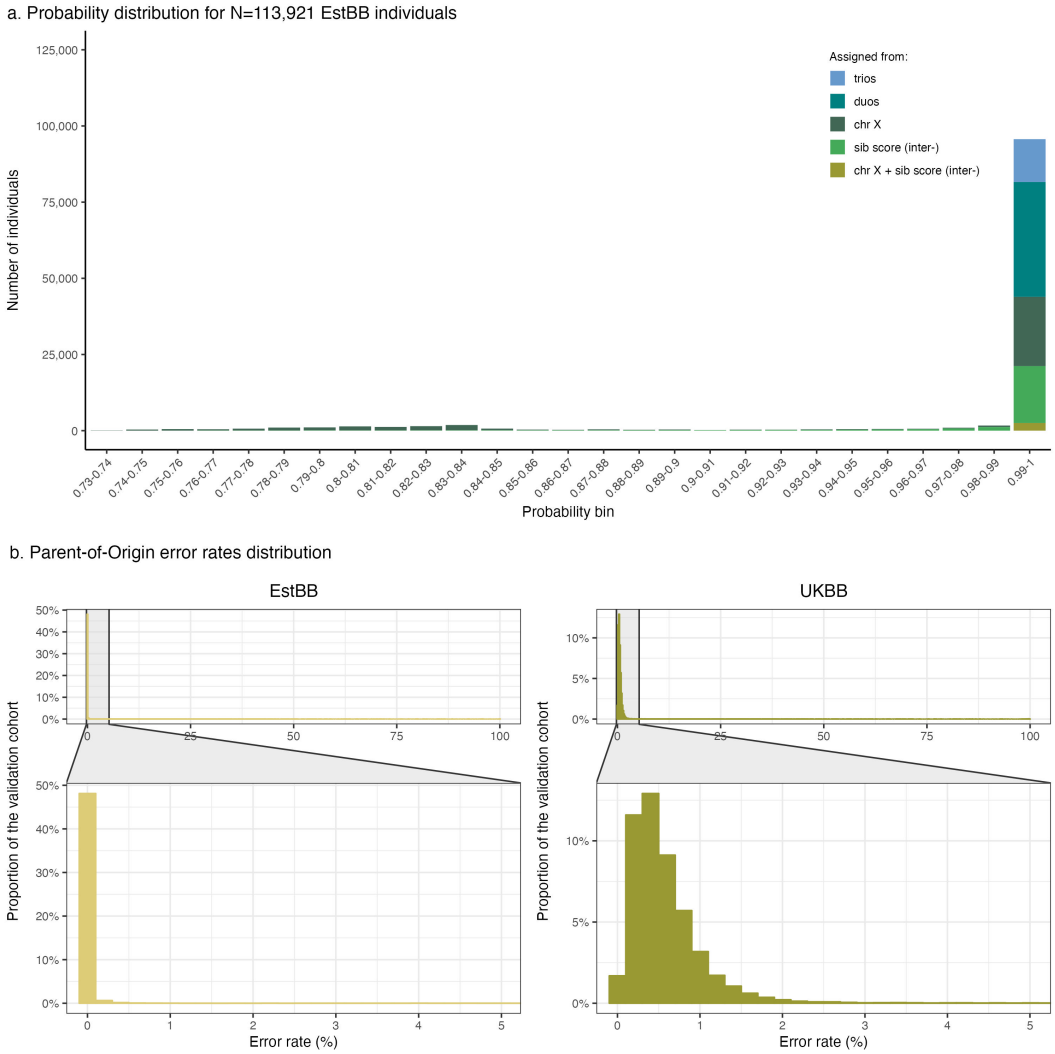

Supplementary Fig. 22 | Parent-of-origin probability distribution and error rates in the Estonian Biobank. a) Distribution of PofO probabilities for N=113,921 individuals in the Estonian Biobank, color-coded by the source of inference (e.g., chromosome X data, sibling score from inter-chromosomal phased data, duos, and trios). Most individuals exhibit high PofO probabilities, reflecting the accuracy of the approach. **b**) Comparison of PofO error rate distributions between the Estonian Biobank (EstBB) and UK Biobank (UKBB) validation cohorts. The EstBB shows consistently lower error rates, likely attributed to the higher number of close relatives per individual, which enhances IBD detection and improves inter-chromosomal phasing accuracy. Zoomed panels show the error rates below 5%, highlighting the robustness of PofO inference in both biobanks.

Supplementary Tables

PHENAME	N	N males	N females
Waist circumference	105688	58938	46750
Hip circumference	105688	58938	46750
Standing height	105688	58938	46750
Birth weight	105688	58938	46750
Body mass index	105688	58938	46750
TS ratio	105656	58915	46741
Body fat percentage	105688	58938	46750
Whole body water mass	105688	58938	46750
Basal metabolic rate	105688	58938	46750
Leg fat percentage	105688	58938	46750
Leg fat-free mass	105688	58938	46750
Arm fat percentage	105688	58938	46750
Arm fat-free mass	105688	58938	46750
Trunk fat percentage	105688	58938	46750
Trunk fat-free mass	105688	58938	46750
White blood cell	105688	58938	46750
Red blood cell	105688	58938	46750
Platelet count	105688	58938	46750
Lymphocyte count	105688	58938	46750
Monocyte count	105688	58938	46750
Neutrophill count	105688	58938	46750
Eosinophill count	105688	58938	46750
Basophill count	105688	58938	46750
Nucleated red blood cell count	105688	58938	46750
Reticulocyte count	105688	58938	46750
Microalbumin in urine	105682	58934	46748
Creatinine	105682	58934	46748
Sodium in urine	105675	58931	46744
Albumin	105688	58938	46750
Alkaline phosphatase	105688	58938	46750
Alanine aminotransferase	105688	58938	46750
Apoliprotein A	105688	58938	46750
Apoliprotein B	105688	58938	46750
Aspartate aminotransferase	105688	58938	46750
Direct bilirubin	105688	58938	46750
Urea	105688	58938	46750
Calcium	105688	58938	46750
Cholesterol	105688	58938	46750
Creatinine	105688	58938	46750
C-reactive protein	105688	58938	46750
Cystatin C	105688	58938	46750
Gamma glutamyltransferase	105688	58938	46750
Glucose	105688	58938	46750
Glycated haemoglobin	105688	58938	46750
HDL cholesterol	105688	58938	46750
IGF-1	105688	58938	46750
LDL direct	105688	58938	46750
Lipoprotein A	105688	58938	46750
Oestradiol	105688	58938	46750
Phosphate	105688	58938	46750
Rheumatoid factor	105688	58938	46750
SHBG	105688	58938	46750
Total bilirubin	105688	58938	46750
Testosterone	105688	58938	46750
Total protein	105688	58938	46750
Triglycerides	105688	58938	46750
Urate	105688	58938	46750
Vitamin D	105688	58938	46750
Type 2 diabetes	9409 (95080)	6556 (51564)	2854 (43517)

Supplementary Table 1 | UK Biobank traits selected for this study.
PHENAME: phenotype name; N: number of individuals (selected as (i) self-reported as white British, confirmed by PCA, according to UK Biobank field 22006; (ii) having a PofO probability > 0.99, as defined for the differential GWAS[3]). For type 2 diabetes, we indicated cases and controls.

				Published studies					Current study				
	PHENAME	RSID	ID	BETA PAT	P PAT	BETA MAT	P MAT	P DIFF	BETA PAT	P PAT	BETA MAT	P MAT	P DIFF
Kim et al., HGG Adv 2021	HDL-C	rs12154627*	7_130422934_T_C	0.0300	6.40E-02	0.1300	2.10E-16	3.10E-06	0.0139	2.76E-02	0.0463	1.93E-13	6.20E-04
	triglyceride	rs12154627*	7_130422934_T_C	-0.0100	5.60E-01	-0.1000	1.40E-09	1.30E-04	-0.0151	2.69E-02	-0.0465	8.94E-12	1.00E-03
	platelets	rs10146962*	14_101170540_T_C	0.0400	6.30E-02	-0.1000	2.30E-11	7.80E-10	-0.0180	9.17E-03	-0.0964	3.73E-44	9.22E-16
Zoledziewska et al., Nat Genet 2015	Height	rs143840904*	11_2813322_C_T	0.0021	9.65E-01	-0.2740	3.98E-08	7.55E-05	-0.0226	1.37E-01	-0.1831	9.13E-32	5.21E-13
	Height	rs2075870*	11_2790019_G_A	-0.0172	7.93E-01	-0.2730	6.97E-08	2.00E-04	-0.0246	8.31E-02	-0.1439	3.00E-23	3.89E-09
	Height	rs149658560*	11_2767262_G_A	-0.0121	8.18E-01	-0.2970	2.93E-07	3.00E-04	-0.0066	6.13E-01	-0.0917	6.47E-12	7.09E-06
Granot-Hershkovitz et al., EJHG 2020	Height	rs1042136	6_33048628_A_C	-0.0230	1.55E-08	0.0050	4.21E-01	1.39E-04	-0.0160	3.54E-03	-0.0062	2.57E-01	1.90E-01
Benonisdottir et al., Nat Comm 2016	Height	rs147239461*	11_1986402_G_T	-0.1200	5.90E-13	0.0560	9.40E-04	1.20E-13	-0.0484	2.80E-05	0.0395	4.92E-04	4.89E-08
	Height	rs7482510	11_2190591_C_G	-0.0650	5.10E-11	0.0180	7.60E-02	4.70E-09	-0.0189	2.71E-04	0.0002	9.71E-01	4.15E-03
	Height	rs143840904*	11_2813322_C_T	0.0570	4.20E-02	-0.2600	2.00E-17	1.60E-14	-0.0226	1.37E-01	-0.1831	9.13E-32	5.21E-13
	Height	rs41286560*	14_101349454_G_T	-0.1200	2.20E-08	0.0670	1.70E-03	7.40E-10	-0.0519	5.03E-05	0.0168	1.87E-01	1.46E-04
Kong et al., Nature 2009	T2D	rs2334499*	11_1696849_C_T	1.35 (OR)	4.70E-10	0.86 (OR)	2.00E-03	4.10E-11	0.1391	2.19E-07	-0.0737	6.05E-03	2.16E-08
Hofmeister et al., Nat Comm 2022	telomere length	rs2735940*	5_1296486_A_G	0.0088	4.60E-01	-0.1215	2.10E-19	4.30E-13	0.014	4.59E-02	-0.100	3.12E-49	2.84E-32
	platelets	rs59228823*	14_101185187_G_C	-0.0110	5.80E-01	-0.1230	6.80E-16	2.30E-08	-0.015	4.68E-02	-0.104	2.14E-42	2.42E-16
Juliusdottir et al., Nat Genet 2021	birth weight	rs9855896	3_14287150_A_G	0.039	4.90E-05	-0.017	1.30E-01	1.65E-04	-0.009	4.29E-01	0.019	8.74E-02	7.59E-02
	birth weight	rs6575803	14_101257755_C_T	0.094	8.30E-17	0.009	5.20E-01	6.00E-07	-0.049	2.03E-03	-0.014	3.75E-01	1.48E-01
	birth weight	rs2296528	20_57274151_G_C	0.037	3.80E-06	-0.012	2.10E-01	4.72E-05	0.032	1.64E-03	0.022	3.45E-02	4.68E-01
	birth weight	rs76094073	6_109288036_C_G	-0.007	5.20E-01	0.06	1.60E-05	2.80E-04	0.042	2.89E-03	0.039	5.84E-03	8.63E-01
	birth weight	rs2529415	7_50736662_C_T	-0.004	6.70E-01	0.039	1.50E-04	7.86E-04	-0.001	9.25E-01	-0.017	8.40E-02	2.39E-01
	birth weight	rs2901307	10_124128443_C_T	0.001	8.50E-01	0.044	2.20E-06	7.03E-05	0.026	5.52E-03	0.031	7.07E-04	6.63E-01
	birth weight	rs231848	11_2735557_A_G	-0.003	7.00E-01	0.051	8.10E-08	9.70E-06	0.005	6.19E-01	-0.019	4.41E-02	7.32E-02
	birth weight	rs2928148	15_41401550_G_A	0.002	8.00E-01	0.045	1.30E-06	1.62E-04	0.016	8.77E-02	0.026	7.09E-03	4.88E-01

Supplementary Table 2 | Replication of previously published Parent-of-origin effects.

PHENAME: phenotype name; RSID: variant rs id; ID: chromosome_position(hg19)_reference allele_alternative allele; BETA and P denote effect sizes and P-values; PAT, MAT, and DIFF denote paternal, maternal and differential tests; *: associations replicated in our study.

CHR	GENPOS	ID	A0	A1	A1FREQ	BETA PAT	SE PAT	P PAT	BETA MAT	SE MAT	P MAT	BETA DIFF	SE DIFF	P DIFF	BETA ADD	SE ADD	P ADD	PHENAME	Status	Locus
2	54422548	rs7562908	A	G	0.026	0.148	0.021	1.06E-12	0.043	0.021	3.86E-02	-0.104	0.029	4.17E-04	-0.099	0.015	2.80E-11	TS ratio	novel	ACYP2
3	46058335	rs6809223	T	C	0.734	-0.049	0.007	1.62E-11	-0.015	0.007	4.20E-02	-0.034	0.010	8.80E-04	-0.032	0.005	5.24E-10	Basophill count	novel	CCR1, CCR3, XCR1
3	156795468	rs13322435	A	G	0.403	-0.072	0.009	1.05E-14	-0.038	0.009	3.15E-05	-0.033	0.013	1.12E-02	-0.055	0.007	4.24E-17	Birth weight	novel	TIPARP
5	72399063	rs10223082	T	C	0.667	-0.052	0.008	9.54E-12	-0.014	0.008	6.50E-02	-0.037	0.011	5.12E-04	-0.033	0.005	9.51E-10	Calcium	novel	FCHO2
7	73026378	rs17145750	C	T	0.162	0.015	0.009	9.68E-02	0.063	0.009	9.07E-13	-0.048	0.013	1.18E-04	0.039	0.006	4.60E-10	IGF-1	novel	MLXIPL
11	2157793	rs3213217	A	T	0.236	0.096	0.008	1.44E-34	0.058	0.008	2.01E-13	0.038	0.011	5.72E-04	0.077	0.006	7.74E-44	IGF-1	novel	IGF2

Supplementary Table 3 | Parent-of-Origin effect genome-wide per phenotype.

CHR: chromosome; GENPOS: genetic position (hg19); ID: variant rs id; A0: reference allele; A1: assessed allele; A1FREQ: A1 allele frequency. BETA, SE and P denote effect sizes, standard errors and P-values; PAT, MAT, DIFF and ADD denote paternal, maternal, differential and additive tests. PHENAME: phenotype name.

Chromosome	Region start	Region end	Genes overlapping region
chr1	68011644	69016459	ARHI
chr2	80015483	81031487	LRRTM1
chr4	89117065	90118980	NAPIL5
chr6	56682421	57691161	PRIM2
chr6	143761436	144885734	PLAGL1,HYMAI
chr6	159890130	161376014	IGF2R,SLC22A2,SLC22A3
chr7	50154712	51361157	GRB10
chr7	93714535	95425726	SGCE,PEG10,PPP1R9A
chr7	96149701	97154142	DLX5
chr7	129432993	130918860	CPA4,MEST,KLF14
chr8	949568	2156642	DLGAP2
chr8	140113081	141215299	KCNK9
chr11	1516405	3686539	H19,IGF2,IGF2AS,INS,KCNQ1,KCNQ1DN,CDKN1C,SLC22A1LS,SLC22A1L,PHLDA2,OSBPL5
chr11	5911654	7479277	SMPD1,ZNF215
chr11	31909324	32957086	WT1
chr14	100693252	101827367	DLK1,MEG3
chr15	23310105	24432449	MKRN3,MAGEL2,NDN
chr15	24700069	26608348	SNURF,IPW,UBE3A,ATP10A
chr16	2986109	3993490	ZNF597
chr18	44054572	45056448	TCEB3C
chr19	56785919	57852075	ZIM2,PEG3
chr20	35649606	36652091	NNAT
chr20	41643052	42670534	L3MBTL
chr20	56914783	57986249	NESP55,GNAS1

Supplementary Table 4 | Imprinted regions.

Imprinted regions extracted from Kong *et al.*[5] and lifted over to hg19.

CHR	GENPOS	ID	A0	A1	A1FREQ	BETA PAT	SE PAT	P PAT	BETA MAT	SE MAT	P MAT	BETA DIFF	SE DIFF	P DIFF	BETA ADD	SE ADD	P ADD	Tested trait
11	1918083	rs7105710	T	C	0.546	0.001	0.005	8.18E-01	-0.013	0.005	8.00E-03	0.014	0.007	4.10E-02	-0.006	0.003	8.70E-02	Sitting height
11	2040272	rs77708343	A	G	0.039	-0.055	0.012	8.51E-06	0.046	0.012	1.21E-04	-0.101	0.017	4.17E-09	-0.003	0.009	6.95E-01	Sitting height
11	2813322	rs143840904	C	T	0.019	-0.044	0.018	1.30E-02	-0.131	0.018	6.61E-13	0.087	0.025	3.80E-04	-0.086	0.013	1.06E-11	Sitting height

Supplementary Table 5 | Replication of standing height association with sitting height.

CHR: chromosome; GENPOS: genetic position (hg19); ID: variant rs id; A0: reference allele; A1: assessed allele; A1FREQ: A1 allele frequency. BETA, SE and P denote effect sizes, standard errors and P-values; PAT, MAT, DIFF and ADD denote paternal, maternal, differential and additive tests. PHENAME: phenotype name.

CHR	GENPOS	ID	A0	A1	A1FREQ	BETA PAT	SE PAT	P PAT	BETA MAT	SE MAT	P MAT	BETA DIFF	SE DIFF	P DIFF	BETA ADD	SE ADD	P ADD	Tested trait
11	1918083	rs7105710	T	C	0.5461	0.011	0.015	4.77E-01	-0.0387	0.015	9.60E-03	0.0494	0.0212	1.95E-02	-0.014	0.0106	1.84E-01	Comparative height size at age 10
11	2040272	rs77708343	A	G	0.0394	-0.118	0.039	2.30E-03	0.0708	0.0381	6.32E-02	-0.1904	0.0542	4.00E-04	-0.022	0.0271	4.16E-01	Comparative height size at age 10
11	2813322	rs143840904	C	T	0.0188	-0.07	0.056	2.10E-01	-0.3206	0.0572	2.07E-08	0.2323	0.0774	2.70E-03	-0.1913	0.0398	1.56E-06	Comparative height size at age 10
11	1702929	rs10838787	G	A	0.425	-0.002	0.013	8.82E-01	-0.0126	0.0132	3.40E-01	0.0097	0.0186	6.03E-01	-0.0073	0.0094	4.36E-01	Comparative body size at age 10
11	2040272	rs77708343	A	G	0.0394	-0.026	0.034	4.42E-01	0.0257	0.0334	4.42E-01	-0.0501	0.0474	2.90E-01	0.0002	0.0237	9.92E-01	Comparative body size at age 10
20	57216538	rs80116540	A	G	0.0753	0.012	0.026	6.46E-01	-0.0553	0.0263	3.52E-02	0.0662	0.0368	7.21E-02	-0.0215	0.0186	2.47E-01	Comparative body size at age 10
11	1702929	rs10838787	G	A	0.4268	-0.029	0.009	2.30E-03	0.0068	0.0095	4.72E-01	-0.0353	0.0133	8.00E-03	-0.0111	0.0067	9.88E-02	Birth weight
11	2040272	rs77708343	A	G	0.0397	-0.057	0.024	1.88E-02	0.0304	0.0236	1.98E-01	-0.0881	0.0339	9.30E-03	-0.012	0.0169	4.78E-01	Birth weight
20	57216538	rs80116540	A	G	0.0763	-0.006	0.019	7.42E-01	0.0208	0.0186	2.64E-01	-0.0248	0.0262	3.44E-01	0.0074	0.0132	5.76E-01	Birth weight

Supplementary Table 6 | Replication of associations with early childhood traits.

CHR: chromosome; GENPOS: genetic position (hg19); ID: variant rs id; A0: reference allele; A1: assessed allele; A1FREQ: A1 allele frequency. BETA, SE and P denote effect sizes, standard errors and P-values; PAT, MAT, DIFF and ADD denote paternal, maternal, differential and additive tests. PHENAME: phenotype name.

CHR	GENPOS	ID	A0	A1	BETA DIFF COMB	SE DIFF COMB	P DIFF COMB	DIFF BETA MALES	DIFF SE MALES	DIFF P MALES	DIFF BETA FEMALES	DIFF SE FEMALES	DIFF P FEMALES	Pz	PHENAME
6	144274210	rs12528876	T	C	-0.057	0.012	2.96E-06	-0.059	0.016	2.68E-04	-0.055	0.018	2.62E-03	8.62E-01	IGF-1
7	130009312	rs10239342	T	G	0.045	0.009	1.87E-06	0.052	0.011	2.42E-06	0.040	0.016	9.73E-03	5.34E-01	SHBG
7	130016470	rs62471721	G	A	-0.057	0.010	6.51E-09	-0.071	0.014	2.03E-07	-0.043	0.014	1.52E-03	1.54E-01	Triglycerides
7	130017940	rs4731690	A	G	0.041	0.009	1.92E-06	0.043	0.012	2.62E-04	0.040	0.013	1.89E-03	8.51E-01	HDL cholesterol
7	130463192	rs6467315	C	G	0.043	0.009	2.20E-06	0.021	0.011	5.05E-02	0.070	0.015	5.03E-06	9.52E-03	Hip circumference
11	1702929	rs10838787	G	A	0.228	0.038	1.87E-09	0.208	0.046	7.56E-06	0.269	0.066	4.47E-05	4.49E-01	Type 2 diabetes
11	1702929	rs10838787	G	A	0.078	0.009	2.77E-17	0.084	0.013	2.29E-10	0.068	0.013	8.53E-08	4.03E-01	Glycated haemoglobin
11	**1703564**	**rs4417225***	**C**	**T**	**0.057**	**0.011**	**7.40E-08**	**0.087**	**0.015**	**4.79E-09**	**0.020**	**0.015**	**1.93E-01**	**1.38E-03**	**Glucose**
11	1918083	rs7105710	T	C	0.032	0.006	1.99E-08	0.027	0.008	7.01E-04	0.039	0.009	3.89E-06	2.69E-01	Standing height
11	1920285	rs4264135	A	G	-0.046	0.009	2.22E-07	-0.046	0.012	1.42E-04	-0.049	0.013	1.72E-04	8.67E-01	Urate
11	1998031	rs170102	G	A	-0.067	0.009	5.98E-14	-0.069	0.012	2.98E-09	-0.065	0.014	1.69E-06	8.34E-01	Cystatin C
11	2003944	rs217215	T	G	0.054	0.008	4.94E-11	0.055	0.011	4.15E-07	0.054	0.013	2.00E-05	9.43E-01	Creatinine
11	2040272	rs77708343	A	G	-0.077	0.015	1.63E-07	-0.086	0.020	1.11E-05	-0.066	0.022	2.99E-03	4.94E-01	Whole body water mass
11	2040272	rs77708343	A	G	-0.083	0.015	7.53E-08	-0.089	0.020	1.43E-05	-0.075	0.023	1.24E-03	6.68E-01	Basal metabolic rate
11	2040272	rs77708343	A	G	-0.085	0.015	1.80E-08	-0.088	0.020	1.05E-05	-0.081	0.023	4.44E-04	8.22E-01	Leg fat-free mass
11	2040272	rs77708343	A	G	-0.088	0.015	2.18E-09	-0.061	0.020	2.61E-03	-0.120	0.022	2.88E-08	4.51E-02	Standing height
11	2041348	rs78507815	G	T	-0.065	0.013	3.61E-07	-0.078	0.017	4.57E-06	-0.050	0.019	9.55E-03	2.71E-01	Trunk fat-free mass
11	2813322	rs143840904	C	T	0.152	0.021	5.21E-13	0.131	0.029	4.48E-06	0.179	0.031	1.15E-08	2.53E-01	Standing height
11	2858295	rs2299620	C	T	0.116	0.024	2.23E-06	0.133	0.035	1.52E-04	0.096	0.034	4.23E-03	4.48E-01	Glycated haemoglobin
14	101185187	rs59228823	G	C	0.082	0.011	1.92E-14	0.078	0.014	5.83E-08	0.086	0.016	5.43E-08	7.05E-01	Platelet count
15	25983333	rs146982369	C	G	0.208	0.044	2.59E-06	0.193	0.059	1.12E-03	0.227	0.066	6.15E-04	7.00E-01	Total protein
16	3412861	rs7188903	A	G	-0.053	0.011	6.14E-07	-0.056	0.014	6.83E-05	-0.049	0.016	2.00E-03	7.25E-01	IGF-1
20	57216538	rs80116540	A	G	0.074	0.014	2.06E-07	0.051	0.018	5.35E-03	0.099	0.022	7.47E-06	9.69E-02	Body fat percentage
20	57216538	rs80116540	A	G	0.078	0.014	3.39E-08	0.049	0.017	4.70E-03	0.110	0.023	1.36E-06	3.42E-02	Arm fat percentage
20	57226079	rs6026426	C	G	0.085	0.018	1.29E-06	0.061	0.022	5.63E-03	0.112	0.028	6.97E-05	1.51E-01	Trunk fat percentage
20	57484934	rs3730173	C	T	0.071	0.014	5.32E-07	0.062	0.019	9.03E-04	0.081	0.021	1.59E-04	5.21E-01	Leg fat percentage
3	169482335	rs2293607	T	C	-0.055	0.011	5.70E-07	-0.053	0.015	3.50E-04	-0.058	0.016	4.22E-04	8.44E-01	TS ratio
4	164012901	rs11100479	C	T	0.057	0.012	6.25E-07	0.057	0.016	3.00E-04	0.059	0.017	5.41E-04	9.20E-01	TS ratio
5	1285974	rs7705526	C	A	-0.068	0.010	5.82E-11	-0.056	0.014	5.87E-05	-0.080	0.015	1.33E-07	2.48E-01	TS ratio
14	101176212	rs12881545	G	C	-0.072	0.010	2.34E-13	-0.067	0.013	3.90E-07	-0.078	0.015	8.92E-08	5.98E-01	Platelet count
11	2857194	rs2237895	A	C	-0.040	0.009	2.16E-05	-0.041	0.013	2.05E-03	-0.038	0.013	2.86E-03	8.91E-01	Glycated haemoglobin
11	2813322	rs143840904	C	T	0.152	0.021	5.21E-13	0.131	0.029	4.48E-06	0.179	0.031	1.15E-08	2.53E-01	Standing height

Supplementary Table 7 | Sex-specificity of Parent-of-Origin effects.

CHR: chromosome; GENPOS: genetic position (hg19); ID: variant rs id; A0: reference allele; A1: assessed allele; A1FREQ: A1 allele frequency. DIFF BETA, DIFF SE and DIFF P denote effect sizes, standard errors and P-values for the differential test; COMB, MALES, and FEMALES denote combined sex, males only and females only. P_Z: denotes the P-values for the comparison tests between males-specific and females-specific coefficients using a Z-score approach; PHENAME: phenotype name.

CHR	GENPOS HG38	UKBB SNP	ASSESSED SNP	LD	A0	A1	N	BETA DIFF	SE DIFF	P DIFF	BETA PAT	SE PAT	P PAT	BETA MAT	SE MAT	P MAT	PHECODE
11	1896853	rs7105710	**rs7105710**		T	C	61630	0.027	0.007	1.13E-04	0.019	0.005	1.20E-04	-0.009	0.005	7.39E-02	Standing height
11	1902116	rs77708343	rs145861779	0.48	C	T	61630	-0.040	0.016	1.56E-02	-0.044	0.012	2.12E-04	-0.006	0.012	6.36E-01	Standing height
11	2792092	rs143840904	**rs143840904**		C	T	61630	0.162	0.028	7.94E-09	-0.005	0.020	7.98E-01	-0.175	0.021	1.70E-17	Standing height
11	1682334	rs4417225	**rs4417225**		C	T	80403	0.046	0.012	1.92E-04	0.030	0.009	5.87E-04	-0.017	0.009	5.81E-02	Glucose
11	1682334	rs10838787	**rs4417225**	1.00	C	T	85050	0.189	0.050	1.47E-04	0.092	0.035	9.60E-03	-0.101	0.035	4.17E-03	Type 2 diabetes
11	1682334	rs10838787	**rs4417225**	1.00	C	T	20203	0.078	0.018	1.03E-05	0.055	0.013	1.45E-05	-0.025	0.013	4.83E-02	Glycated haemoglobin
11	2837065	rs2299620	rs2299620		C	T	20203	0.130	0.048	6.79E-03	0.060	0.034	8.07E-02	-0.070	0.034	3.83E-02	Glycated haemoglobin
7	130378099	rs4731690	**rs4731690**		A	G	81884	0.016	0.003	6.86E-08	0.009	0.002	1.18E-05	-0.007	0.002	1.01E-03	HDL cholesterol
7	130376629	rs62471721	**rs62471721**		G	A	81884	-0.036	0.008	1.91E-05	-0.012	0.006	5.21E-02	0.024	0.006	4.74E-05	Triglycerides
7	130778999	rs6467315	rs10954284	1.00	T	A	55874	-0.008	0.010	4.07E-01	0.001	0.007	8.78E-01	0.009	0.007	1.81E-01	Hip circumference
11	1899055	rs217215	**rs4264135**	0.61	A	G	77270	-0.058	0.008	4.40E-12	-0.028	0.006	2.21E-06	0.030	0.006	4.27E-07	Creatinine
11	1899055	rs170102	rs4264135	0.61	A	G	21851	0.042	0.015	5.38E-03	0.028	0.011	8.99E-03	-0.014	0.011	1.86E-01	Cystatin C
14	100709875	rs12881545	**rs12881545**		G	C	67266	-0.102	0.010	1.17E-23	0.010	0.007	1.69E-01	0.111	0.007	1.99E-54	Platelet count
14	100718850	rs59228823	**rs59228823**		G	C	67266	0.078	0.011	2.97E-13	-0.007	0.008	3.55E-01	-0.087	0.008	4.49E-30	Platelet count

Supplementary Table 8 | Replication of parent-of-origin effects in the Estonian Biobank cohort.

CHR: chromosome; GENPOS: genetic position (hg38); UKBB SNP: variant exhibiting POE on the trait in the UK Biobank (UKBB); ASSESSED SNP: variant tested for POE in the Estonian Biobank (EstBB); LD: Linkage Disequilibrium (LD) between the UKBB variant and the assessed variant, if not the same variant. LD was computed in the UK Biobank cohort; A0: reference allele of the assessed variant in the EstBB; A1: assessed allele of the assessed variant in the EstBB; N: number of individuals with available trait levels (includes individuals both homozygous and heterozygous for the assessed variant); BETA, SE and P denote effect sizes, standard errors and P-values; PAT, MAT and DIFF denote paternal, maternal and differential tests. PHENAME: phenotype name.